ISTANBUL TECHNICAL UNIVERSITY ★ GRADUATE SCHOOL

INVESTIGATION OF STRETCHING EFFECT WITH MIXED FINITE ELEMENT FORMULATIONS FOR LAMINATED BEAMS AND PLATES

M.Sc. THESIS

Doğan KANIĞ

Department of Civil Engineering

Structural Engineering Programme

DECEMBER 2023

ISTANBUL TECHNICAL UNIVERSITY ★ GRADUATE SCHOOL

INVESTIGATION OF STRETCHING EFFECT WITH MIXED FINITE ELEMENT FORMULATIONS FOR LAMINATED BEAMS AND PLATES

M.Sc. THESIS

Doğan KANIĞ
(501211006)

Department of Civil Engineering

Structural Engineering Programme

Thesis Advisor: Assoc. Prof. Dr. Akif KUTLU

DECEMBER 2023

ISTANBUL TEKNİK ÜNİVERSİTESİ ★ LİSANSÜSTÜ EĞİTİM ENSTİTÜSÜ

TABAKALI KOMPOZİT KİRİŞ VE PLAKLAR İÇİN KARIŞIK SONLU ELEMAN FORMÜLASYONLARI İLE ENİNE ŞEKİL DEĞİŞTİRME ETKİSİNİN İNCELENMESİ

YÜKSEK LİSANS TEZİ

Doğan KANIĞ
(501211006)

İnşaat Mühendisliği Anabilim Dalı

Yapı Mühendisliği Programı

Tez Danışmanı: Doç. Dr. Akif KUTLU

ARALIK 2023

Doğan KANIĞ, a M.Sc student of ITU Graduate School student ID 501211006, successfully defended the thesis/dissertation entitled “INVESTIGATION OF STRETCHING EFFECT WITH MIXED FINITE ELEMENT FORMULATIONS FOR LAMINATED BEAMS AND PLATES”, which he prepared after fulfilling the requirements specified in the associated legislations, before the jury whose signatures are below.

Thesis Advisor :	**Assoc. Prof. Dr. Akif KUTLU** Istanbul Technical University	.....
Jury Members :	**Prof. Dr. Nihal ERATLI** Istanbul Technical University	.....
	Assoc. Prof. Dr. Mehmet Dördüncü Erciyes University	.....

Date of Submission : 8 December 2023
Date of Defense : 29 December 2023

To my family,

FOREWORD

I currently completing my thesis for the M.Sc. degree in structural engineering from Istanbul Technical University's civil engineering department. The work I carried out on this thesis has greatly impacted my practical expertise. First of all, I would like to express my sincere thanks to Assistant Professor Dr. Akif KUTLU, who performed the role my thesis advisor. He provided me with competent assistance and unwavering support throughout the research process. The way that my work has developed has been greatly influenced by his excellent coaching. Additionally, I would like to sincerely thank to my colleague Yonca BAB, for her consistent backing and important contribution to widening my academic outlook. In addition, I want to express my sincere gratitude to my family for their inspiration, guidance, and patiently support during the whole study process. I am also thankful to Turkish Science Dissemination Foundation 'İlim Yayma Vakfı (İYV)', which greatly facilitated the completion of this research.

December 2023 Doğan KANIĞ

(Civil Engineer)

TABLE OF CONTENTS

Page

ABBREVIATIONS

CBT **:** Classical Beam Theory
CPT **:** Classical Plate Theory
CLT : Classical Lamination Theory
DLWM : Discrete Layerwise Methods
ESL **:** Equivalent Single Layer
FEM **:** Finite Element Method
FSDT **:** First Order Shear Deformation Theory
HSDT **:** Higher Order Shear Deformation Theory
ILWM **:** Integrate Layerwise Methods
LWT **:** Layer wise Theories
ZZ **:** Zig-zag Theory

SYMBOLS

$\delta \Pi_{HR}$	: First variation of the functional
$\boldsymbol{\varepsilon}^{\mathbf{u}}$	: Strain vector in terms of displacement components
$\boldsymbol{\varepsilon}^{\boldsymbol{\sigma}}$	: Strain vector in terms of the stress components
$\boldsymbol{\sigma}^{\boldsymbol{\sigma}}$	: Stress vector
δ	: Variation operator
$\hat{\mathbf{t}}$	: Traction vector
Γ	: Boundary of the structure
E_1, E_2, E_3	: Young's moduli
v_{ij}	: Poison's ratio
G_{23}, G_{31}, G_{12}	: Shear moduli
GD	: Geometry-Displacement matrix
θ	: Angle measured from x-axis to material axis 1
$\bar{Q}$	: Transformed reduced stiffnesses
$f(z)$	: Shear functions
$g(z)$	: A function which represents the variation of the transverse normal strain along the beam thickness (= d$f(z)$ / dz)
h	: Thickness of the structure in transverse direction
z	: Any coordinate along the thickness
u	: Midplane displacement in x direction
v	: Midplane displacement in y direction
w	: Midplane displacement in z direction
β	: A variable used to describe the stretching effect
θ_x	: Shear rotation about y axis
θ_y	: Shear rotation about x axis
$\sigma_{\alpha}^{(k)}$	: In-plane stress components at k^{th} layer ($\alpha = xx, yy, xy$)
$\sigma_{\alpha}^{(k)}$	: Transverse shear stress components at k^{th} layer ($\alpha = xz, yz$)

σ^0 : Initial stress matrix

N_α : In-plane resultants of stress components ($\alpha = xx, yy, xy$)

M_α : Resultant moments of stress components ($\alpha = xx, yy, xy$)

M_α^f : Resultant higher order moments of stress components ($\alpha = xx, yy, xy$)

M_{zz}^f : Transverse normal stress resultant

Q_α : Resultants of transverse shear components ($\alpha = xz, yz$)

b : Beam width

N : Total number of layers

$\mathbf{E_Q}$: Material constant matrix

$\mathbf{Z}$: A function of thickness coordinate

$\mathbf{P}$: Stress resultants

$\mathbf{e^u}$: Strain measures in terms of kinematical variables

$\mathbf{E}$: Section stiffness matrix

$\mathbf{e^P}$: Stress measures in terms of stress resultants

$\mathbf{p}$: Applied load vector

L : Beam length

$\mathbf{K}$: System matrix

$\mathbf{F}$: External force vector

$\mathbf{X}$: Unknown vector

A : Plate area

$u^*_{,\alpha}, v^*_{,\alpha}$: First derivative of in-plane displacements in laminate continuum in terms of α ($\alpha = x, y, z$)

$w^*_{,\alpha}$: First derivative of deflection in laminate continuum in terms of α ($\alpha = x, y$)

K : Bulk modulus

G : Representative shear modulus

i : Imaginary number unit

N_b : Buckling load

D : Flexural rigidity

LIST OF TABLES

Page

LIST OF FIGURES

INVESTIGATION OF STRETCHING EFFECT WITH MIXED FINITE ELEMENT FORMULATIONS FOR LAMINATED BEAMS AND PLATES

SUMMARY

A complete knowledge of the behavior of structural applications under applied loads is necessary for the engineering design process. Finite element formulations have been shown to be one of the most effective analysis method in engineering applications. This information is crucial since it has always been a top objective for engineers and researchers to offer solutions that are as accurate as possible.

Construction, biomechanics, mobile, industrial, aerospace, defense, and nuclear engineering are just a few of the engineering fields where composite structures are increasingly widely employed. In the constructions in which they are used, a variety of composite materials, which are based on the collaboration of many materials, provide some advantages including sound, temperature, water insulation, fire prevention and so on. In the structural design of composite materials, load bearing capability, failure load, and damage detection are crucial factors. Regarding to find a closer solution to expected results of all those parameters, a proper static analysis is unavoidable. It will be effective to choose the right and efficient formulation that reflects the real physics behavior accurate enough because either the financial condition or other factors may not be available for experimental work.

The modeling and analysis of laminated composite beams and plates using higher order shear deformation theory (HSDTs) is performed in this thesis. This thesis' main goal is to introduce the stretching effect with the higher order shear deformation theory into a single formulation using polynomial, exponential, and trigonometric functions. To develop a weak form based on the generalized displacement fields of the higher order shear deformation theories, the notion of virtual displacements is used within a mixed formulation. In order to adequately represent the nonlinear and parabolic variability of transverse shear stress, it is discovered that even for the different functions, results with elasticity method theoretically compatible with used HSDT model. In addition, when compared to the theories that are already accessible in the literature, presented higher order shear deformation theory converges the responses for laminated composite plates and beams.

The first variation of the functional for both laminated beam and plate structures are obtained through the application of the Hellinger-Reissner variational principle. Due to this, displacements and stress resultants, namely two independent fields, are included in finite element equations. Two-noded, one-dimensional straight elements are utilized for the laminated beams, whereas four-noded, two-dimensional quadrilateral elements are used for laminated plates. While the generated functional initially had C^1 continuity, as an advantage of the mixed finite element formulation integration by parts is performed resulting with functionals requiring only C^0 continuity. The kinematical variables of the beam model involve one deflection, one

axial displacement, one additional deflection parameter to introduce transverse stretching, and one shear rotation. The plate's kinematics consist of deflection parameters w and β, two in-plane displacement u and v, representing the displacement components for x and y directions, and shear rotations θ_x and θ_y associated with y and x axes, respectively.

One advantage of this mixed finite element method is the accurate derivation of displacements and stress components at the nodes. To compute axial stress and in-plane shear stress Hooke's law is employed, while with the help of the equilibrium equations of elasticity, transverse shear components are acquired. To demonstrate the applicability of the proposed mixed finite element formulation, different types of examples for composite beams and plates based on various higher order shear deformation theories are presented. In addition, buckling analysis is performed for isotropic plate and laminated composite beams using the presented theory. The performance of the proposed solution procedure is evaluated through comparison and convergence assessments with various layouts and boundary conditions.

TABAKALI KOMPOZİT KİRİŞ VE PLAKLAR İÇİN KARIŞIK SONLU ELEMAN FORMÜLASYONLARI İLE ENİNE ŞEKİL DEĞİŞTİRME ETKİSİNİN İNCELENMESİ

ÖZET

Mühendislik tasarım süreci için, taşıyıcı elemana etkiyen yükler altında ilgili yapısal uygulamaların davranışı hakkında yeterince bilgi edinilmelidir. Bu nedenle, mühendisler ve araştırmacılar, genellikle analiz sürecinde en etkili çözüm yöntemlerinden biri olarak sonlu eleman formülasyonlarını tercih ederler. Bu sayede gerçek hayat problemleri için mümkün olduğunca gerçekçi çözümler en verimli ve güvenilir şekilde elde edilebilmektedir.

Günümüzde, inşaat, biyomekanik, otomobil, endüstriyel, havacılık, savunma ve nükleer mühendisliksektörleri kompozit yapıların giderek yaygınlaştığı mühendislik alanlarından sadece birkaçıdır. Bu malzemeler birbirinden farklı özellikte en az iki malzemenin bir araya gelip uygun entegrasyon ile birlikte çalışma prensibine dayanır. Kompozit malzemelerin temel avatantajı oluşturulan kompozit yapının gerçekleştirilen tasarım ile bir araya getirilen malzemelerin güçlü yönlerinin ortaya çıkarılıp zayıf yönlerine karşı tedbir oluşturulabilmesidir. Bu sebeple, kompozit malzemelerin kullanımı, yapılar için ısı, ses ve su yalıtımı sağlama, yangına karşı direnç gibi birçok olumlu özellik sunar. Bir yapısal sistemde kullanılacak kompozit malzemenin taşıyabileceği maksimum yükü belirlemek ve malzeme hasarına neden olabilecek kopma veya sıyrılma gibi durumları tespit etmek son derece önemlidir. Bu gibi durumların tespiti için tasarım sürecinde kullanılacak kompozit malzemeden oluşturulmuş yapının statik davranışını uygun yöntemlerle detaylıca incelemek önemlidir. Deneysel analizlerin yapılması da elbette önemlidir; ancak fiziksel koşulların sınırlı olması ve yüksek bütçe ihtiyacı gibi nedenlerden dolayı bu analizler tercih edilemeyebilir. Bu durumda, gerçek probleme en yakın fiziksel modeli belirlemek ve ardından uygun teorik çalışmalarla analiz yapmak daha sağlıklı ve tercih edilebilir bir yol olmaktadır.

Yüksek mertebe kayma deformasyon teorisi (YMKT) kullanılarak tabakalı kompozit kiriş ve plakların modellenmesi ve karışık sonlu elemanlar kullanılarak analizi bu tezde bir araya getirilmiştir. Bu tezin başlıca amacı, kalınlık boyunca enine şekil değiştirme etkisini dahil ederek tüm yüksek mertebeli kayma deformasyon teorilerinin polinom, üstel ve trigonometrik fonksiyonlarla birlikte tek bir formülasyonda sentezleyebilen bir sonlu eleman formülasyonunun geliştirilmesidir. Bu tezde, sayısal çözüm formülasyonunun oluşturulmasında Hellinger-Reissner prensibi kullanılmıştır ve bu prensibe dayalı olarak kiriş ve plak denklemleri için ayrı ayrı elde edilen fonksiyonelin ilk varyasyonu yer almaktadır. Bu sayede yer değiştirme ve gerilme bileşkesi türündeki iki farklı bölge değişkenlerini bir arada içeren karışık sonlu eleman denklemleri elde edilmiştir. Yüksek mertebeli kayma deformasyon teorilerinin genelleştirilmiş yer değiştirme alanlarına dayanan zayıf bir

form elde etmek için virtüel iş denklemi karışık sonlu elemanlar çerçevesi içinde kullanılmıştır. Tabakalı kompozit kiriş ve plak mekanik modellerinde Yüksek Mertebe Kayma Teorisi göz önünde bulundurulmuş ve bu sayede Birinci Mertebe Kayma Deformasyon Teorisinde (BMKT) ihtiyaç duyulan kayma düzeltme katsayısına olan ihtiyaç ortadan kaldırılmıştır. Tabakalı kompozit yapıların mekanik davranışlarının incelenmesinde mühim bir konu olan kesit çarpılmasını (enine kayma gerilmesi kaynaklı) aktarmak üzere bir çok kayma deformasyon teorisi, farklı türlerde kayma fonksiyonları üzerinden araştırmacılar tarafından ortaya atılmıştır. Bu tezde, tabakalı kiriş ve plak elemanlar için fonksiyonelin durağanlığını temsil eden ilk varyasyonu, Hellinger-Reissner varyasyon ilkesi kullanılarak türetilmiştir. Bu nedenle, çalışma için sonlu eleman denklemlerine yer değiştirme ve gerilme bileşenleri olmak üzere iki bağımsız alan dahil edilmiştir. Problemin kiriş açısından ayrıştırılması için iki düğümlü, bir boyutlu düz elemanlar kullanılmış, problemin plak kısmı için ise dört düğümlü, iki boyutlu dörtgen elemanlar kullanılmıştır. Bu çalışmada gerçekleştirilen tabakalı kompozit plak analizleri ve sayısal örnekleri için birbirinden farklı dört araştırmacının kayma şekil değiştirme fonksiyonları kullanılmış ve birbirleri ile (ve literatürdeki diğer tabakalanma teorileri ve çözüm yöntemleri ile) karşılaştırılmıştır.

Sonlu eleman ayrıklaştırması sırasında, kirişler için iki düğüm noktalı, tek boyutlu düz (geometrik olarak doğrusal) elemanlar ve plaklar için ise dört düğüm noktalı, iki boyutlu ve genel dörtgen elemanlar kullanılmıştır. Oluşturulan fonksiyonel başlangıçta C^1 sürekliliğine sahip iken karışık sonlu eleman formülasyonunun bir avantajı olarak matematiksel operasyonlar ile nihayetinde C^0 sürekliliğini gerektiren bir yapı oluşturulmuştur. Tabakalı kompozit kirişin yer değiştirme alanı, bir çökme, bir eksenel yer değiştirme, bir enine şekil değiştirme parametresi ve bir kayma dönmesi ifadesinden oluşurken, plak yer değiştirme alanı iki çökme bileşeni w ve β, iki düzlem içi yer değiştirme u ve v, ve θ_x ile θ_y olmak üzere iki kayma dönmesi ifadesinden meydana gelmektedir.

Sunulan karışık sonlu eleman çözüm yönteminin önemli bir avantajı, düğüm noktalarında deplasmanların ve gerilme bileşenlerinin doğru bir şekilde türetilmesidir. Gerçekleştirilen analizlerde, normal gerilmelerin ve düzlem içi kayma gerilmesi hesabında Hooke yasası ve enine kayma gerilmesi bileşenleri için ise elastisite teorisinin denge denklemleri kullanılmıştır. Önerilen karışık sonlu eleman formulasyonunun geçerliliğini ve uygulanabilirliğini göstermek amacıyla, yüksek mertebeden kayma deformasyon teorisine dayalı farklı örnekler sunulmuştur. Ayrıca izotropik bir plak ve lamine kompozit kirişler için burkulma analizi yapılmıştır. Önerilen çözüm prosedürünün performansı, çeşitli tabakalanma düzenleri ve sınır koşulları altında karşılaştırma ve yakınsama değerlendirmeleri aracılığıyla değerlendirilmiştir.

1. INTRODUCTION

The flexural analysis of laminated composite beams and plates including the transverse stretching effect using mixed finite element formulation based on Higher Order Shear Deformation Theory is the main focus of this thesis. The mixed finite element formulation is derived using the Hellinger-Reissner variational principle. A inhouse FORTRAN code is used to implement the numerical procedures. This section, after providing an overview, presents a literature review on the theories and analyses of laminated composite beams and plates and concludes with presenting the aim and scope of the thesis study.

1.1 Overview

In simulating the response of laminated beam, plate, or shell structures, mechanical models can be categorized into three basic theories: 3D theories, Equivalent Single Layer Theories (ESLT), and Layer-Wise Theories (LWT). 3D theories offer highly accurate predictions of displacement and stress components for laminated structures in numerical analyses. However, using 3D elements to represent a laminated structure can be expensive, especially when dealing with structures having many layers with different material distributions. LWTs also provide quite accurate structural characteristics, but they are also computationally high-demanding, similar to 3D approaches. On the other hand, ESLTs represent the laminated structure using a fixed number of kinematical variables independent of material layouts. It is important to note that the accuracy of a formulation designed for laminated structures depends on both the assumptions of the structural theory and the used numerical method. To design laminated composite structures accurately, it's essential to precisely determine mechanical characteristics like displacements and stress components. Various theories and solution methods have been developed to improve predictions of these structural properties.

1.2 Literature Survey

Several papers on the mechanical analysis of beam and plate structures are available in the literature. To be more specific, laminated composite beams and plates have been the subject of numerous essential works and a selection of them is presented here. The subject related reference books are listed in each section. Then, the position of the present thesis has been clarified in the literature.

1.2.1 Laminated Composite Beams

Composite materials are widely used in various engineering fields such as construction, biomechanics, automobile, industry, nuclear, aircraft and space. These materials are based on the principle that at least two materials with different properties come and work together with appropriate integration. The main advantage of composite materials is that the strengths of the materials of the composite structure are revealed against the weaknesses. Depending on the maximum load that the composite material to be used in a structural system can bear, it is important to determine the damage characteristics such as matrix failure or bond failure of the material in the composite structure at the design stage. To make the necessary predictions regarding the integrity of the structures, it is necessary to examine the static behavior of the composite structure to be designed in detail with appropriate analysis methods. Experimental analysis yields realistic results, while they are often not an option due to limited physical conditions and exaggerated budget requirements. From this point of view, it is a more efficient and preferable solution to determine the model closest to the real physical problem and then perform analysis with appropriate theoretical studies.

The elements used to model the structural systems can be examined mainly under three main types: beam, plate and shell elements. Beams are one-dimensional structural members which have one dimension relatively larger than the other two dimensions. Plates represent planar systems whose two dimensions are relatively larger next to the third dimension. In the shell, again, the two dimensions are relatively larger next to the third dimension, but this time the selected element has a curved geometry. It is very important to accurately determine the stress components across the section for all these three thin-walled structural members. For this purpose, many beam and plate theories have been developed from past to present,

also elasticity-based solutions have been presented. In the existing literature, several theories have been developed to analyze the static, dynamic, and other mechanical behaviors exhibited by beams. The well-known theories include Classical Beam Theory (CBT), First-Order Beam Theory (FSDT), High-Order Beam Theory (HSDT), and Zig-Zag Theory (ZZ). The Bernoulli-Euler theory, commonly known as CBT, was put forward by Euler [1] and Bernoulli [2] around 280 years ago and it was the best available theory for thin beams for a long time. As an example of the implementation of CBT, Boley [3] and Modaress [4] can be given for the recent application of this theory. Timoshenko's [5] FSDT takes rotational inertia and first-order shear effects into account, for the theory requires the selection of an appropriate shear correction factor for better accuracy, particularly for thick and heterogeneous structures. This correction factor aims to reduce the errors introduced by the assumptions of the theory. Wagner and Gruttman [6] as well as Lee and Jang [7] investigated composite beams using the FSDT. Lal [8] conducted a study on the damping of bending vibrations of beams by exploring how the transverse shear deformation affects the beam's response. It is shown that the calculation of the shear correction factor depends on the geometry of the structure, how its layers are arranged and the conditions at its edges, and type of loading. As a result, using FSDT can be difficult, especially when analyzing very thick and heterogenous structures. To stress eliminate the need of the shear correction factor[9,10], some researchers, like Reddy [11], Reissner [12], and Soldatos [13], made an effort to introduce an improved approach to express a parabolic variation of the transverse shear. Thus, for the analysis of layered beams and plates, called higher-order shear theory (HSDT) have been systematically applied.

Chandrashekhara and Bangera [14] conducted a study on the free vibration characteristics of laminated composite beams. They employed the Higher-order Shear Deformation Theory (HSDT) and considered the influence of Poisson’s ratio, a factor often overlooked in one-dimensional analyses. Different versions of the HSDT with various shear functions and transverse axial deformations, have been proposed by various researchers to create better transverse shear deformations.

1.2.2 Laminated Composite Plates

The development of the plate theories in the historical aspect is mainly driven by the inclusion of transverse shear deformation in the models. From the simplest to more advanced ones, they can be mentioned as Classical Plate/Thin Plate (Kirchhoff) Theory, First Order Shear Deformation Theory (FSDT), Higher Order Shear Deformation Theory (HSDT) and Zig-zag Theory (ZZ) covering various approaches on emphasizing the shear deformation into the kinematics of the plate. According to the needs of the problems and to overcome the limitations of the assumptions made in each theory, more advanced models are proposed in time.

The Classical Plate Theory (CPT) ignores transverse shear stresses hence its application is limited to thin plates with low order heterogeneity in material distribution [15]. Classical Plate theory is firstly asserted by Kirchhoff [16]; thereby his name is referred when defining this theory. Love [17] is also one of the pioneer researchers who mentioned about CPT. Classical Lamination Theory (CLT) is the application of the CPT in laminated composite structures. Reissner and Stavsky [18] considered bending and stretching effect for the first time in the scope of CLT. Whitney and Leissa [19] used a Fourier series method to solve bending, free vibration and buckling problems of thin laminated plates. Ewing et al. [20] investigated the validity of reduced bending stiffness method on the flexural analyses of laminated composite plates based on CLT. Danielson and Tielking [21] employed the Ritz method to examine membrane type boundary conditions on the flexural behavior of unsymmetrical laminated plates based on CLT. Lin and Jen [22] investigated the flexural behavior of thin laminated composite plates by using Chebyshev collocation method.

Timoshenko [5] introduced the so called Timoshenko beam theory which sets light to the first-order shear deformation theory (FSDT) for plates. Mindlin [23] and Reissner [24] are the first researchers who proposed plate and shell theories considering transverse shear deformation effects. In literature, the generalization of the homogeneous isotropic Mindlin plate theory to the arbitrarily laminated anisotropic plates is called Yang, Norris and Stavsky (YNS) theory. Reddy derived a C^0 class finite element based on YNS theory for the stress and free vibration analyses of arbitrarily laminated composite plates. Noor and Burton [25] presented a two-phase (predictor-corrector) analysis procedure for laminated composite plates for a better

prediction of the flexural and dynamic characteristics. Voyiadjis and Pecquet [26] developed a finite element formulation incorporating bending and stretching elements for the stress analysis of composite plates based on a refined deformation theory which accounts transverse stretching. Auricchio and Sacco [27] reported mixed finite element formulations based on FSDT and Hu-Washizu variational principle which takes transverse shear stress components as primary variable of the laminated composite plate. Dorduncu et al. [28] performed peridynamic analysis of laminated composite plated based on FSDT to predict stress components. Ma and Wang [29] investigated buckling and bending problems for circular plates, which are functionally graded, with CPT, FSDT, and TSDT. Although the FSDT improved CPT by introducing an average cross-sectional rotation, its accuracy on predicting stress components is limited when the plate is thick and/or has highly heterogeneous material distribution. Moreover, it violates the zero transverse shear stress conditions at the top and bottom surfaces of the plate [30,31].

In order to introduce a better description of the transverse shear deformation for laminated composite plates several Higher Order Shear Deformation Theories (HSDT) has been developed. The main advantage of the HSDT over FSDT is that it eliminates the need for a shear correction factor. HSDTs aim to impose a transverse shear stress distribution over the cross-section such that the zero transverse shear stresses are obtained at the top and bottom surfaces of the laminate. Some HSDT approaches involve additional kinematic variables dependent to expansion of in-plane displacements in polynomial forms. Computationally efficient HSDTs developed for plate structures include six kinematic variables in case the stretching effect along the thickness is added. As an early attempt, Reddy [11] proposed a simple HSDT plate model to calculate the displacements and stresses of anisotropic laminated composite plates. The third order HSDT presented by Reddy [11] has been quite famous, although there were some earlier attempts about this subject [32]. In a general classification of HSDTs the in-plane displacement components of the laminated plate's cross-sections are expressed in terms of trigonometric [33–35], hyperbolic [36–38], and exponential functions [39–41]. The work of Shankara and Iyengar [42] is claimed to be the first attempt in developing a finite element formulation for the bending analysis of laminated composite plates based on the Reddy's third order shear deformation theory [11]. Lim [43] introduced a mixed

finite element formulation for the linear and large deflection analyses of laminated composite plates based on a HSDT. Ahmed and Basu [44] formulated p-version finite elements based on the HSDT for modelling cylindrical and general bending of laminated composite plates. Sadek [45] proposed three different elements (one of them considers thickness stretching) utilizing first-order and higher-order terms for the in-plane displacement components for the flexural analysis of laminated composite plates. Cheung and Shenglin [46] investigated the flexural properties of laminated composite plates using a hybrid stress quadrilateral four-noded finite element method that relies on a HSDT. In this approach, the initial trial of layer stresses is restricted through an energy-based approach. Ferreira et al. [47] employed Reddy's third-order theory within the framework of the radial basis function method for the analysis of laminated composite beams and plates. Aydogdu [48] introduced a new HSDT based on an inverse approach relying on 3D elasticity solutions and investigated dynamic and flexural behavior of laminated beams and plates. Nguyen et al. [49] collected HSDTs under a unified formulation by representing the shear functions in approximate and equivalent polynomials and also introduced four new polynomial based HSDTs for the analysis of composite plates also considered some parameters related strain components including the stretching effect. Ferreira et al. [50] adopted a meshless method relying on multiquadratic radial basis functions for stress analyses of laminated composite plates based on a trigonometric HSDT. Mantari et al. [51] proposed a trigonometric shear deformation theory adjusted by a parameter to give closest results to the 3D elasticity solution. Mantari and Soares [52] developed a generalized HSDT involving five kinematical variables (as in FSDT) to represent existing HSDTs and develop new ones. Nguyen-Xuan et al. [53] formulated an isogeometric finite element approach for the stress analysis of sandwich plates based on a fifth-order odd polynomial shear deformation theory. Thai et al. [54] utilized the non-uniform rational B-splines (NURBS) for the isogeometric analysis laminated composite plates based on third order shear deformation theory covering flexural, free-vibration and stability solutions. Shi et al. [55] performed the flexural, free vibration, and stability analyses of laminated composite plates by incorporating a new hyperbolic tangent shear deformation theory with isogeometric analysis. Madenci et al. [56] developed a four node mixed finite element method relying on Gâteaux differential method for the flexural analysis of laminated composite plates based on HSDT. Kant and Pandya [57] conducted static

analysis of asymmetrical laminated composite plates based on the HSDT. Although HSDTs may increase the accuracy of kinematical and stress components compared to CPT and FSDT, generally they do not provide a continuous transverse shear stress distribution at the material interfaces. To overcome this problem, elasticity theory is implemented in this study for calculation of transverse shear stress.

To eliminate the insufficiencies of prior theories, zigzag theories have evolved for the assessment of layered structures. Carrera [58] and Gherlone [59] published comprehensive literatures on zigzag theory improvement. Tessler et al. [60] suggested a refined form of zigzag theory which is also a revised form of first-order shear deformation theory applied in each layer of the laminated composite and sandwich plates. Barut et al. [61] performed static analysis of laminated composite and sandwich plates based on refined ZZ theory using a C^0 continuous triangular finite element formulation. Hasim et al. [62] investigated the static behavior of laminated plates using the isogeometric refined ZZ theory. Dorduncu [63] performed static analysis of functionally graded sandwich plates by incorporating peridynamic differential operator with refined ZZ theory. Kutlu et al. [64] developed a new mixed FEM to examine the static behavior of laminated thin and thick composite plates applying the refined ZZ theory. Sahoo and Singh [65] implemented a new trigonometric zigzag theory to elastic composite and sandwich plates and displayed its application on various boundary conditions. In their study, static and dynamic analyses were performed based on finite element methods and various types of problems were solved including free vibration and buckling. Cho and Oh [66] studied on mechanical-electrical-thermal behavior of laminated composite plates using a higher-order zigzag theory. In their article, a finite element formulation is also adopted for the bending analyses of simply supported and cantilevered plates. These theories keep the number of kinematic variables constant and improve the in-plane displacement fields by employing piece-wise continuous functions. Consequently, they are like LW in terms of maintaining an agreeable accuracy and they are also like ESL in terms of low computational cost.

There are examples of several different mixed finite element formulations in the literature. In this thesis a mixed finite element formulation is employed to investigate the flexural behavior of laminated composite beams and plates with a two-field variational principle. Ermis et al. [67] performed the free vibration analysis of

functionally graded curved beams resting on orthotropic Pasternak foundations using a mixed finite element formulation.. Orthotropic material properties are implemented depending on the correspondence principle. Pereira and Freitas [68] developed a hybrid mixed finite element model for the static analysis of Mindlin plates. Gendy et al. [69] performed free vibration and stability analyses of laminated composite plates and shells for different boundary conditions including free, simply supported, and fixed supported edges. Kutlu and Omurtag [70] conducted bending analysis of elliptic plates under large deflection. They utilized a mixed finite element formulation within the framework of the Hellinger-Reissner principle. The orthotropic elastic foundation was implemented to the analysis that represents Mindlin's assumptions in the plate formulation. The numerical solution of the nonlinear problem involved the implementation of the Newton-Raphson iteration scheme. Interpretations of the results focused on assessing the impact of parameters, such as foundation characteristics and principal directions, on the responses of elliptic plates.

1.3 Objectives and Scope

The fundamental objective of the current thesis is to introduce a new mixed finite element formulation, which includes the effect of stretching, for laminated composite beams and plates obeying a unified higher order shear deformation theory that can employ any shear function based on HSDT. To achieve this objective, static and buckling analyses of beams and plates are conducted using a mixed variational formulation.

In this thesis a unified HSDT is implemented for the mechanical model of laminated composite beams and plates because CBT and CPT neglect the transverse shear deformation, and the FSDT needs a shear correction factor. For the implemented mixed FEM formulation, the shear functions proposed by Reissner [12], Reddy [11], Touratier [71] and Nguyen-Xuan et al. [49] are implemented. The Hellinger-Reissner principle is employed to describe the energy statement of beams and plates. The adopted finite element functional is in a mixed form and assigns nodal unknowns in terms of displacements and stress resultants. In generation of the finite element equations of the transversely deformable laminated beams and plates, two-node and four-node elements are implemented associated with linear and bilinear shape

functions, respectively. Integrals of shape functions are calculated numerically over two-point and 2×2 Gaussian schemes for beams and plates, respectively. By solving the finite element equations, the stress resultants, as well as the components of deflection and rotation terms are directly calculated at the nodal points. In this way the strain components can be computed at the nodal points using compliance matrices without a need to spatial derivatives. Thus, the accuracy of the axial and in-plane shear stress components are improved when compared to the displacement-based finite element calculations with the help of thickness expansion [72]. Transverse shear stresses for laminated beams and plates are obtained along the section by placing the calculated axial stresses in the equilibrium equations presented by the theory of elasticity. Convergence analyses are performed with increasing the number of elements, and comparison analyses were carried out considering the elasticity solutions in the literature alongside various numerical solutions. Subsequently, numerous examples are demonstrated involving various layout schemes, boundary, and loading conditions to illustrate the effectiveness of the presented finite element formulation in the displacement and stress calculation of laminated composite beams and plates. Furthermore, buckling analysis of isotropic plate and composite beams are examined with different materials and boundary conditions.

2. FORMULATION OF LAMINATED BEAMS AND PLATES

2.1 Lamination Theories for Beams and Plates

Plates are two-dimensional (ignorable thickness) structural components used as load-bearing members primarily or secondary to beams, which are classified as one-dimensional (ignorable thickness and depth) structural elements.

2.1.1 Classical Lamination Theory

Classical Lamination Theory analyzes laminated composite structures by using the of Kirchhoff's classical theory. This theory, which assumes that the center of the surface is perpendicular to the cross-section both before and after deformation, is appropriate for thin beams or plates (with a thickness to length ratio less than 0.05). However, it does not account for transverse shear deformation.

2.1.2 Lamination Theory Based on First Order Shear Deformation

The consequences of transverse shear deformation are taken into account by this theory, frequently referred to as the first-order shear deformation theory for laminated structures. This hypothesis states that the center surface of the laminated structure is not parallel to the straight cross-section.

2.1.3 Lamination Theories Based on Higher Order Shear Deformation

Zero shear stresses at the top and bottom of the structure cross-section is the purpose of the Higher Order Shear Deformation Theory (HSDT) by using higher order functions (trigonometric, exponential, or polynomial). The addition of any shear correction factor is not necessary for HSDT, in contrast to other theories.

2.1.4 Other Theories

Equivalent single layer (ESL) and Layer-wise theories are the two basic categories for plate theories. Zig-zag (ZZ) theories are a part of the CPT, FSDT, and HSDT subcategories of ESL theories. Sections 2.1.1-2.1.3 covered the first three ESL

theories. The benefit of zigzag theories is that the number of kinematical variables does not rise as the number of layers increases.

Contrarily, Layer-wise theories, which gain from the kinematical formulations of ESL theories, resemble quasi 3-D theories more [73]. When using 1D interpolation functions, layer-wise theories can be described in two ways: either as a collection of separate layers or as structures defined by stress and/or displacement zones along the thickness direction.

Discrete Layer-wise Methods (DLWM) and Integrate Layer-wise Methods (ILWM) are two further subcategories of layer-wise theories depending on thickness. Interlaminar linkages influence stress equilibrium and displacement continuity in DLWM when individual layers are collected. Reddy proposed ILWM, which have been created for application in failure analysis, piezo laminates, and sandwich structures.

2.2 Hellinger-Reissner Mixed Principle

Using the Hellinger-Reissner principle yields a mixed form of functional suitable for deriving mixed finite element formulations. According to the Hellinger-Reissner principle, the first variation of the functional which stands for an mechanical problem may be written as follows:

$$\delta\Pi_{HR} = \int_V \left(\boldsymbol{\varepsilon}^{\mathbf{u}} - \boldsymbol{\varepsilon}^{\boldsymbol{\sigma}}\right)^T \delta\boldsymbol{\sigma}^{\boldsymbol{\sigma}} \mathrm{d}V + \int_V \left(\left(\boldsymbol{\sigma}^{\boldsymbol{\sigma}}\right)^T \delta\boldsymbol{\varepsilon}^{\mathbf{u}} - \mathbf{q}^T \delta\mathbf{u}\right) \mathrm{d}V - \int_\Gamma \hat{\mathbf{t}}^T \delta\mathbf{u} \mathrm{d}\Gamma = 0 \qquad (2.1)$$

Equation (2.1) can be divided into three parts: the compatibility equations are represented by the first integral, the virtual work principle involving two independent fields (displacements and stresses) is represented by the second volume integral, and the boundary terms are represented by the third part of the integral. A thorough explanation of the terminology is as follows: $\delta\Pi_{HR}$ is first variation of the functional, $\boldsymbol{\varepsilon}^{\mathbf{u}}$ is the strain vector in terms of displacement components, $\boldsymbol{\varepsilon}^{\boldsymbol{\sigma}}$ is the strain vector defined in terms of the stress components, $\boldsymbol{\sigma}^{\boldsymbol{\sigma}}$ is the stress vector, $\mathbf{q}$ denotes applied load, δ is the variation operator and $\hat{\mathbf{t}}$ is the traction vector at the boundary (Γ) of the structure.

2.3 Stiffness Terms of an Orthotropic Layer

In this section stress-strain relations are formulated to calculate the stiffness parameters of an orthotropic material. First, due to the compliance matrix's symmetry, the stress-strain relations' 36 terms are reduced to 21. The universal anisotropic material, that does not have a symmetry plane, can be represented as [74]:

$$\begin{Bmatrix} \sigma_{xx} \\ \sigma_{yy} \\ \sigma_{xy} \\ \sigma_{yz} \\ \sigma_{xz} \\ \sigma_{zz} \end{Bmatrix} = \begin{bmatrix} \overline{C_{11}} & \overline{C_{12}} & \overline{C_{16}} & \overline{C_{14}} & \overline{C_{15}} & \overline{C_{13}} \\ \overline{C_{12}} & \overline{C_{22}} & \overline{C_{26}} & \overline{C_{24}} & \overline{C_{25}} & \overline{C_{23}} \\ \overline{C_{16}} & \overline{C_{26}} & \overline{C_{66}} & \overline{C_{34}} & \overline{C_{35}} & \overline{C_{36}} \\ \overline{C_{14}} & \overline{C_{24}} & \overline{C_{34}} & \overline{C_{44}} & \overline{C_{45}} & \overline{C_{46}} \\ \overline{C_{15}} & \overline{C_{25}} & \overline{C_{35}} & \overline{C_{54}} & \overline{C_{55}} & \overline{C_{56}} \\ \overline{C_{13}} & \overline{C_{23}} & \overline{C_{36}} & \overline{C_{46}} & \overline{C_{56}} & \overline{C_{33}} \end{bmatrix} \begin{Bmatrix} \varepsilon_{xx} \\ \varepsilon_{yy} \\ \gamma_{xy} \\ \gamma_{yz} \\ \gamma_{xz} \\ \varepsilon_{zz} \end{Bmatrix} \tag{2.2}$$

If there is just one symmetry plane, the material is termed monoclinic and the stress-strain coefficients are reduced to 13, in which 1-2 plane alignment is:

$$\begin{Bmatrix} \sigma_{xx} \\ \sigma_{yy} \\ \sigma_{xy} \\ \sigma_{zz} \\ \sigma_{xz} \\ \sigma_{yz} \end{Bmatrix} = \begin{bmatrix} \overline{C_{11}} & \overline{C_{12}} & \overline{C_{16}} & \overline{C_{13}} & 0 & 0 \\ \overline{C_{12}} & \overline{C_{22}} & \overline{C_{26}} & \overline{C_{23}} & 0 & 0 \\ \overline{C_{16}} & \overline{C_{26}} & \overline{C_{66}} & \overline{C_{36}} & 0 & 0 \\ \overline{C_{13}} & \overline{C_{23}} & \overline{C_{36}} & \overline{C_{33}} & 0 & 0 \\ 0 & 0 & 0 & 0 & \overline{C_{55}} & \overline{C_{45}} \\ 0 & 0 & 0 & 0 & \overline{C_{54}} & \overline{C_{44}} \end{bmatrix} \begin{Bmatrix} \varepsilon_{xx} \\ \varepsilon_{yy} \\ \gamma_{xy} \\ \varepsilon_{zz} \\ \gamma_{xz} \\ \gamma_{yz} \end{Bmatrix} \tag{2.3}$$

With the rearrangement the equation (2.3) becomes:

$$\begin{Bmatrix} \sigma_{xx} \\ \sigma_{yy} \\ \sigma_{xy} \\ \sigma_{yz} \\ \sigma_{xz} \\ \sigma_{zz} \end{Bmatrix} = \begin{bmatrix} \overline{C_{11}} & \overline{C_{12}} & \overline{C_{16}} & 0 & 0 & \overline{C_{13}} \\ \overline{C_{12}} & \overline{C_{22}} & \overline{C_{26}} & 0 & 0 & \overline{C_{23}} \\ \overline{C_{16}} & \overline{C_{26}} & \overline{C_{66}} & 0 & 0 & \overline{C_{36}} \\ 0 & 0 & 0 & \overline{C_{44}} & \overline{C_{45}} & 0 \\ 0 & 0 & 0 & \overline{C_{54}} & \overline{C_{55}} & 0 \\ \overline{C_{13}} & \overline{C_{23}} & \overline{C_{36}} & 0 & 0 & \overline{C_{33}} \end{bmatrix} \begin{Bmatrix} \varepsilon_{xx} \\ \varepsilon_{yy} \\ \gamma_{xy} \\ \gamma_{yz} \\ \gamma_{xz} \\ \varepsilon_{zz} \end{Bmatrix} \tag{2.4}$$

The governing expression of each orthotropic layer in its local coordinate is:

$$\begin{Bmatrix}\sigma_1\\ \sigma_2\\ \sigma_3\\ \sigma_4\\ \sigma_5\\ \sigma_6\end{Bmatrix}=\begin{bmatrix}C_{11} & C_{12} & C_{13} & 0 & 0 & 0\\ C_{12} & C_{22} & C_{23} & 0 & 0 & 0\\ C_{13} & C_{23} & C_{33} & 0 & 0 & 0\\ 0 & 0 & 0 & C_{44} & 0 & 0\\ 0 & 0 & 0 & 0 & C_{55} & 0\\ 0 & 0 & 0 & 0 & 0 & C_{66}\end{bmatrix}\begin{Bmatrix}\varepsilon_1\\ \varepsilon_2\\ \varepsilon_3\\ \gamma_{23}\\ \gamma_{31}\\ \gamma_{12}\end{Bmatrix} \tag{2.5}$$

For an anisotropic material, the inverse relation between strain and stress is specified over compliance parameters, which are 21 constants associated with the material.

$$\begin{Bmatrix}\varepsilon_{xx}\\ \varepsilon_{yy}\\ \gamma_{xy}\\ \gamma_{yz}\\ \gamma_{xz}\\ \varepsilon_{zz}\end{Bmatrix}=\begin{bmatrix}\overline{S_{11}} & \overline{S_{12}} & \overline{S_{16}} & \overline{S_{14}} & \overline{S_{15}} & \overline{S_{13}}\\ \overline{S_{12}} & \overline{S_{22}} & \overline{S_{26}} & \overline{S_{24}} & \overline{S_{25}} & \overline{S_{23}}\\ \overline{S_{16}} & \overline{S_{26}} & \overline{S_{66}} & \overline{S_{34}} & \overline{S_{35}} & \overline{S_{36}}\\ \overline{S_{14}} & \overline{S_{24}} & \overline{S_{34}} & \overline{S_{44}} & \overline{S_{45}} & \overline{S_{46}}\\ \overline{S_{15}} & \overline{S_{25}} & \overline{S_{35}} & \overline{S_{54}} & \overline{S_{55}} & \overline{S_{56}}\\ \overline{S_{13}} & \overline{S_{23}} & \overline{S_{36}} & \overline{S_{46}} & \overline{S_{56}} & \overline{S_{33}}\end{bmatrix}\begin{Bmatrix}\sigma_{xx}\\ \sigma_{yy}\\ \sigma_{xy}\\ \sigma_{yz}\\ \sigma_{xz}\\ \sigma_{zz}\end{Bmatrix} \tag{2.6}$$

The constitutive equations for a monoclinic substance with 13 independent constants (1-2 plane symmetry) are given as:

$$\begin{Bmatrix}\varepsilon_{xx}\\ \varepsilon_{yy}\\ \gamma_{xy}\\ \gamma_{yz}\\ \gamma_{xz}\\ \varepsilon_{zz}\end{Bmatrix}=\begin{bmatrix}\overline{S_{11}} & \overline{S_{12}} & \overline{S_{16}} & 0 & 0 & \overline{S_{13}}\\ \overline{S_{12}} & \overline{S_{22}} & \overline{S_{26}} & 0 & 0 & \overline{S_{23}}\\ \overline{S_{16}} & \overline{S_{26}} & \overline{S_{66}} & 0 & 0 & \overline{S_{36}}\\ 0 & 0 & 0 & \overline{S_{44}} & \overline{S_{45}} & 0\\ 0 & 0 & 0 & \overline{S_{54}} & \overline{S_{55}} & 0\\ \overline{S_{13}} & \overline{S_{23}} & \overline{S_{36}} & 0 & 0 & \overline{S_{33}}\end{bmatrix}\begin{Bmatrix}\sigma_{xx}\\ \sigma_{yy}\\ \sigma_{xy}\\ \sigma_{yz}\\ \sigma_{xz}\\ \sigma_{zz}\end{Bmatrix} \tag{2.7}$$

In terms of engineering constants, the compliance matrix components of an orthotropic material are as follows:

$$\left[S_{ij}\right]=\begin{bmatrix} \frac{1}{E_1} & -\frac{v_{21}}{E_2} & -\frac{v_{31}}{E_3} & 0 & 0 & 0 \\ -\frac{v_{12}}{E_1} & \frac{1}{E_2} & -\frac{v_{32}}{E_3} & 0 & 0 & 0 \\ 0 & 0 & \frac{1}{G_{12}} & 0 & 0 & 0 \\ 0 & 0 & 0 & \frac{1}{G_{23}} & 0 & 0 \\ 0 & 0 & 0 & 0 & \frac{1}{G_{31}} & 0 \\ -\frac{v_{13}}{E_1} & -\frac{v_{23}}{E_2} & \frac{1}{E_3} & 0 & 0 & 0 \end{bmatrix} \tag{2.8}$$

In Equation (2.8), Young's moduli in specified material orientations are represented by E_1, E_2, and E_3 in the equation. Poisson's ratio is represented by v_{ij} and shear moduli in the 2-3, 3-1, and 1-2 planes are represented by G_{23}, G_{31}, and G_{12}, respectively.

The inverse relations between stiffness and compliance matrices can be given as follows:

$$\begin{aligned} &C_{11}=\frac{S_{22}S_{33}-S_{23}^2}{S} \;,\; C_{12}=\frac{S_{13}S_{23}-S_{12}S_{33}}{S} \;,\; C_{13}=\frac{S_{12}S_{23}-S_{13}S_{22}}{S} \\ &C_{22}=\frac{S_{33}S_{11}-S^2{}_{13}}{S} \;,\; C_{23}=\frac{S_{12}S_{13}-S_{23}S_{11}}{S} \;,\; C_{33}=\frac{S_{11}S_{22}-S^2{}_{12}}{S} \\ &C_{44}=\frac{1}{S_{44}} \;,\; C_{55}=\frac{1}{S_{55}} \;,\; C_{66}=\frac{1}{S_{66}} \end{aligned} \tag{2.9}$$

where

$$S=S_{11}S_{22}S_{33}-S_{11}S_{23}^2-S_{22}S_{13}^2-S_{33}S_{12}^2+2S_{12}S_{23}S_{13} \tag{2.10}$$

Finally, stiffness terms can be expressed in terms of the engineering constants as [49]:

$$C_{11}=\frac{E_1(1-\nu_{23}\nu_{32})}{\Delta} \quad , \quad C_{12}=\frac{E_1(\nu_{21}+\nu_{31}\nu_{23})}{\Delta}$$
$$C_{13}=\frac{E_1(\nu_{31}+\nu_{21}\nu_{32})}{\Delta}=\frac{\nu_{13}+\nu_{12}\nu_{23}}{E_1E_2\Delta}$$
$$C_{22}=\frac{E_2(1-\nu_{13}\nu_{31})}{\Delta} \quad , \quad C_{23}=\frac{E_2(\nu_{32}+\nu_{12}\nu_{31})}{\Delta}=\frac{\nu_{23}+\nu_{21}\nu_{13}}{E_1E_3\Delta} \qquad (2.11)$$
$$C_{33}=\frac{E_3(1-\nu_{12}\nu_{21})}{\Delta} \quad , \quad C_{44}=G_{23} \quad , \quad C_{55}=G_{31} \quad , \quad C_{66}=G_{12}$$
$$\Delta=1-\nu_{12}\nu_{21}-\nu_{23}\nu_{32}-\nu_{31}\nu_{13}-2\nu_{21}\nu_{32}\nu_{13}$$

2.4 Arbitrarily Oriented Orthotropic Material

The principal material orientations of orthotropic elements sometimes correspond to their global coordinates. Hence, it is necessary to carry out the conversion of stress-strain relationships between these coordinate systems.

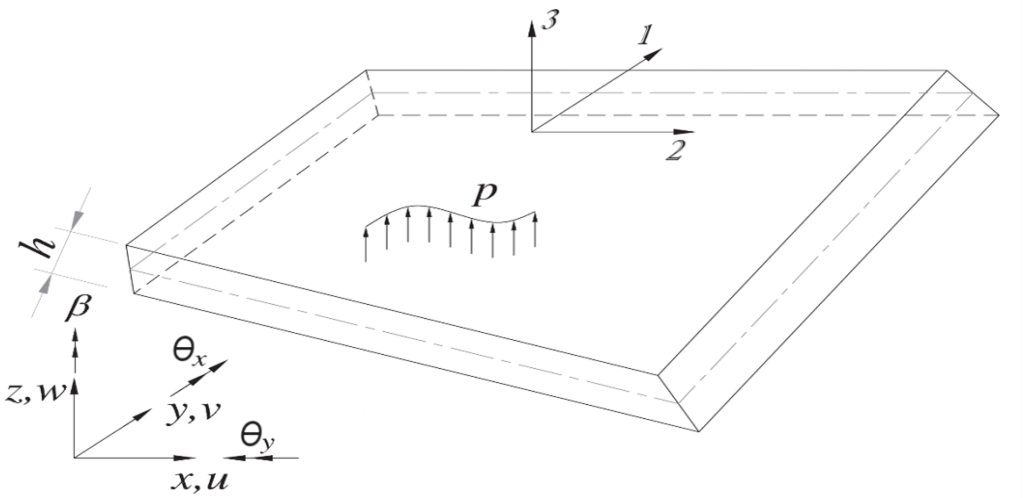

Figure 2.1 : A composite layer consisting global directions with thickness h

In the Figure 2.1, the relation between the stress components in material coordinates 1, 2 and 3 and stress components in global directions *x*, *y* and *z* is given by [9]:

$$\begin{Bmatrix}\sigma_{xx}\\ \sigma_{yy}\\ \tau_{xy}\\ \tau_{yz}\\ \tau_{xz}\\ \sigma_{zz}\end{Bmatrix}=\begin{bmatrix}\cos^2\theta & \sin^2\theta & -\sin 2\theta & 0 & 0 & 0\\ \sin^2\theta & \cos^2\theta & \sin 2\theta & 0 & 0 & 0\\ \sin\theta\cos\theta & -\sin\theta\cos\theta & \cos^2\theta-\sin^2\theta & 0 & 0 & 0\\ 0 & 0 & 0 & \cos\theta & \sin\theta & 0\\ 0 & 0 & 0 & -\sin\theta & \cos\theta & 0\\ 0 & 0 & 0 & 0 & 0 & 1\end{bmatrix}\begin{Bmatrix}\sigma_1\\ \sigma_2\\ \sigma_3\\ \sigma_4\\ \sigma_5\\ \sigma_6\end{Bmatrix} \quad (2.12)$$

The angle θ indicates the measurement from the x-axis of the global coordinates to the 1-axis of the material coordinates. Likewise, the strain transformation is also provided as:

$$\begin{Bmatrix}\varepsilon_{xx}\\ \varepsilon_{yy}\\ \varepsilon_{xy}\\ \varepsilon_{yz}\\ \varepsilon_{xz}\\ \varepsilon_{zz}\end{Bmatrix}=\begin{bmatrix}\cos^2\theta & \sin^2\theta & -\sin 2\theta & 0 & 0 & 0\\ \sin^2\theta & \cos^2\theta & \sin 2\theta & 0 & 0 & 0\\ \sin\theta\cos\theta & -\sin\theta\cos\theta & \cos^2\theta-\sin^2\theta & 0 & 0 & 0\\ 0 & 0 & 0 & \cos\theta & \sin\theta & 0\\ 0 & 0 & 0 & -\sin\theta & \cos\theta & 0\\ 0 & 0 & 0 & 0 & 0 & 1\end{bmatrix}\begin{Bmatrix}\begin{Bmatrix}\varepsilon_1\\ \varepsilon_2\\ \varepsilon_3\end{Bmatrix}\\ \begin{Bmatrix}\varepsilon_4\\ \varepsilon_5\\ \varepsilon_6\end{Bmatrix}\end{Bmatrix} \quad (2.13)$$

Transformations can be defined for stress and strain briefly:

$$\begin{aligned}\sigma_p &= T\ \sigma_m\\ \varepsilon_p &= T\ \varepsilon_m\end{aligned} \quad \text{or} \quad \begin{bmatrix}\sigma_x\\ \sigma_y\\ \tau_{xy}\\ \tau_{yz}\\ \tau_{xz}\\ \sigma_{zz}\end{bmatrix}=T^{-1}\begin{bmatrix}\sigma_1\\ \sigma_2\\ \sigma_3\\ \sigma_4\\ \sigma_5\\ \sigma_6\end{bmatrix},\ \begin{bmatrix}\varepsilon_{xx}\\ \varepsilon_{yy}\\ \frac{\gamma_{xy}}{2}\\ \frac{\gamma_{yz}}{2}\\ \frac{\gamma_{xz}}{2}\\ \varepsilon_{zz}\end{bmatrix}=T^{-1}\begin{bmatrix}\varepsilon_1\\ \varepsilon_2\\ \frac{\gamma_{12}}{2}\\ \frac{\gamma_{23}}{2}\\ \frac{\gamma_{13}}{2}\\ \varepsilon_{33}\end{bmatrix} \quad (2.14)$$

where $[T]$ is [9]:

$$T=\begin{bmatrix}\cos^2\theta & \sin^2\theta & -\sin 2\theta & 0 & 0 & 0\\ \sin^2\theta & \cos^2\theta & \sin 2\theta & 0 & 0 & 0\\ \sin\theta\cos\theta & -\sin\theta\cos\theta & \cos^2\theta-\sin^2\theta & 0 & 0 & 0\\ 0 & 0 & 0 & \cos\theta & \sin\theta & 0\\ 0 & 0 & 0 & -\sin\theta & \cos\theta & 0\\ 0 & 0 & 0 & 0 & 0 & 1\end{bmatrix}_{6x6} \quad (2.15)$$

The term special orthotropic lamina refers to materials with same orientations in both global coordinates and material geometry.

$$\begin{Bmatrix} \sigma_1 \\ \sigma_2 \\ \tau_{12} \\ \tau_{23} \\ \tau_{13} \\ \sigma_3 \end{Bmatrix} = \begin{bmatrix} Q_{11} & Q_{12} & Q_{16} & 0 & 0 & Q_{13} \\ Q_{21} & Q_{22} & Q_{26} & 0 & 0 & Q_{23} \\ Q_{61} & Q_{62} & Q_{66} & 0 & 0 & Q_{36} \\ 0 & 0 & 0 & Q_{44} & Q_{45} & 0 \\ 0 & 0 & 0 & Q_{54} & Q_{55} & 0 \\ Q_{31} & Q_{32} & Q_{63} & 0 & 0 & Q_{33} \end{bmatrix} \begin{Bmatrix} \varepsilon_1 \\ \varepsilon_2 \\ \gamma_{12} \\ \gamma_{23} \\ \gamma_{13} \\ \varepsilon_3 \end{Bmatrix} \tag{2.16}$$

The condensed form of the relations in equation (2.16) is:

$$\begin{Bmatrix} \sigma_1 \\ \sigma_2 \\ \gamma_{12} \\ \gamma_{23} \\ \gamma_{13} \\ \sigma_3 \end{Bmatrix} = Q \begin{Bmatrix} \varepsilon_1 \\ \varepsilon_2 \\ \gamma_{12} \\ \gamma_{23} \\ \gamma_{13} \\ \varepsilon_3 \end{Bmatrix} \tag{2.17}$$

Finally, stress-strain relations in $x-y$ global directions are:

$$\begin{Bmatrix} \sigma_{xx} \\ \sigma_{yy} \\ \sigma_{xy} \\ \sigma_{yz} \\ \sigma_{xz} \\ \sigma_{zz} \end{Bmatrix} = \begin{bmatrix} \overline{Q}_{11} & \overline{Q}_{12} & \overline{Q}_{16} & 0 & 0 & \overline{Q}_{13} \\ \overline{Q}_{12} & \overline{Q}_{22} & \overline{Q}_{26} & 0 & 0 & \overline{Q}_{23} \\ \overline{Q}_{16} & \overline{Q}_{26} & \overline{Q}_{66} & 0 & 0 & \overline{Q}_{36} \\ 0 & 0 & 0 & \overline{Q}_{44} & \overline{Q}_{45} & 0 \\ 0 & 0 & 0 & \overline{Q}_{45} & \overline{Q}_{55} & 0 \\ \overline{Q}_{13} & \overline{Q}_{23} & \overline{Q}_{36} & 0 & 0 & \overline{Q}_{33} \end{bmatrix} \begin{Bmatrix} \varepsilon_{xx} \\ \varepsilon_{yy} \\ \gamma_{xy} \\ \gamma_{yz} \\ \gamma_{xz} \\ \varepsilon_{zz} \end{Bmatrix} \tag{2.18}$$

where

$$\left[\overline{Q}\right] = T^{-1} Q \; T^{-T} \tag{2.19}$$

The relation between $\overline{Q_{ij}}$ and Q_{ij} can be written as;

$$\begin{Bmatrix} \overline{Q}_{11} \\ \overline{Q}_{12} \\ \overline{Q}_{22} \\ \overline{Q}_{16} \\ \overline{Q}_{26} \\ \overline{Q}_{66} \end{Bmatrix} = \begin{pmatrix} c^4 & 2c^2s^2 & s^4 & 4c^2s^2 \\ c^2s^2 & c^4+s^4 & c^2s^2 & -4c^2s^2 \\ s^4 & 2c^2s^2 & c^4 & 4c^2s^2 \\ -c^3s & cs(c^2-s^2) & cs^3 & 2cs(c^2-s^2) \\ -cs^3 & cs(c^2-s^2) & c^3s & 2cs(c^2-s^2) \\ c^2s^2 & -2c^2s^2 & c^2s^2 & (c^2-s^2)^2 \end{pmatrix} \begin{pmatrix} Q_{11} \\ Q_{12} \\ Q_{22} \\ Q_{66} \end{pmatrix} \tag{2.20}$$

Here, c represents the $\cos\theta$, where s denotes for $\sin\theta$. The open form of the formulation in equation (2.20) is:

$$\begin{aligned} \overline{Q_{11}} &= Q_{11}\cos^4\theta + 2(Q_{12}+2Q_{66})\sin^2\theta\cos^2\theta + Q_{22}\sin^4\theta \\ \overline{Q_{12}} &= (Q_{11}+Q_{22}-4Q_{66})\sin^2\theta\cos^2\theta + Q_{12}(\sin^4\theta+\cos^4\theta) \\ \overline{Q_{22}} &= Q_{11}\sin^4\theta + 2(Q_{12}+2Q_{66})\sin^2\theta\cos^2\theta + Q_{22}\cos^4\theta \\ \overline{Q_{16}} &= (Q_{11}-Q_{22}-2Q_{66})\sin\theta\cos^3\theta + (Q_{12}-Q_{22}+2Q_{66})\sin^3\theta\cos\theta \\ \overline{Q_{26}} &= (Q_{11}-Q_{12}-2Q_{66})\sin^3\theta\cos\theta + (Q_{12}-Q_{22}+2Q_{66})\sin\theta\cos^3\theta \\ \overline{Q_{66}} &= (Q_{11}+Q_{12}-2Q_{12}-2Q_{66})\sin^2\theta\cos^2\theta + Q_{66}(\sin^4\theta+\cos^4\theta) \end{aligned} \tag{2.21}$$

The transformed reduced stiffness terms related to transverse shear components and stretching effect (transverse axial deformation components) can be formulated as [49]:

$$\left\{ \begin{bmatrix} \overline{Q}_{44} \\ \overline{Q}_{45} \end{bmatrix}; \begin{bmatrix} \overline{Q}_{13} \\ \overline{Q}_{36} \end{bmatrix} \right\} = \begin{bmatrix} c^2 & s^2 \\ cs & -cs \\ s^2 & c^2 \end{bmatrix} \left\{ \begin{bmatrix} Q_{44} \\ Q_{45} \end{bmatrix}; \begin{bmatrix} Q_{13} \\ Q_{36} \end{bmatrix} \right\}, \ \overline{Q}_{13} = Q_{13} \tag{2.22}$$

Open form of (2.22) is:

$$\begin{aligned} \overline{Q}_{13} &= Q_{13}\cos^2\theta - 2Q_{36}\cos\theta\sin\theta + Q_{23}\sin^2\theta \\ \overline{Q}_{23} &= Q_{23}\cos^2\theta + 2Q_{36}\cos\theta\sin\theta + Q_{13}\sin^2\theta \\ \overline{Q}_{33} &= Q_{33} \\ \overline{Q}_{44} &= Q_{44}\cos^2\theta + Q_{55}\sin^2\theta \\ \overline{Q}_{55} &= Q_{55}\cos^2\theta + Q_{44}\sin^2\theta \end{aligned} \tag{2.23}$$

For an orthotropic material, the interaction around transverse shear stresses and transverse shear strains can be summed up in the following manner :

$$\begin{bmatrix}\sigma_4\\ \sigma_5\end{bmatrix}=\begin{bmatrix}Q_{44} & Q_{45}\\ Q_{54} & Q_{55}\end{bmatrix}\begin{bmatrix}\gamma_{23}\\ \gamma_{13}\end{bmatrix} \quad , \quad Q_{44}=G_{23} \quad , \quad Q_{55}=G_{13} \tag{2.24}$$

Shear stresses and strains can be transformed from material dimensions to cartesian coordinates as illustrated below:

$$\begin{bmatrix}\tau_{yz}\\ \tau_{xz}\end{bmatrix}=\begin{bmatrix}\cos\theta & \sin\theta\\ -\sin\theta & \cos\theta\end{bmatrix}\begin{bmatrix}\sigma_4\\ \sigma_5\end{bmatrix} \quad , \quad \begin{bmatrix}\gamma_{yz}\\ \gamma_{xz}\end{bmatrix}=\begin{bmatrix}\cos\theta & \sin\theta\\ -\sin\theta & \cos\theta\end{bmatrix}\begin{bmatrix}\gamma_{23}\\ \gamma_{13}\end{bmatrix} \tag{2.25}$$

2.5 Higher Order Shear Deformation Function

Variety of shear functions, namely "$f(z)$" exist in the literature for Higher Order Beam/Plate theories, adjusting how stress and strain are distributed throughout the thickness of the beam or plate. The shear functions used in Higher Order Beam/Plate theories can be categorized as polynomial, exponential, or trigonometric. Over time, several researchers have developed such functions for beams and plates. Reissner [12], Reddy [11], Touratier [71], Soldatos [13], Nguyen-Xuan et al. [49], Karama et al. [40], Mantari et al. [51], Thai et al. [54] and Singh and Singh [65] are some of the researchers who have chronologically contributed to this field.

Table 2.1 presents shear functions utilized in the analysis of laminated composite beams and plates within the scope of this thesis as;

Table 2.1 : Shear functions used in this study

Researcher	$f(z)$	Analysis
Reissner	$\frac{5z}{4}(1-\frac{4z^2}{3h^2})$	Plate
Reddy	$z(1-\frac{4z^2}{3h^2})$	Plate+Beam
Touratier	$\frac{h}{\pi}\sin(\frac{\pi}{h}z)$	Plate
Nguyen-Xuan et al.	$\frac{7}{8}z-\frac{2}{h^2}z^3+\frac{2}{h^4}z^5$	Plate

In the table 2.1, $f(z)$ denotes for shear function, h represents thickness while z represents any coordinate along the thickness (see Figure 2.2).

2.6 Mixed FEM for Laminated Composite Beam

In this section, a detailed explanation of the Mixed Finite Element Method for statically loaded laminated beams (loaded along the beam axis) is provided. The formulation of the current study is incorporated with the Hellinger Reissner variational principle and the Higher Order Beam Theory.

2.6.1 Kinematic Relations

The geometric center of the cross-section of a laminated composite beam, when loaded in the xz plane, is defined by the x-axis, and the cross-section accommodates the yz-axes (refer to Figure 2.2 for visualization).

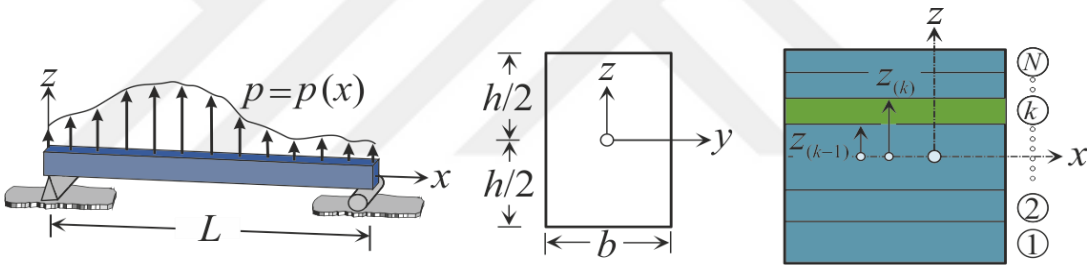

Figure 2.2. : Laminated composite beam a) Beam axes b) Cross section dimensions of beam c) Beam lamination

The axial displacement and deflection field of the beam under the effect of distributed load acting along the central axis in the z direction can be described, respectively, according to the Higher Order Beam Theory, as follows [49]:

$$\left.\begin{aligned} u^*(x,z) &= u(x) - z\,w_{,x}(x) + f(z)\theta_x(x) \\ w^*(x,z) &= w(x) + g(z)\beta \end{aligned}\right\} \qquad (2.26)$$

where $u^*(x,z)$, $w^*(x,z)$ are displacements in laminate section and $u(x,z)$ $w(x,z)$ are axial displacement and deflection of mid surface, respectively. $\theta_x(x,z)$

is the rotation of cross sections about y axes and an additional parameter β is introduced as a transverse deformation component to account normal strain in the thickness direction. Here, the function $g(z) = f_{,z}$ expresses the distribution of stretching through the thickness.

The formulation introduces the kinematic variables $\mathbf{u} = \{u \quad w \quad \theta_x \quad \beta\}^T$ and the strain components involve second order differentiations. The strain field associated with this displacement field requires C^1 continuity in the classical displacement type finite element formulations. Some studies [79,80] include additional rotations to replace those second order derivative by first order derivatives obtain C^0 type continuity requirement. In this study, without introducing any additional rotation, C^0 continuity requirement is provided thanks to the two independent field approach of the mixed finite element formulation.

2.6.2 Strain Components of Higher Order Beam Theories

Strain components along the beam section can be written over the displacement field described in equation (2.26) :

$$\left.\begin{aligned} \varepsilon_{xx} &= u^*_{,x} = u_{,x} - z\, w_{,xx} + f(z)\theta_{x,x} \\ \gamma_{xz} &= u^*_{,z} + w^*_{,x} = g(z)\theta_x(x) + g(z)\beta_{,x} \\ \varepsilon_z &= w_{,z} = g_{,z}(z)\beta \end{aligned}\right\} \tag{2.27}$$

The presence of the comma in the subscript reflects that the derivatives are computed with respect to the axis terms specified after the comma.

2.6.2.1 Strain Measures in Matrix Form

Strain measures in equation (2.27) can be given as follows:

$$\varepsilon_0 = u_{,x} \;,\; \varepsilon_1 = -w_{,xx} \;,\; \varepsilon_2 = \theta_{x,x} \;,\; \varepsilon_3 = \beta_{,x} + \theta_x \;,\; \varepsilon_4 = \beta \tag{2.28}$$

Then, the strain components at a global coordinate system on the beam's cross-section can be described as a combination of strain components and beam curvatures as :

$$\begin{Bmatrix}\varepsilon_{xx}\\ \gamma_{xz}\\ \varepsilon_{xx}\end{Bmatrix}=\begin{Bmatrix}\varepsilon_0\\ 0\\ 0\end{Bmatrix}+z\begin{Bmatrix}\varepsilon_1\\ 0\\ 0\end{Bmatrix}+f(x)\begin{Bmatrix}\varepsilon_2\\ 0\\ 0\end{Bmatrix}+g(z)\begin{Bmatrix}0\\ \varepsilon_3\\ 0\end{Bmatrix}+g_{,z}(z)\begin{Bmatrix}0\\ 0\\ \varepsilon_4\end{Bmatrix} \tag{2.29}$$

2.6.3 Constitutive Relations

The stress-strain relations in the k^{th} layer of the laminated composite beam (Figure 2.2c) can be written as follows by using Hooke law:

$$\begin{Bmatrix}\sigma_{xx}\\ \sigma_{xz}\\ \sigma_{zz}\end{Bmatrix}^{(k)}=\begin{bmatrix}\overline{Q}_{11} & 0 & \overline{Q}_{13}\\ 0 & \overline{Q}_{55} & 0\\ \overline{Q}_{31} & 0 & \overline{Q}_{33}\end{bmatrix}^{(k)}\begin{Bmatrix}\varepsilon_{xx}\\ \gamma_{xz}\\ \varepsilon_{zz}\end{Bmatrix}^{(k)} \tag{2.30}$$

In the equation (2.30), $\overline{Q}_{11}$, $\overline{Q}_{13}$, $\overline{Q}_{31}$, $\overline{Q}_{33}$ and $\overline{Q}_{55}$ correspond transformed material stiffness terms, which are calculated in equation (2.21) while $\sigma_{xx}^{(k)}$, $\sigma_{xz}^{(k)}$, and $\sigma_{zz}^{(k)}$ are the axial normal stress, transverse shear stress, transverse normal stress components respectively in the k^{th} layer of the laminated beam.

2.6.4 Equilibrium Equations

The stress resultants of the laminated beam are obtained by integrating the stress and moments of stress components along the beam thickness. N_{xx} denotes the axial force, M_{xx} represents the bending moment, while M_{xx}^{f} indicates the higher-order bending moment Q_{xz} signifies the shear force, and M_{zz}^{f} corresponds to the transverse normal stress component and are calculated as:

$$\begin{aligned}&\left(N_{xx}\quad M_{xx}\quad M_{xx}^{f}\quad Q_{xz}\quad M_{zz}^{f}\right)\\ &\quad=b\sum_{k=1}^{N}\int_{z_{(k-1)}}^{z_{(k)}}\left(\sigma_{xx}^{(k)}\quad z\sigma_{xx}^{(k)}\quad f(z)\sigma_{xx}^{(k)}\quad g(z)\sigma_{xz}^{(k)}\quad \left(g_{,z}(z)\right)^2\sigma_{zz}^{(k)}\right)\mathrm{d}z\end{aligned} \tag{2.31}$$

In equation (2.31), b represents the beam width (as shown in Figure 2.2b), and N is the total number of layers. When the constitutive relations from equation (2.31) is substituted into equation (2.30), the relationship between stress components and strain measures. $\mathbf{e^u}=[\varepsilon_0\quad \varepsilon_1\quad \varepsilon_2\quad \varepsilon_3\quad \varepsilon_4]^T$ is obtained as:

$$\mathbf{P} = \mathbf{E}\mathbf{e}^{\mathbf{u}} \quad \text{or} \quad \begin{Bmatrix} N_{xx} \\ M_{xx} \\ M_{xx}^{f} \\ Q_{xz} \\ M_{zz}^{f} \end{Bmatrix} = \begin{bmatrix} A_{11} & B_{11} & E_{11} & 0 & J_{13} \\ B_{11} & D_{11} & F_{11} & 0 & L_{13} \\ E_{11} & F_{11} & H_{11} & 0 & O_{13} \\ 0 & 0 & 0 & A^{s} & 0 \\ J_{13} & L_{13} & O_{13} & 0 & P_{33} \end{bmatrix} \begin{Bmatrix} \varepsilon_0 \\ \varepsilon_1 \\ \varepsilon_2 \\ \varepsilon_3 \\ \varepsilon_4 \end{Bmatrix} \tag{2.32}$$

In the equation (2.32), $\mathbf{E}$ is the sectional-stiffness matrix and its terms can be calculated as follows:

$$\left(A_{ij} \quad B_{ij} \quad D_{ij} \quad E_{ij} \quad F_{ij} \quad H_{ij} \right) = b \sum_{k=1}^{N} \int_{z_{(k-1)}}^{z_{(k)}} \bar{Q}_{ij}^{(k)} \left(1 \;\; z \;\; z^2 \;\; f(z) \;\; zf(z) \;\; f(z)^2 \right) \mathrm{d}z \tag{2.33}$$

$$\left(L_{13} \quad O_{13} \right) = b \sum_{k=1}^{N} \int_{z_{(k-1)}}^{z_{(k)}} \bar{Q}_{13}^{(k)} \left(zg'(z) \quad f(z)g(z) \right) \mathrm{d}z \tag{2.34}$$

$$A^{s} = \begin{pmatrix} A^{s1} & A^{s12} \\ A^{s12} & A^{s2} \end{pmatrix}$$
$$A^{s} = b \sum_{k=1}^{N} \int_{z_{(k-1)}}^{z_{(k)}} \bar{Q}_{55}^{(k)} \left(f'(z)^2 \quad f'(z)g(z) \;\; g(z)^2 \right) \mathrm{d}z \tag{2.35}$$

$$P_{33} = b \sum_{k=1}^{N} \int_{z_{(k-1)}}^{z_{(k)}} \bar{Q}_{33}^{(k)} \left(g'(z) \right)^2 \mathrm{d}z \tag{2.36}$$

The compliance matrix $\mathbf{S} = \mathbf{E}^{-1}$ can be defined using equation (2.32) as follows:

$$\mathbf{e}^{\mathbf{P}} = \mathbf{S}\mathbf{P} \quad \text{or} \quad \begin{Bmatrix} \varepsilon_0 \\ \varepsilon_1 \\ \varepsilon_2 \\ \varepsilon_3 \\ \varepsilon_4 \end{Bmatrix} = \begin{bmatrix} A'_{11} & B'_{11} & E'_{11} & 0 & J'_{13} \\ B'_{11} & D'_{11} & F'_{11} & 0 & L'_{13} \\ E'_{11} & F'_{11} & H'_{11} & 0 & O'_{13} \\ 0 & 0 & 0 & A^{s} & 0 \\ J'_{13} & L'_{13} & O'_{13} & 0 & P'_{33} \end{bmatrix} \begin{Bmatrix} N_{xx} \\ M_{xx} \\ M_{xx}^{f} \\ Q_{xz} \\ M_{zz}^{f} \end{Bmatrix} \tag{2.37}$$

In equation (2.37), $\mathbf{e}^{\mathbf{P}}$ represents strain measures in terms of stress resultants. The equilibrium equations are provided below in beam theory, considering the higher-order shear effects:

$$\left.\begin{aligned} N_{xx,x} &= 0 \\ p + M_{xx,xx} &= 0 \\ M^{f}_{xx,x} - Q_{xz} &= 0 \\ M^{f}_{zz} + Q_{xz,x} &= 0 \end{aligned}\right\} \tag{2.38}$$

2.6.5 Functional and Finite Element Equations

The Hellinger-Reissner functional for a three-dimensional description of mechanical systems is described in equation (2.1). Instead of stress and strain components, strain measures and stress resultants are used when it is reduced to beam form.

$$\delta\Pi_{HR} = \int_{L} \left(\mathbf{e}^{\mathbf{u}} - \mathbf{e}^{\mathbf{P}}\right)^{T} \delta\mathbf{P}\,\mathrm{d}L + \int_{L} \left(\mathbf{P}^{T}\delta\mathbf{e}^{\mathbf{u}} - \mathbf{p}^{T}\delta\mathbf{u}\right)\mathrm{d}L - \int_{\Gamma} \hat{\mathbf{t}}^{T}\delta\mathbf{u}\,\mathrm{d}\Gamma = 0 \tag{2.39}$$

While $\mathbf{e}^{\mathbf{P}}$ accumulates strain measurements in terms of stress resultants in equation (2.39), $\mathbf{e}^{\mathbf{u}} = [\varepsilon_0 \quad \varepsilon_1 \quad \varepsilon_2 \quad \varepsilon_3 \quad \varepsilon_4]^{T}$ represents the strain variables vector stated using kinematic relations, $\mathbf{p}$ stands for the applied load operating transversely along the beam and $\mathbf{P}$ reflects the stress resultants vector.

The first variant of the laminated composite beam functional can be represented in an open form by combining equations (2.27), (2.38) and (2.39).

$$\begin{aligned} \delta\Pi_{HR} = {} & \int_{L}\left[u_{,x}\delta N_{xx,x} - \left(\overline{A}_{11}N_{xx} + \overline{B}_{11}M_{xx} + \overline{E}_{11}M^{f}_{xx} + \overline{J}_{13}M^{f}_{zz}\right)\delta N_{xx}\right]\mathrm{d}L \\ & + \int_{L}\left[w_{,x}\delta M_{xx,x} - \left(\overline{B}_{11}N_{xx} + \overline{D}_{11}M_{xx} + \overline{F}_{11}M^{f}_{xx} + \overline{L}_{13}M^{f}_{zz}\right)\delta M_{xx}\right]\mathrm{d}L \\ & + \int_{L}\left[\theta_{x,x} - \left(\overline{E}_{11}N_{xx} + \overline{F}_{11}M_{xx} + \overline{H}_{11}M^{f}_{xx} + \overline{O}_{13}M^{f}_{zz}\right)\delta M^{f}_{xx}\right]\mathrm{d}L \\ & + \int_{L}\left[(\theta_{x} + \beta_{,x}) - \left(\overline{A}^{s}_{55}Q_{xz}\right)\right]\delta Q_{xz}\,\mathrm{d}L \\ & + \int_{L}\left[\beta - (\overline{J}_{13}N_{xx} + \overline{L}_{13}M_{xx} + \overline{O}_{13}M^{f}_{xx} + \overline{P}_{33}M^{f}_{zz})\delta M^{f}_{zz}\right]\mathrm{d}L - \int_{L}\delta w p\,\mathrm{d}L \\ & + \int_{L}\left(N_{xx}\,\delta u_{,x} + M_{xx,x}\,\delta w_{,x} + M^{f}_{xx}\delta\theta_{x,x} + Q_{xz}\delta\theta_{x} + M^{f}_{zz}\delta\beta\right)\mathrm{d}L - \int_{\Gamma}\hat{\mathbf{t}}^{T}\delta\mathbf{u}\,\mathrm{d}\Gamma = 0 \end{aligned} \tag{2.40}$$

The terms L and Γ in equation (2.40) stand for the beam length and beam boundary respectively. Both field variables of the displacement and force-moment type are included in this equation. One of the benefits of the mixed finite element formulation is that the first variation of the functional described in equation (2.40)

substitutes first-order derivatives with the second-order derivatives by partial integration. Hence, the shape functions used in the finite element discretization are providing simply a C^0 continuity.

2.6.6 Finite Element Discretization

The discretization of the laminated beam domain is made by adopting two-noded elements having linear interpolation functions as shown in Figure 2.3. The shape functions are formulated as follows for each local ξ coordinate defined within the domain $-1 \le \xi \le 1$:

$$\varphi_i(\xi) = \tfrac{1}{2}\left(1 + \xi\xi_i\right), \quad i = 1,2 \tag{2.41}$$

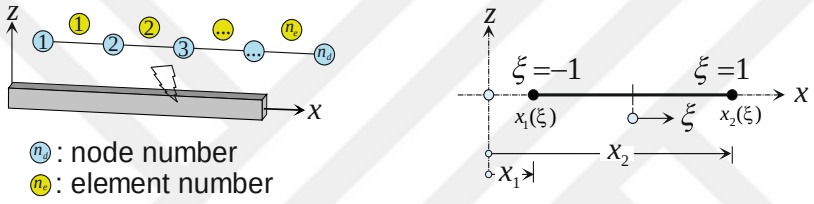

(a) **(b)**

Figure 2.3 : Finite element description a) Linear two-noded element discretization in beam field b) Global and local coordinate systems in a general element

After the discretization process, the mixed finite element formulation for the laminated composite beam can be represented in closed form. The equations incorporate the equilibrium equations and constitutive relations at each node of the finite elements, considering the applied boundary conditions and loading on the beam:

$$\mathbf{KX = F} \tag{2.42}$$

In the equation (2.42), $\mathbf{K}$ represents system matrix, $\mathbf{F}$ denotes external force vector and $\mathbf{X}$, which has an open form in the equation (2.43), is named as unknown vector.

$$\mathbf{X}^i = \left[u^i \quad w^i \quad \theta_x^i \quad N_{xx}^i \quad M_{xx}^i \quad M_{xx}^{fi} \quad Q_{xz}^i \quad M_{zz}^f \right]^T \tag{2.43}$$

By solving equation (2.42) for the laminated composite beam, both displacement and stress resultant field variables are directly obtained at the nodes. Consequently, employing equation (2.42) allows for direct calculation of strain measures through matrix operations without the need for numerical derivative operations. By utilizing kinematic and constitutive relations, the distribution of axial stress components along the cross-section can also be obtained at the nodes. This approach offers more efficient method then the case in which stretching effect is ignored in terms of displacement, stress and strain distributions throughout the laminated composite beam during the analysis process.

2.6.7 Stress Calculations

The conventional approach of calculating transverse shear stresses using constitutive relations can produce inaccurate results especially in laminated sections. For this reason, to obtain more realistic values of transverse shear stress and normal stress components, the equilibrium equations of the theory of elasticity are considered. By incorporating these equilibrium equations, the transverse shear stress and transverse normal stress components can be determined at any given thickness coordinate as follows:

$$\sigma_{xz} = -\int_{-h}^{z} (\partial \sigma_{xx} / \partial x) \mathrm{d}\bar{z} \tag{2.44}$$

$$\sigma_{zz} = -\int_{-h}^{z} (\partial \sigma_{xz} / \partial x) \mathrm{d}\bar{z} \tag{2.45}$$

2.7 Mixed FEM for Laminated Composite Plate

In this section, a detailed derivation of the Mixed Finite Element Method for statically loaded laminated plates is explained. The formulation of the current study is incorporated with the Hellinger Reissner variational principle and the Higher Order Plate Theory.

2.7.1 Kinematic Relations

A laminated composite plate with its mid-plane oriented along the xy axis is shown in Figure 2.4. A transverse load $p = p(x, y)$ is applied to the plate in the direction of the z-axis.

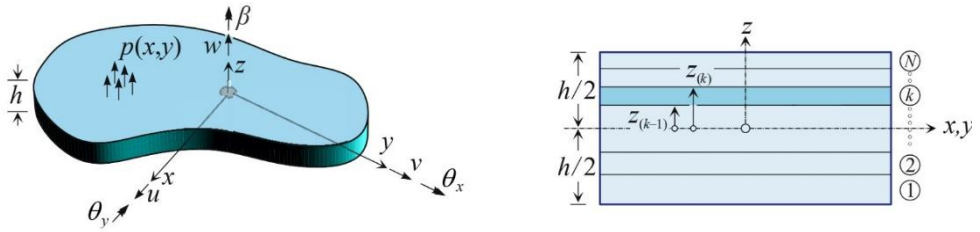

(a) **(b)**

Figure 2.4: Laminated composite plate a) Axes of plate and kinematic variables of the plate in positive directions b) Lamination of the plate

The axial displacement components (in positive *x* and *y* directions) and deflection field of the laminated plate is given as follows based on the higher order shear deformation theory:

$$u^*(x, y, z) = u(x, y) - z\, w_{,x}(x, y) + f(z)\theta_x(x, y) \tag{2.46}$$

$$v^*(x, y, z) = v(x, y) - z\, w_{,y}(x, y) + f(z)\theta_y(x, y) \tag{2.47}$$

$$w^*(x, y, z) = w(x, y) + g(z)\beta \tag{2.48}$$

In the equation (2.46), $w(x, y, z)$ represents the deflection term while $\theta_x(x, y)$ and $\theta_y(x, y)$ represents cross sectional shear rotations about *y* and *x* axis, respectively and β stands for an additional deflection component in *z* direction where $g(z)$ denotes how stretching effect is distributed through the thickness (Figure 2.4a).

Also, by using the functions given in Table 2.1 distribution of $f(z)$ and $g(z)$ along the thickness direction are described in Figure 2.5 and Figure 2.6, respectively.

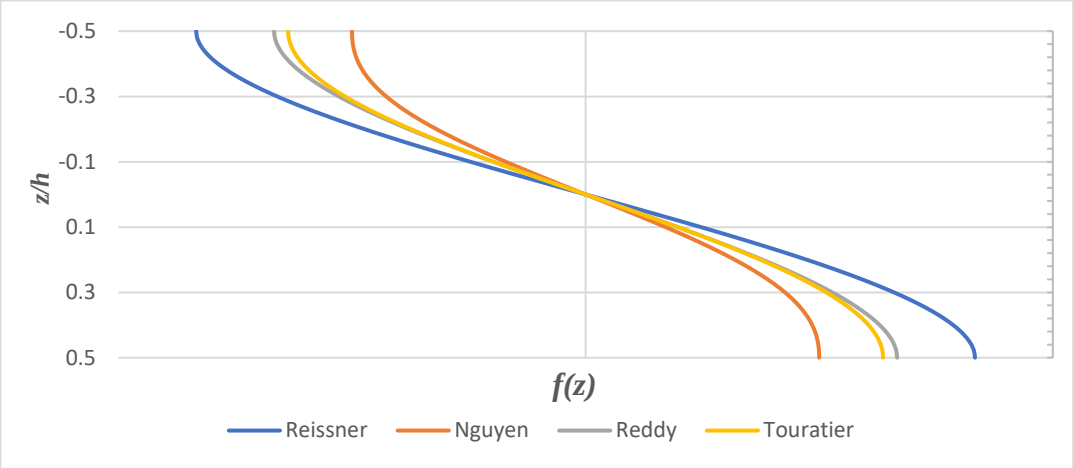

Figure 2.5: Distribution of $f(z)$ through thickness

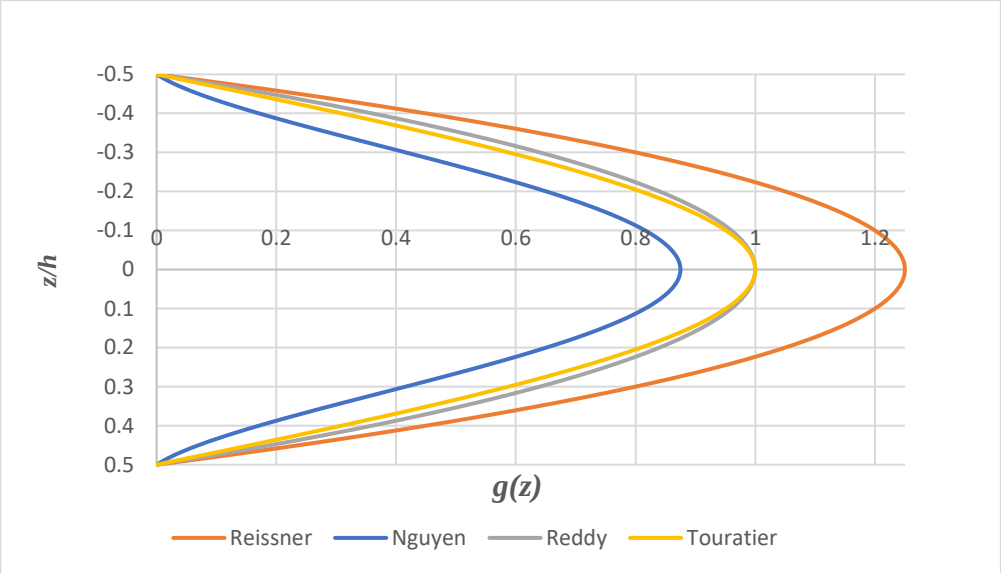

Figure 2.6: Distribution of $g(z)$ through thickness

As illustrated in Figure 2.5, at the middle of the section $(z=0)$, $f(z)=0$ for all functions used in this thesis. From the Figure 2.6, it can be seen that at the top $(z=-h/2)$ and the bottom of the cross section $(z=h/2)$, $g(z)=0$; which meets with the requirements of higher order shear theories zero transverse shear stress values at the top and bottom surfaces of the section.

2.7.2 Strain Components of Higher Order Plate Theories

The strain components throughout the plate domain can be written in terms of the kinematical variable of HSDT described in equation (2.46):

$$
\begin{aligned}
\varepsilon_{xx} &= u^*_{,x} = u_{,x} - z\,w_{,xx} + f\,\theta_{x,x} \\
\varepsilon_{yy} &= v^*_{,y} = v_{,y} - z\,w_{,yy} + f\,\theta_{y,y} \\
\varepsilon_{z} &= w_{,z} = g_{,z}\beta \\
\gamma_{xy} &= u^*_{,y} + v^*_{,x} = u_{,y} + v_{,x} - 2z\,w_{,xy} + f\ \ \theta_{x,y} + \theta_{y,x} \\
\gamma_{yz} &= v^*_{,z} + w^*_{,y} = g\theta_{y} + g\beta_{,y} \\
\gamma_{xz} &= u^*_{,z} + w^*_{,x} = g\theta_{x} + g\beta_{,x}
\end{aligned}
\tag{2.49}
$$

In the equation (2.49), $u^*_{,x}, u^*_{,y}, u^*_{,z}, v^*_{,x}, v^*_{,y}, v^*_{,z}, u^*_{,z}$ represent first derivative of in-plane displacements while $w^*_{,x}, w^*_{,y}$ represent first derivative of deflection in laminate section in terms of related axis.

Strain measures for plate can be given as follows:

$$
\boldsymbol{\varepsilon}_0 = \begin{Bmatrix} u_{,x} \\ v_{,y} \\ u_{,y} + v_{,x} \\ 0 \end{Bmatrix}, \boldsymbol{\varepsilon}_1 = \begin{Bmatrix} -w_{,xx} \\ -w_{,yy} \\ -2w_{,xy} \\ 0 \end{Bmatrix}, \boldsymbol{\varepsilon}_2 = \begin{Bmatrix} \theta_{x,x} \\ \theta_{y,y} \\ \theta_{x,y} + \theta_{y,x} \\ 0 \end{Bmatrix}, \boldsymbol{\varepsilon}_3 = \begin{Bmatrix} 0 \\ 0 \\ 0 \\ \beta \end{Bmatrix}, \boldsymbol{\varepsilon}_S = \begin{Bmatrix} \beta_{,x} + \theta_x \\ \beta_{,y} + \theta_y \\ 0 \\ 0 \end{Bmatrix} \tag{2.50}
$$

2.7.3 Constitutive Relations

The stress-strain relations in the k^{th} layer of the laminated composite plate (Figure 2.1c) can be written as follow by using Hooke's law:

$$
\begin{Bmatrix} \sigma_{xx} \\ \sigma_{yy} \\ \sigma_{xy} \\ \sigma_{yz} \\ \sigma_{xz} \\ \sigma_{zz} \end{Bmatrix} = \begin{bmatrix} \overline{Q}_{11} & \overline{Q}_{12} & \overline{Q}_{16} & 0 & 0 & \overline{Q}_{13} \\ \overline{Q}_{12} & \overline{Q}_{22} & \overline{Q}_{26} & 0 & 0 & \overline{Q}_{23} \\ \overline{Q}_{16} & \overline{Q}_{26} & \overline{Q}_{66} & 0 & 0 & \overline{Q}_{36} \\ 0 & 0 & 0 & \overline{Q}_{44} & \overline{Q}_{45} & 0 \\ 0 & 0 & 0 & \overline{Q}_{45} & \overline{Q}_{55} & 0 \\ \overline{Q}_{13} & \overline{Q}_{23} & \overline{Q}_{36} & 0 & 0 & \overline{Q}_{33} \end{bmatrix} \begin{Bmatrix} \varepsilon_{xx} \\ \varepsilon_{yy} \\ \gamma_{xy} \\ \gamma_{yz} \\ \gamma_{xz} \\ \varepsilon_{zz} \end{Bmatrix} \tag{2.51}
$$

In the equation (2.51), $\overline{Q}_{ij}$ corresponds transformed and reduced material stiffness terms while $\sigma^{(k)}_{ii}$ and $\sigma^{(k)}_{ij}$ denote normal stress and shear stress components, respectively.

2.7.4 Equilibrium Equations

Stress resultants $\mathbf{P} = \left\{ \mathbf{N} \quad \mathbf{M} \quad \mathbf{M}^f \quad \mathbf{V} \quad \mathbf{M}_z^f \right\}^T$ (integrals of stresses and their moments along the thickness direction) and strain measures $\mathbf{e^u} = \left[\boldsymbol{\varepsilon_0} \quad \boldsymbol{\varepsilon_1} \quad \boldsymbol{\varepsilon_2} \quad \boldsymbol{\varepsilon_s} \quad \boldsymbol{\varepsilon_3} \right]^{\mathbf{T}}$ can be related as follows:

$$\mathbf{P} = \mathbf{E}\mathbf{e^u} \quad \text{or} \quad \begin{Bmatrix} \mathbf{N} \\ \mathbf{M} \\ \mathbf{M}^f \\ \boldsymbol{V} \\ \mathbf{M}_z^f \end{Bmatrix} = \begin{bmatrix} \boldsymbol{A} & \boldsymbol{B} & \boldsymbol{E} & \boldsymbol{0} & \boldsymbol{J} \\ \boldsymbol{B} & \boldsymbol{D} & \boldsymbol{F} & \boldsymbol{0} & \boldsymbol{L} \\ \boldsymbol{E} & \boldsymbol{F} & \boldsymbol{H} & \boldsymbol{0} & \boldsymbol{O} \\ \boldsymbol{0} & \boldsymbol{0} & \boldsymbol{0} & \boldsymbol{A_s} & \boldsymbol{0} \\ \boldsymbol{J} & \boldsymbol{L} & \boldsymbol{O} & \boldsymbol{0} & \boldsymbol{P} \end{bmatrix} \begin{Bmatrix} \boldsymbol{\varepsilon_0} \\ \boldsymbol{\varepsilon_1} \\ \boldsymbol{\varepsilon_2} \\ \boldsymbol{\varepsilon_s} \\ \boldsymbol{\varepsilon_3} \end{Bmatrix} \tag{2.52}$$

Where; $\mathbf{N} = \left\{ N_{xx} \quad N_{yy} \quad N_{xy} \right\}^T$, $\mathbf{M} = \left\{ M_{xx} \quad M_{yy} \quad M_{xy} \right\}^T$,

$\mathbf{M}^f = \left\{ M_{xx}^f \quad M_{yy}^f \quad M_{xy}^f \quad M_{zz}^f \right\}^T$ and $\mathbf{Q} = \left\{ Q_{yz} \quad Q_{xz} \right\}^T$. In the equation (2.52), $\mathbf{E}$ is the sectional stiffness matrix and its terms can be calculated as shown below:

$$\begin{aligned}
\left(A_{ij} \quad B_{ij} \quad D_{ij} \right) &= \int_{-h/2}^{+h/2} \bar{Q}_{ij}^{(k)} \left(1 \quad z \quad z^2 \right) \mathrm{d}z \qquad i, j = 1, 2, 6 \\
\left(E_{ij} \quad F_{ij} \quad H_{ij} \right) &= \int_{-h/2}^{+h/2} \bar{Q}_{ij}^{(k)} \left(f(z) \quad zf(z) \quad f(z)^2 \right) \mathrm{d}z \quad i, j = 1, 2, 3, 6 \\
\left(J_{ij} \quad L_{ij} \quad O_{ij} \right) &= \int_{-h/2}^{+h/2} \bar{Q}_{ij}^{(k)} \left(g'(z) \quad zg'(z) \quad f(z)g(z) \right) \mathrm{d}z \quad i, j = 1, 2, 3, 6 \\
\left(P_{ij} \right) &= \int_{-h/2}^{+h/2} \bar{Q}_{ij}^{(k)} \left(g'(z)^2 \right) \quad i, j = 3
\end{aligned} \tag{2.53}$$

$$A^s = b \sum_{k=1}^{N} \int_{z_{(k-1)}}^{z_{(k)}} \bar{Q}_{55}^{(k)} \left(f'(z) \right)^2 \mathrm{d}z \quad ; \quad i, j = 4, 5 \tag{2.54}$$

To provide the expanded form of the equations given above, Equation (2.55) is used [55], here $\mathbf{E_Q}$ represents the material constant matrix;

$$\mathbf{E}_Q = \int_{-h/2}^{h/2} \left(\mathbf{Z}^T \mathbf{Q} \mathbf{Z} \right) \mathrm{d}z \tag{2.55}$$

$\mathbf{Z}$, which is a function of thickness coordinate can be written as ;

$$\mathbf{Z}=\begin{bmatrix} 1 & 0 & 0 & z & 0 & 0 & f(z) & 0 & 0 & 0 & 0 & 0 \\ 0 & 1 & 0 & 0 & z & 0 & 0 & f(z) & 0 & 0 & 0 & 0 \\ 0 & 0 & 1 & 0 & 0 & z & 0 & 0 & f(z) & 0 & 0 & 0 \\ 0 & 0 & 0 & 0 & 0 & 0 & 0 & 0 & 0 & g(z) & 0 & 0 \\ 0 & 0 & 0 & 0 & 0 & 0 & 0 & 0 & 0 & 0 & g(z) & 0 \\ 0 & 0 & 0 & 0 & 0 & 0 & 0 & 0 & 0 & 0 & 0 & g'(z) \end{bmatrix} \tag{2.56}$$

The expanded form of equation (2.52) by using eqn. (2.55) be demonstrated as follows:

$$\begin{Bmatrix} N_{xx} \\ N_{yy} \\ N_{xy} \\ M_{xx} \\ M_{yy} \\ M_{xy} \\ M^f_{xx} \\ M^f_{yy} \\ M^f_{xy} \\ V_{yz} \\ V_{xz} \\ M^f_{zz} \end{Bmatrix} = \begin{bmatrix} A_{11} & A_{12} & A_{16} & B_{11} & B_{12} & B_{16} & E_{11} & E_{12} & E_{16} & 0 & 0 & J_{13} \\ A_{12} & A_{22} & A_{26} & B_{12} & B_{22} & B_{26} & E_{12} & E_{22} & E_{26} & 0 & 0 & J_{23} \\ A_{16} & A_{26} & A_{66} & B_{16} & B_{26} & B_{66} & E_{16} & E_{26} & E_{66} & 0 & 0 & J_{36} \\ B_{11} & B_{12} & B_{16} & D_{11} & D_{12} & D_{16} & F_{11} & F_{12} & F_{16} & 0 & 0 & L_{13} \\ B_{12} & B_{22} & B_{26} & D_{12} & D_{22} & D_{26} & F_{12} & F_{22} & F_{26} & 0 & 0 & L_{23} \\ B_{16} & B_{26} & B_{66} & D_{16} & D_{26} & D_{66} & F_{16} & F_{26} & F_{66} & 0 & 0 & L_{36} \\ E_{11} & E_{12} & E_{16} & F_{11} & F_{12} & F_{16} & H_{11} & H_{12} & H_{16} & 0 & 0 & O_{13} \\ E_{12} & E_{22} & E_{26} & F_{12} & F_{22} & F_{26} & H_{12} & H_{22} & H_{26} & 0 & 0 & O_{23} \\ E_{16} & E_{26} & E_{66} & F_{16} & F_{26} & F_{66} & H_{16} & H_{26} & H_{66} & 0 & 0 & O_{36} \\ 0 & 0 & 0 & 0 & 0 & 0 & 0 & 0 & 0 & A^s_{44} & A^s_{45} & 0 \\ 0 & 0 & 0 & 0 & 0 & 0 & 0 & 0 & 0 & A^s_{54} & A^s_{55} & 0 \\ J_{13} & J_{23} & J_{36} & L_{13} & L_{23} & L_{36} & O_{13} & O_{23} & O_{36} & 0 & 0 & P_{33} \end{bmatrix} \begin{Bmatrix} u_{,x} \\ v_{,y} \\ u_{,y}+v_{,x} \\ -w_{,xx} \\ -w_{,yy} \\ -2w_{,xy} \\ \theta_{x,x} \\ \theta_{y,y} \\ \theta_{x,y}+\theta_{y,x} \\ \beta_{,y}+\theta_y \\ \beta_{,x}+\theta_x \\ \beta \end{Bmatrix} \tag{2.57}$$

The stiffness matrix in Eq. (2.57) is calculated with the MATLAB code given in the Appendix A as well as they are implemented in FORTRAN language for the analyses of the problems presented in this thesis. Also, the corresponded equations of each components of the stiffness matrix, dependent to the shear functions in Table 2.1 are given in Appendix B. Compliance matrix $\mathbf{S}=\mathbf{E}^{-1}$ can be defined by using the equation equation (2.52):

$$\mathbf{e^P}=\mathbf{SP} \quad \text{or} \quad \begin{Bmatrix} \boldsymbol{\varepsilon_0} \\ \boldsymbol{\varepsilon_1} \\ \boldsymbol{\varepsilon_2} \\ \boldsymbol{\varepsilon_s} \\ \boldsymbol{\varepsilon_3} \end{Bmatrix} = \begin{bmatrix} \boldsymbol{A'} & \boldsymbol{B'} & \boldsymbol{E'} & \boldsymbol{0} & \boldsymbol{J'} \\ \boldsymbol{B'} & \boldsymbol{D'} & \boldsymbol{F'} & \boldsymbol{0} & \boldsymbol{L'} \\ \boldsymbol{E'} & \boldsymbol{F'} & \boldsymbol{H'} & \boldsymbol{0} & \boldsymbol{O'} \\ \boldsymbol{0} & \boldsymbol{0} & \boldsymbol{0} & \boldsymbol{A'_s} & \boldsymbol{0} \\ \boldsymbol{J'} & \boldsymbol{L'} & \boldsymbol{O'} & \boldsymbol{0} & \boldsymbol{P'} \end{bmatrix} \begin{Bmatrix} \mathbf{N} \\ \mathbf{M} \\ \mathbf{M}^f \\ \boldsymbol{V} \\ \mathbf{M}^f_z \end{Bmatrix} \tag{2.58}$$

In the equation (2.58), $\mathbf{e^P}$ corresponds strain measures in terms of stress resultants. Equilibrium equations are given as follows for the plate theory, where higher order shear effects are considered:

$$\delta u \neq 0 \quad \Rightarrow N_{xx,x} + N_{xy,y} = 0$$

$$\delta v \neq 0 \quad \Rightarrow N_{xy,x} + N_{yy,y} = 0$$

$$\delta w \neq 0 \quad \Rightarrow M_{xx,xx} + M_{yy,yy} + 2M_{xy,xy} = 0$$

$$\delta \theta_x \neq 0 \quad \Rightarrow M^f_{xx,x} + M^f_{xy,y} - V_{xz} = 0$$

$$\delta \theta_y \neq 0 \quad \Rightarrow M^f_{yy,y} + M^f_{xy,x} - V_{yz} = 0$$

$$\delta \beta \neq 0 \quad \Rightarrow M^f_{zz} + V_{xz,x} + V_{yz,y} = 0$$

2.7.5 Functional and Finite Element Equations

The general version of the Hellinger-Reissner functional for three-dimensional systems is given in equation (2.1). When it is reduced for plate structures, strain measures and stress resultants take the role of the stress and strain components:

$$\delta \Pi_{HR} = \int_A \left(\mathbf{e}^{\mathbf{u}} - \mathbf{e}^{\mathbf{P}} \right)^T \delta \mathbf{P} \, \mathrm{d}A + \int_A \left(\mathbf{P}^T \delta \mathbf{e}^{\mathbf{u}} - \mathbf{p}^T \delta \mathbf{u} \right) \mathrm{d}A - \int_\Gamma \hat{\mathbf{t}}^T \delta \mathbf{u} \, \mathrm{d}\Gamma = 0 \qquad (2.59)$$

While $\mathbf{e}^{\mathbf{P}}$ stands for strain measures defined in terms of stress resultants in equation (2.59), $\mathbf{e}^{\mathbf{u}} = \begin{bmatrix} \varepsilon_0 & \varepsilon_1 & \varepsilon_2 & \varepsilon_s & \varepsilon_3 \end{bmatrix}^T$ represents strain measures expressed using kinematical relations. The middle plane of the plate is symbolized by the letter A while the letter $\mathbf{P}$ accumulates the effects of stress, $\mathbf{p}$ stands for the transverse load that is applied to the plate.

The first variant of the functional obtained for a laminated composite plate can be described by using equations (2.60), (2.61), and (2.50) as:

$$\int_\Omega \left[u_{,x} - \begin{pmatrix} \bar{A}_{11}N_{xx} + \bar{A}_{12}N_{yy} + \bar{A}_{16}N_{xy} \\ +\bar{B}_{11}M_{xx} + \bar{B}_{12}M_{yy} + \bar{B}_{16}M_{xy} \\ +\bar{E}_{11}M^f_{xx} + \bar{E}_{12}M^f_{yy} + \bar{E}_{16}M^f_{xy} \\ +\bar{J}_{13}M^f_{zz} \end{pmatrix} \right] \delta N_{xx} \mathrm{d}A + \int_\Omega \left[v_{,y} - \begin{pmatrix} \bar{A}_{21}N_{xx} + \bar{A}_{22}N_{yy} + \bar{A}_{26}N_{xy} \\ +\bar{B}_{21}M_{xx} + \bar{B}_{22}M_{yy} + \bar{B}_{26}M_{xy} \\ +\bar{E}_{21}M^f_{xx} + \bar{E}_{22}M^f_{yy} + \bar{E}_{26}M^f_{xy} \\ +\bar{J}_{23}M^f_{zz} \end{pmatrix} \right] \delta N_{yy} \mathrm{d}A$$

$$+\int_\Omega \left[u_{,y} + v_{,x} - \begin{pmatrix} \bar{A}_{16}N_{xx} + \bar{A}_{26}N_{yy} + \bar{A}_{66}N_{xy} \\ +\bar{B}_{16}M_{xx} + \bar{B}_{26}M_{yy} + \bar{B}_{66}M_{xy} \\ +\bar{E}_{16}M^f_{xx} + \bar{E}_{26}M^f_{yy} + \bar{E}_{66}M^f_{xy} \\ +\bar{J}_{36}M^f_{zz} \end{pmatrix} \right] \delta N_{xy} \mathrm{d}A +$$

$$\int_\Omega \left[-w_{,xx} - \begin{pmatrix} \bar{B}_{11}N_{xx} + \bar{B}_{12}N_{yy} + \bar{B}_{16}N_{xy} \\ +\overline{D_{11}}M_{xx} + \overline{D_{12}}M_{yy} + \overline{D_{16}}M_{xy} \\ +\bar{F}_{11}M^f_{xx} + \bar{F}_{12}M^f_{yy} + \bar{F}_{16}M^f_{xy} \\ +\bar{L}_{13}M^f_{zz} \end{pmatrix} \right] \delta M_{xx} \mathrm{d}A + \int_\Omega \left[-w_{,yy} - \begin{pmatrix} \bar{B}_{12}N_{xx} + \bar{B}_{22}N_{yy} + \bar{B}_{26}N_{xy} \\ +\overline{D_{12}}M_{xx} + \overline{D_{22}}M_{yy} + \overline{D_{26}}M_{xy} \\ +\bar{F}_{12}M^f_{xx} + \bar{F}_{22}M^f_{yy} + \bar{F}_{26}M^f_{xy} \\ +\bar{L}_{23}M^f_{zz} \end{pmatrix} \right] \delta M_{yy} \mathrm{d}A$$

$$+\int_\Omega \left[-2w_{,xy} - \begin{pmatrix} \bar{B}_{16}N_{xx} + \bar{B}_{26}N_{yy} + \bar{B}_{66}N_{xy} \\ +\overline{D_{16}}M_{xx} + \overline{D_{26}}M_{yy} + \overline{D_{66}}M_{xy} \\ +\bar{F}_{16}M^f_{xx} + \bar{F}_{26}M^f_{yy} + \bar{F}_{66}M^f_{xy} \\ +\bar{L}_{36}M^f_{zz} \end{pmatrix} \right] \delta M_{xy} \mathrm{d}A$$

$$+\int_\Omega \left[\theta_{x,x} - \begin{pmatrix} \overline{E_{11}}N_{xx} + \overline{E_{12}}N_{yy} + \overrightarrow{E_{16}}N_{xy} \\ +\overline{F_{11}}M_{xx} + \overline{F_{12}}M_{yy} + \overline{F_{16}}M_{xy} \\ +\overline{H_{11}}M^f_{xx} + \overline{H_{12}}M^f_{yy} + \overline{H_{16}}M^f_{xy} \\ +\bar{O}_{13}M^f_{zz} \end{pmatrix} \right] \delta M^f_{xx} \mathrm{d}A + \int_\Omega \left[\theta_{y,y} - \begin{pmatrix} \bar{E}_{21}N_{xx} + \bar{E}_{22}N_{yy} + \bar{E}_{26}N_{xy} \\ +\bar{F}_{21}M_{xx} + \bar{F}_{22}M_{yy} + \bar{F}_{26}M_{xy} \\ +\bar{H}_{21}M^f_{xx} + \bar{H}_{22}M^f_{yy} + \bar{H}_{26}M^f_{xy} \\ +\bar{O}_{23}M^f_{zz} \end{pmatrix} \right] \delta M^f_{yy} \mathrm{d}A$$

$$+\int_\Omega \left[\theta_{x,y} + \theta_{y,x} - \begin{pmatrix} \bar{E}_{16}N_{xx} + \bar{E}_{26}N_{yy} + \bar{E}_{66}N_{xy} \\ +\bar{F}_{16}M_{xx} + \bar{F}_{26}M_{yy} + \bar{F}_{66}M_{xy} \\ +\bar{H}_{16}M^f_{xx} + \bar{H}_{26}M^f_{yy} + \bar{H}_{66}M^f_{xy} \\ +\bar{O}_{36}M^f_{zz} \end{pmatrix} \right] \delta M^f_{xy} \mathrm{d}A$$

$$+\int_\Omega \left[\theta_y + \beta_{,y} - \left(\bar{A}^s_{11}V_{yz} + \bar{A}^s_{12}V_{xz} \right) \right] \delta V_{yz} \mathrm{d}A + \int_\Omega \left[\theta_x + \beta_{,x} - \left(\bar{A}^s_{21}V_{yz} + \bar{A}^s_{22}V_{xz} \right) \right] \delta V_{xz} \mathrm{d}A$$

$$-\int_\Omega \delta u q_x \mathrm{d}A - \int_\Omega \delta v q_y \mathrm{d}A - \int_\Omega \delta w q_z \mathrm{d}A - \int_\Omega \delta\theta_x m_x \mathrm{d}A - \int_\Omega \delta\theta_y m_y \mathrm{d}A - \int_\Omega \delta\beta m_z \mathrm{d}A$$

$$-\int_\Omega \left[N_{xx,x} + N_{xy,y} \right] \delta u \mathrm{d}A - \int_\Omega \left[N_{xy,x} + N_{yy,y} \right] \delta v \mathrm{d}A$$

$$-\int_\Omega \left[M_{xx,xx} + M_{yy,yy} + 2M_{xy,xy} \right] \delta w \mathrm{d}A$$

$$-\int_\Omega \left[M^f_{xx,x} + M^f_{xy,y} - V_{xz} \right] \delta\theta_x \mathrm{d}A - \int_\Omega \left[M^f_{yy,y} + M^f_{xy,x} - V_{yz} \right] \delta\theta_y \mathrm{d}A$$

$$-\int_\Omega \left[M^f_{zz,z} + V_{xz,x} + V_{yz,y} \right] \delta\beta \mathrm{d}A$$

$$+\int_S \left(\sigma_{ij} n_j - \hat{t}_i \right) \delta u_i \mathrm{d}S = 0$$

(2.62)

This equation involves both displacement and force-moment type field variables. The second order derivatives in (2.62) are reduced to the first order by using partial integration. In this way, the shape functions to be used in the finite element discretization introduced with C^0 continuity. Thus, the final form of the first variation of the functional is obtained as follows:

$$
\begin{aligned}
&\int_\Omega \left[u_{,x} - \begin{pmatrix} \bar{A}_{11}N_{xx} + \bar{A}_{12}N_{yy} + \bar{A}_{16}N_{xy} \\ +\bar{B}_{11}M_{xx} + \bar{B}_{12}M_{yy} + \bar{B}_{16}M_{xy} \\ +\bar{E}_{11}M^f_{xx} + \bar{E}_{12}M^f_{yy} + \bar{E}_{16}M^f_{xy} \\ +\bar{J}_{13}M^f_{zz} \end{pmatrix} \right] \delta N_{xx} \mathrm{d}A + \int_\Omega \left[v_{,y} - \begin{pmatrix} \bar{A}_{12}N_{xx} + \bar{A}_{22}N_{yy} + \bar{A}_{26}N_{xy} \\ +\bar{B}_{12}M_{xx} + \bar{B}_{22}M_{yy} + \bar{B}_{26}M_{xy} \\ +\bar{E}_{12}M^f_{xx} + \bar{E}_{22}M^f_{yy} + \bar{E}_{26}M^f_{xy} \\ +\bar{J}_{23}M^f_{zz} \end{pmatrix} \right] \delta N_{yy} \mathrm{d}A \\
&+\int_\Omega \left[u_{,y} + v_{,x} - \begin{pmatrix} \bar{A}_{16}N_{xx} + \bar{A}_{26}N_{yy} + \bar{A}_{66}N_{xy} \\ +\bar{B}_{16}M_{xx} + \bar{B}_{26}M_{yy} + \bar{B}_{66}M_{xy} \\ +\bar{E}_{16}M^f_{xx} + \bar{E}_{26}M^f_{yy} + \bar{E}_{66}M^f_{xy} \\ +\bar{J}_{36}M^f_{zz} \end{pmatrix} \right] \delta N_{xy} \mathrm{d}A + \int_\Omega \left[w_{,x}\delta M_{xx,x} - \begin{pmatrix} \bar{B}_{11}N_{xx} + \bar{B}_{12}N_{yy} + \bar{B}_{16}N_{xy} \\ +\bar{D}_{11}M_{xx} + \bar{D}_{12}M_{yy} + \bar{D}_{16}M_{xy} \\ +\bar{F}_{11}M^f_{xx} + \bar{F}_{12}M^f_{yy} + \bar{F}_{16}M^f_{xy} \\ +\bar{L}_{13}M^f_{zz} \end{pmatrix} \right] \delta M_{xx} \mathrm{d}A \\
&+\int_\Omega \left[w_{,y}\delta M_{yy,y} - \begin{pmatrix} \bar{B}_{12}N_{xx} + \bar{B}_{22}N_{yy} + \bar{B}_{26}N_{xy} \\ +\bar{D}_{12}M_{xx} + \bar{D}_{22}M_{yy} + \bar{D}_{26}M_{xy} \\ +\bar{F}_{12}M^f_{xx} + \bar{F}_{22}M^f_{yy} + \bar{F}_{26}M^f_{xy} \\ +\bar{L}_{23}M^f_{zz} \end{pmatrix} \right] \delta M_{yy} \mathrm{d}A + \int_\Omega \left[\theta_{x,x} - \begin{pmatrix} \bar{E}_{11}N_{xx} + \bar{E}_{12}N_{yy} + \bar{E}_{16}N_{xy} \\ +\bar{F}_{11}M_{xx} + \bar{F}_{12}M_{yy} + \bar{F}_{16}M_{xy} \\ +\bar{H}_{11}M^f_{xx} + \bar{H}_{12}M^f_{yy} + \bar{H}_{16}M^f_{xy} \\ +\bar{O}_{13}M^f_{zz} \end{pmatrix} \right] \delta M^f_{xx} \mathrm{d}A \\
&+\int_\Omega \left[w_{,x}\delta M_{xy,y} + w_{,y}\delta M_{xy,x} - \begin{pmatrix} \bar{B}_{16}N_{xx} + \bar{B}_{26}N_{yy} + \bar{B}_{66}N_{xy} \\ +\bar{D}_{16}M_{xx} + \bar{D}_{26}M_{yy} + \bar{D}_{66}M_{xy} \\ +\bar{F}_{16}M^f_{xx} + \bar{F}_{26}M^f_{yy} + \bar{F}_{66}M^f_{xy} \\ +\bar{L}_{36}M^f_{zz} \end{pmatrix} \delta M_{xy} \right] \mathrm{d}A \\
&+\int_\Omega \left[\theta_{y,y} - \begin{pmatrix} \bar{E}_{12}N_{xx} + \bar{E}_{22}N_{yy} + \bar{E}_{26}N_{xy} \\ +\bar{F}_{12}M_{xx} + \bar{F}_{22}M_{yy} + \bar{F}_{26}M_{xy} \\ +\bar{H}_{12}M^f_{xx} + \bar{H}_{22}M^f_{yy} + \bar{H}_{26}M^f_{xy} \\ +\bar{O}_{23}M^f_{zz} \end{pmatrix} \right] \delta M^f_{yy} \mathrm{d}A \\
&+\int_\Omega \left[\theta_{x,y} + \theta_{y,x} - \begin{pmatrix} \bar{E}_{16}N_{xx} + \bar{E}_{26}N_{yy} + \bar{E}_{66}N_{xy} \\ +\bar{F}_{16}M_{xx} + \bar{F}_{26}M_{yy} + \bar{F}_{66}M_{xy} \\ +\bar{H}_{16}M^f_{xx} + \bar{H}_{26}M^f_{yy} + \bar{H}_{66}M^f_{xy} \\ +\bar{O}_{36}M^f_{zz} \end{pmatrix} \right] \delta M^f_{xy} \mathrm{d}A + \int_\Omega \left[\beta - \begin{pmatrix} \bar{J}_{13}N_{xx} + \bar{J}_{23}N_{yy} + \bar{J}_{36}N_{xy} \\ +\bar{L}_{13}M_{xx} + \bar{L}_{23}M_{yy} + \bar{L}_{36}M_{xy} \\ +\bar{O}_{13}M^f_{xx} + \bar{O}_{23}M^f_{yy} + \bar{O}_{36}M^f_{xy} \\ +\bar{P}_{33}M^f_{zz} \end{pmatrix} \right] \delta M^f_{zz} \mathrm{d}A \\
&+\int_\Omega \left[\beta_{,x} - \left(\bar{A}^s_{21}V_{yz} + \bar{A}^s_{22}V_{xz} \right) \right] \delta V_{xz} \mathrm{d}A + \int_\Omega \left[\beta_{,y} - \left(\bar{A}^s_{11}V_{yz} + \bar{A}^s_{12}V_{xz} \right) \right] \delta V_{yz} \mathrm{d}A \\
&+\int_\Omega \left[\theta_y - \left(\bar{A}^s_{11}V_{yz} + \bar{A}^s_{12}V_{xz} \right) \right] \delta V_{yz} \mathrm{d}A + \int_\Omega \left[\theta_x - \left(\bar{A}^s_{21}V_{yz} + \bar{A}^s_{22}V_{xz} \right) \right] \delta V_{xz} \mathrm{d}A \\
&-\int_\Omega \delta u q_x \mathrm{d}A - \int_\Omega \delta v q_y \mathrm{d}A - \int_\Omega \delta w q_z \mathrm{d}A - \int_\Omega \delta\theta_x m_x \mathrm{d}A - \int_\Omega \delta\theta_y m_y \mathrm{d}A - \int_\Omega \delta\beta m_z \mathrm{d}A \\
&+\int_\Omega \begin{pmatrix} N_{xx}\delta u_{,x} + M_{xx,x}\,\delta w_{,x} + M^f_{xx}\delta\theta_{x,x} + N_{yy}\delta v_{,y} + M_{yy,y}\delta w_{,y} + M^f_{yy}\delta\theta_{y,y} \\ +N_{xy}\delta u_{,y} + N_{xy}\delta v_{,x} + M_{xy,x}\,\delta w_{,y} + M_{xy,y}\,\delta w_{,x} + M^f_{xy}\delta\theta_{x,y} + M^f_{xy}\delta\theta_{y,x} \\ +M^f_{zz}\delta\beta + V_{xz}\delta\beta_{,x} + V_{yz}\delta\beta_{,y} + V_{yz}\delta\theta_y + V_{xz}\delta\theta_x \end{pmatrix} \mathrm{d}A + \int_S \hat{t}_i \delta u_i \mathrm{d}S = 0
\end{aligned}
\tag{2.63}
$$

The details of the integration by part procedures adopted here are presented as follows:

$$
\begin{aligned}
-\int_A w_{,xx}\delta M_{xx}\,dA &= \int_A w_{,x}\delta M_{xx,x}\,dA - \int_\Gamma w_{,x}n_x\delta M_{xx}\,d\Gamma \\
-\int_A w_{,yy}\delta M_{yy}\,dA &= \int_A w_{,y}\delta M_{yy,y}\,dA - \int_\Gamma w_{,y}n_y\delta M_{yy}\,d\Gamma \\
-\int_A w_{,xy}\delta M_{xy}\,dA &= \int_A w_{,x}\delta M_{xy,y}\,dA - \int_\Gamma w_{,x}n_y\delta M_{xy}\,d\Gamma \\
-\int_A w_{,xy}\delta M_{xy}\,dA &= \int_A w_{,x}\delta M_{xy,x}\,dA - \int_\Gamma w_{,y}n_x\delta M_{xy}\,d\Gamma
\end{aligned}
\tag{2.64}
$$

2.7.6 Finite Element Discretization

Based on the equation (2.63), the laminated plate's finite element matrices are calculated using four-noded quadrilateral elements with bi-linear form functions. Within the domains of $-1 \le \xi \le 1$ and $-1 \le \eta \le 1$, the interpolation of field variables takes place in the local coordinates ξ and η of the master element. The shape function's expression is provided by :

$$
\varphi_i(\xi,\eta) = \tfrac{1}{4}\left(1+\xi\xi_i\right)\left(1+\eta\eta_i\right), \quad i = (1,2,3,4) \tag{2.65}
$$

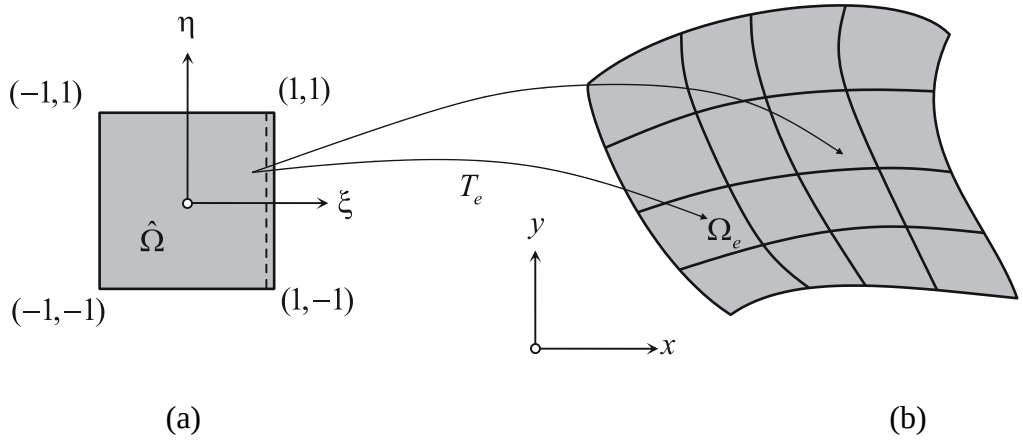

Figure 2.7 : Four-noded linear element discretization in plate field a) Local coordinate systems b) Global coordinates and element allocation

Using the nodal unknowns, field variables are acquired through a plate element with nodes $i = (1,2,3,4)$ by utilizing the interpolation functions φ_i in Appendix C.

The comprehensive closed form of the finite element formulation for the laminated composite plate after discretization is as :

$$\mathbf{KX = F} \tag{2.66}$$

In the equation (2.66), $\mathbf{K}$ is the system matrix, $\mathbf{F}$ is external force vector where $\mathbf{X}$ refers to unknown vector.

$$\mathbf{X}^i = \left[u^i \quad v^i \quad w^i \quad \theta_x^i \quad \theta_y^i \quad \beta^i \quad N_{xx}^i \quad N_{yy}^i \quad N_{xy}^i \quad M_{xx}^i \quad M_{yy}^i \quad M_{xy}^i \quad M_{xx}^{fi} \quad M_{yy}^{fi} \quad M_{xy}^{fi} \quad Q_{yz}^i \quad Q_{xz}^i \quad M_{zz}^{fi} \right]^T \tag{2.67}$$

Upon solving equation (2.66), the field variables representing both displacement and stress components of the laminated composite plate are directly obtained at the nodes. Consequently, eq. (2.58) can be employed to compute strain measures through matrix operations without resorting to numerical derivatives. By using the kinematic and constitutive relations, the distribution of stress components across the cross-section can be determined at the nodes. To calculate the transverse shear stress components for laminated composite plates, the equilibrium equations of the elasticity theory are used instead of Hooke's law as follows [49]:

$$\tau_{xz} = -\int (\sigma_{xx,x} + \tau_{xz,y}) dz, \;\; \tau_{yz} = -\int (\tau_{xy,x} + \sigma_{yy,y}) dz \tag{2.68}$$

2.7.7 Buckling Analysis

Buckling analysis is a crucial aspect of structural design, and various theories have been developed to study the buckling behavior of composite structures. Also, composite buckling analysis is a complex and multifaceted field, with various theories and models available to help people to understand and predict the buckling behavior of composite structures.

In this thesis, a mixed finite element solution is presented for the buckling analysis of an composite beam and isotropic plate considering the higher-order shear effects. All of the deformations, which will be mentioned in next part, are used in with the higher order beam theory, namely based on the shear function suggested by Reddy, to formulate the field equations for the problem. The system and geometric matrices of the laminated beam based on HSDT are expressed in a mixed form. Two noded linear and four noded quadrilateral elements are used to discretize the laminated beam and plate and to obtain finite element equations. Through a

condensation method, the stress resultant type field variables are removed from the finite element equations, yielding a classical eigen-value system in terms of displacements. Some examples are presented to test the convergence behavior of the proposed numerical formulation in numerical examples part. By assuming the axial forces to be constant in the buckling analysis $(\delta N_{xx} = \delta N_{yy} = \delta N_{xy})$ and avoiding transverse external loads, also considering the in-plane normal forces as constant ($N_{xx} = \overline{N}_{xx}$, $N_{yy} = \overline{N}_{yy}$, $N_{xy} = \overline{N}_{xy}$, $M_{zz}^{f} = \overline{M}_{zz}^{f}$) the expression of the eigenvalue problem representing buckling analysis is obtained as follows:

$$\left(\begin{bmatrix} [\mathbf{k}_{ss}] & [\mathbf{k}_{su}] \\ [\mathbf{k}_{us}] & [\mathbf{k}_{uu}] \end{bmatrix} - \lambda_b \begin{bmatrix} [\mathbf{0}] & [\mathbf{0}] \\ [\mathbf{0}] & [\mathbf{K}_g] \end{bmatrix} \right) \begin{Bmatrix} \{\mathbf{M}\}^T \\ \{\mathbf{U}\}^T \end{Bmatrix} = \begin{Bmatrix} \{\mathbf{0}\} \\ \{\mathbf{0}\} \end{Bmatrix} \tag{2.69}$$

Here, λ_b represents the assumed constant in-plane critical force for the problem, known as the buckling load. By removing stress resultant type quantities from the system, the system of equations is simplified to one that only involve displacement-related terms. Thus, by applying static condensation, the condensed matrix gets the form:

$$[\mathbf{K}^*] = [\mathbf{k}_{uu}] - [\mathbf{k}_{su}]^{\mathrm{T}} [\mathbf{k}_{ss}]^{-1} [\mathbf{k}_{su}] \tag{2.70}$$

Hence, the eigenvalue expression becomes as follows:

$$\left([\mathbf{K}^*] - \lambda_b [\mathbf{K}_g] \right) \{\mathbf{U}^T\} = \{\mathbf{0}\} \tag{2.71}$$

The solution of this equation in terms of λ_b represents the buckling loads, and the corresponding buckling mode shapes are represented by the vector $\mathbf{U}$. $\mathbf{K_g}$ is called the geometric matrix.

Here geometric matrix calculation can be given as :

$$[\mathbf{K}_g] = \int [GD]^T [\sigma^0] [GD] dV \tag{2.72}$$

Here, GD represents the geometry-displacement matrix where σ^0 is used for initial stress matrix.

3. NUMERICAL EXAMPLES

Several numerical examples are presented to demonstrate the effectiveness of the proposed mixed finite element formulation for calculating stress and displacement components under static loading for laminated composite beams and plates. The obtained results are thoroughly analyzed and interpreted. To achieve these outcomes, a FORTRAN-based program has been improved by the author, which allows for the implementation and execution of the proposed finite element method. The initial step involves examining the convergence behavior of the numerical solution method. To assess the accuracy of the formulation and its numerical implementation, comparisons are made with the reference solutions provided by Pagano [80] for plates, which are widely accepted as benchmark solutions in the literature for 3D elasticity analysis. By comparing the results obtained from the proposed mixed finite element formulation with the reference solutions, the validity and reliability of the numerical method are tested. The convergence analysis provided valuable insights into the convergence rate of the proposed method and ensured that it yields accurate results to predict the stress and displacement fields for laminated composite beams and plates under static loading conditions. Subsequently, solutions were presented for various lamination, loading, and support conditions, aiming to investigate the effectiveness of the proposed formulation. The obtained results were compared with studies conducted by Reddy [11] (simple higher-order theory) for plates, Ferreira et al. [50], (layer-wise theory), Shi et al. [55], (a new higher-order shear deformation theory), and Kapuria and Kulkarni [75], (third-order zigzag theory) for plates. Additionally, for laminated composite beams, comparisons are made with studies conducted by Kulkarni and Kapuria [76] (third-order theory), Hasim [62] (isogeometric zigzag formulation), Vidal and Polit [77] (sinusoidal zigzag), Khdeir and Reddy [78] (analytical solution of higher-order theory), Zenkour [79] (simple higher-order theory), and Aydogdu [48]. The materials used for those analyses are listed as follows:

Material 1: $E_1 / E_2 = 25, E_1 / E_3 = 25, G_{12} = G_{13} = 0.5E_2, G_{23} = 0.2E_2$

$\nu_{12} = \nu_{13} = \nu_{23} = 0.25$

Material 2: $(E_1 = 181,\ E_2 = E_3 = 10.3,\ G_{12} = G_{13} = 7.17,\ G_{23} = 2.87)$[GPa],

$\nu_{12} = \nu_{13} = 0.28, \nu_{23} = 0.33$

Material 3: $(E_1 = 172.5,\ E_2 = E_3 = 6.9,\ G_{12} = G_{13} = 3.45,\ G_{23} = 1.38)$[GPa],

$\nu_{12} = \nu_{13} = \nu_{23} = 0.25$

Material 4: $(E_1 = 40,\ E_2 = E_3 = 1,\ G_{12} = G_{13} = 0.6,\ G_{23} = 0.5)$[GPa]

$\nu_{12} = 0.25$

3.1 Laminated Composite Beam Examples

3.1.1 Symmetric-Antisymmetric Layered Beam under Sinusoidal Load

This example investigates simple supported symmetric and antisymmetric laminated beams subjected to a distributed sinusoidal transverse load denoted by $p(x) = p_0 \sin(\pi x/L)$ along its axis. The cross-section layouts of the laminated composite beam are described as [0/90] and [0/90/0] as given in Figure 3.1. For those layouts, the material lamination angles are specified as follows:

[0/90]: The cross-section consists of two layers of equal thickness formed with same material. The first half of the total layers are oriented at 0 degrees (aligned with the beam axis), and the second half of total layers are oriented at 90 degrees (perpendicular to the beam axis).

[0/90/0]: The cross-section comprises three layers of equal thickness, all formed with identical materials. The first and third layers are oriented at 0 degrees, and the middle layer is oriented at 90 degrees.

In both cases, the laminated beam is composed of layers of equal thickness, all made from Material 1 and the specific orientations of these layers are given by the lamination angles. The values of $\rho = 4, 20, 40$ are taken to represent the beam span-thickness ratio. Solutions are then obtained by employing different numbers of elements, denoted as $n_e = 10, 20, 30, 40$ along the beam. This approach was adopted

to study and analyze the convergence behavior of the deflection and stress components with respect to the refinement of the finite element mesh.

Nondimensional deflection and stress components are given in the nondimensional form, which is given below;

$$\bar{w} = \frac{10^2 E_2 h^3 b w(L/2,0)}{p_0 L^4} \quad , \quad \bar{\sigma}_{xx} = \frac{b}{p_0}\sigma_{xx}(L/2,-h/2) \tag{3.1}$$

MHBT (Mixed Higher Order Beam Theory) represents the theory used in this thesis. As it can be observed from Table 3.1, the values for both displacement and stress components converge with increasing the number of elements. For very thick beams, the displacement results show noticeable differences compared to elasticity results, which is expected due to the higher-order theory used. Even with the case considering the stretching effect improves the results when it is compared with the study where stretching it is ignored. Furthermore, it has been observed that the stress values obtained in this study for the symmetrical laminated case are compatible with the elasticity solution with better approximation than the case in which stretching effect is excluded. These findings prove that the proposed mixed higher order beam theory provides more accurate stress predictions for symmetrical laminated beams in comparison to the deflection results compared to the rather advanced solution methods, given in the Table 3.1. Besides, the performance of the MHBT is similar for each thickness configurations. Although antisymmetric loading is a compelling lamination scenario, the computational solution produces highly realistic results. To illustrate the convergence values, from the axial stress aspect, in the comparison between the elasticity solution in Table 1 and the finest element mesh for $\rho = 40$, the symmetrical structure has a difference of 0.23%, while the antisymmetric structure has a difference of 0.11%.

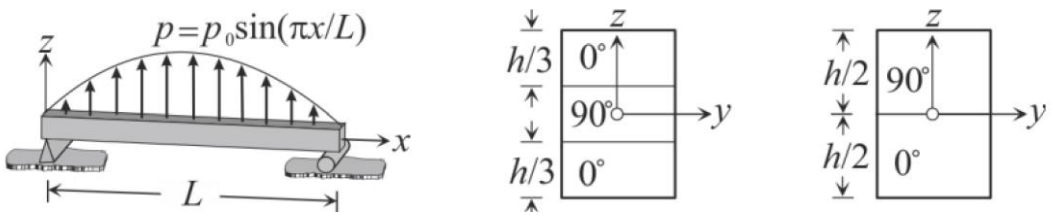

Figure 3.1 : Sinusoidal loaded [0/90/0] and [0/90] oriented simply supported beam

Table 3.1 : Stress components and deflections of simply supported laminated composite beams under sinusoidal loading

Layups		Theory	$\rho = 4$			$\rho = 20$			$\rho = 40$		
			$\bar{w}$	$\bar{\sigma}_{xx}$	$\bar{\sigma}_{xz}$	$\bar{w}$	$\bar{\sigma}_{xx}$	$\bar{\sigma}_{xz}$	$\bar{w}$	$\bar{\sigma}_{xx}$	$\bar{\sigma}_{xz}$
[0/90/0]^a	MHBT ($\varepsilon_z \neq 0$)	($n_e = 10$)	2.672	-18.638	1.427	0.594	-259.35	8.586	0.5333	-1009.6	17.227
		($n_e = 20$)	2.706	-18.754	1.454	0.606	-260.95	8.725	0.5331	-1015.8	17.560
		($n_e = 30$)	2.712	-18.775	1.459	0.607	-261.25	8.755	0.5344	-1016.9	17.609
		($n_e = 40$)	2.715	-18.783	1.460	0.608	-261.35	8.766	0.5348	-1017.4	17.630
	($\varepsilon_z = 0$)	($n_e = 40$)	2.697	-16.981	1.556	0.602	-259.22	8.788	0.533	-1015.3	17.641
		Hasim	2.804	-15.9	1.44	0.6134	-258.9	8.681	0.5362	-1015.3	17.563
		Vidal and Polit	2.803	-19.5	1.42	0.6151	-265.4	8.699	0.5371	-1024.4	17.540
		Pagano (Exact)	2.8899	-18.8	1.432	0.618	-263.2	8.748	0.5379	-1019.7	17.761
[0/90]^b	MHBT ($\varepsilon_z \neq 0$)	($n_e = 10$)	4.3737	-33.4	2.909	2.6556	-698.7	14.327	2.6000	-2774.3	28.641
		($n_e = 20$)	4.4284	-33.6	2.963	2.6885	-702.0	14.595	2.6329	-2790.6	29.177
		($n_e = 30$)	4.4385	-33.7	2.973	2.6946	-702.8	14.646	2.6389	-2793.8	29.277
		($n_e = 40$)	4.4461	-33.7	2.977	2.6968	-703.1	14.663	2.6410	-2795.7	29.313
	($\varepsilon_z = 0$)	($n_e = 40$)	4.4461	-33.6	2.976	2.6968	-703.1	14.663	2.6410	-2795.0	29.313
		Hasim	4.5175	-26.8	2.871	2.6996	-692.5	14.644	2.6419	-2785.1	29.372
		Vidal and Polit	4.5438	-31.8	2.843	2.7036	-703.6	14.574	2.6450	-2803.1	29.174
		Pagano (Exact)	4.7076	-30.0	2.706	2.7092	-699.7	14.620	2.6462	-2793.0	29.325

In the name of giving some details of the converged values, regarding the comparison made with the elasticity solution for $\rho = 40$ and $n_e = 40$ in Table 3.1, it can be noted that the normal stress of the symmetrical layouts has a difference of 0.43%, while the antisymmetric one has a difference of 0.07%. Also, it should be pointed out that including the stretching effect $(\varepsilon_z \neq 0)$ has improved the predictions for each parameter in comparison with the results of Bab and Kutlu [81], where the stretching effect is neglected $(\varepsilon_z = 0)$.

Figure 3.2 shows the shear stress distribution in the thickness direction for the sinusoidally loaded laminated composite beam with [0/90/0] layout. Results are given for $\rho = 40$ ratio and 40 elements. The results of MHBT are also compared with the solutions offered by Pagano [80] and Hasim [62]. As it can be seen in the figure that the transverse shear stress values obtained from all three solutions overlapped.

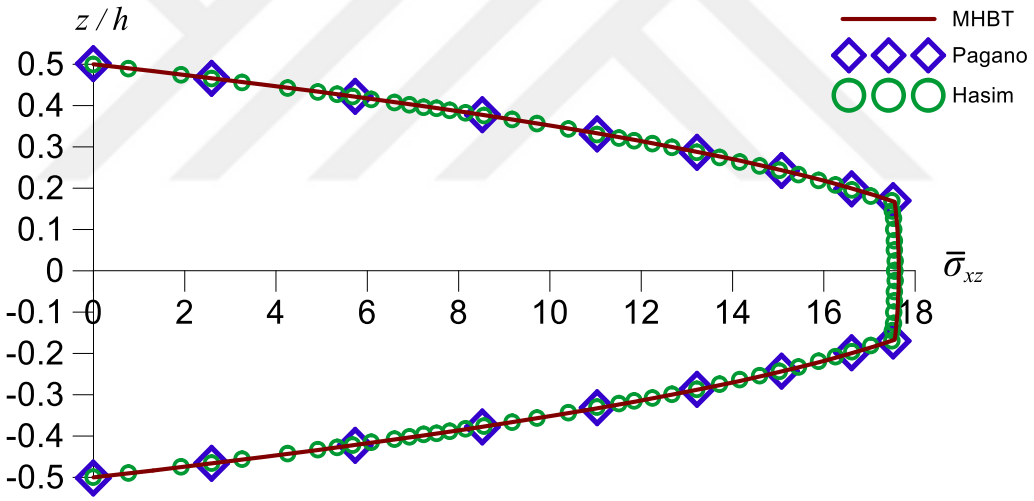

Figure 3.2 : Transverse shear stress distribution in a sinusoidal loaded, simply supported laminated composite beam (Material 1)

Figure 3.3 illustrates the comparison between the shear force computed through the performed numerical method and the shear force derived from the classical equilibrium equations of the composite beam. Due to the assumptions of the higher order beam theory, shear force sets up an equilibrium state including higher order moments. Hence, the shear force is computed through the finite element solution, directly taken as the field parameter, differs from the resultant of the shear stress distributed through the cross-sectional area. If it is desired to compute the classical transverse shear force using the MHBT, integrals of transverse shear components

derived from elasticity's equilibrium equations across the cross-section can be accumulated.

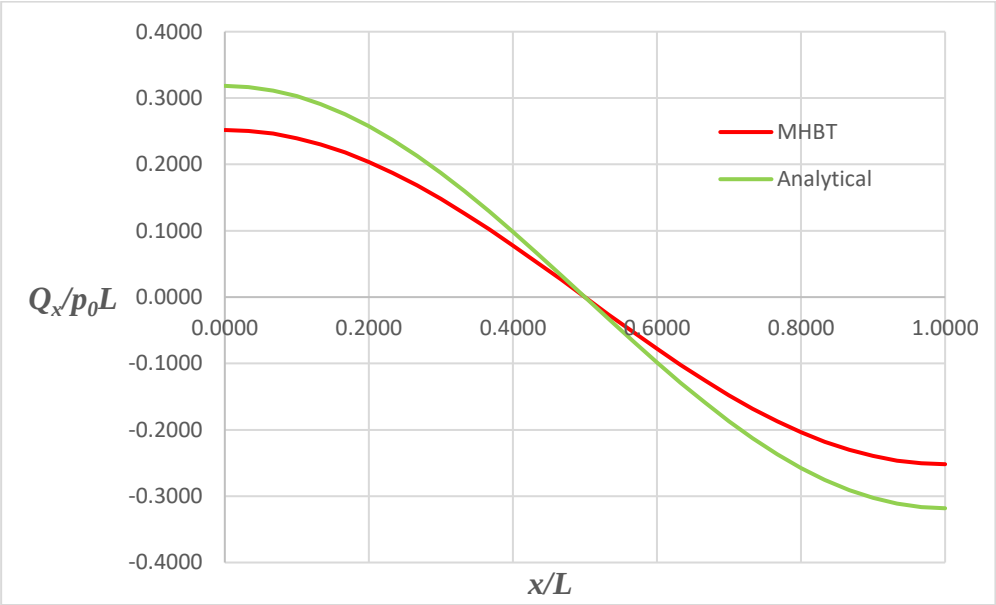

Figure 3.3 : Shear force distribution in a laminated composite beam with sinusoidal load and simply supports (Material 1)

Figure 3.4 shows a comparison between the bending moment distribution of the analytical solution for a symmetrically laminated composite beam subjected to sinusoidal loading and the bending distribution obtained using the mixed finite element method. The results show that the proposed finite element method accurately represents the equilibrium equations, aligning well with the observed moment distribution.

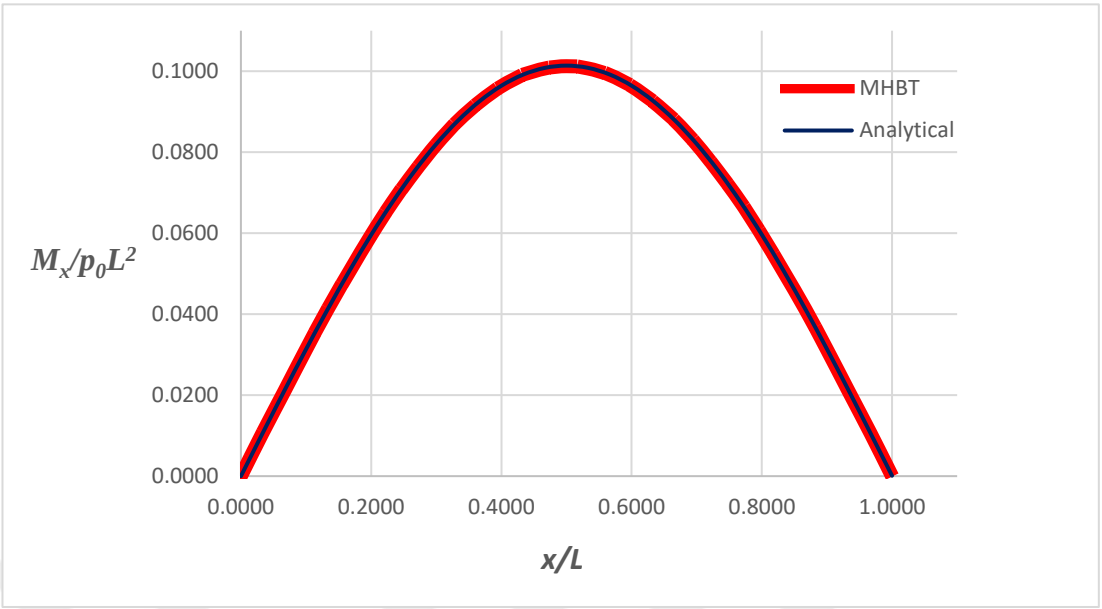

Figure 3.4 : Moment distribution in a sinusoidal loaded, simply supported laminated composite beam with ρ = 20 and 30 elements (Material 1**)**

Deflections along the beam axis for simply supported and simply sliding supported conditions under sinusoidal loading of antisymmetric beam is shown in Figure 3.5. The maximum deflection value for the simply-sliding case is 1.93 times that of the simply-simply case. The coupling between the axial force and the bending moment in the simply-simply case causes a more rigid behavior than the simply sliding case.

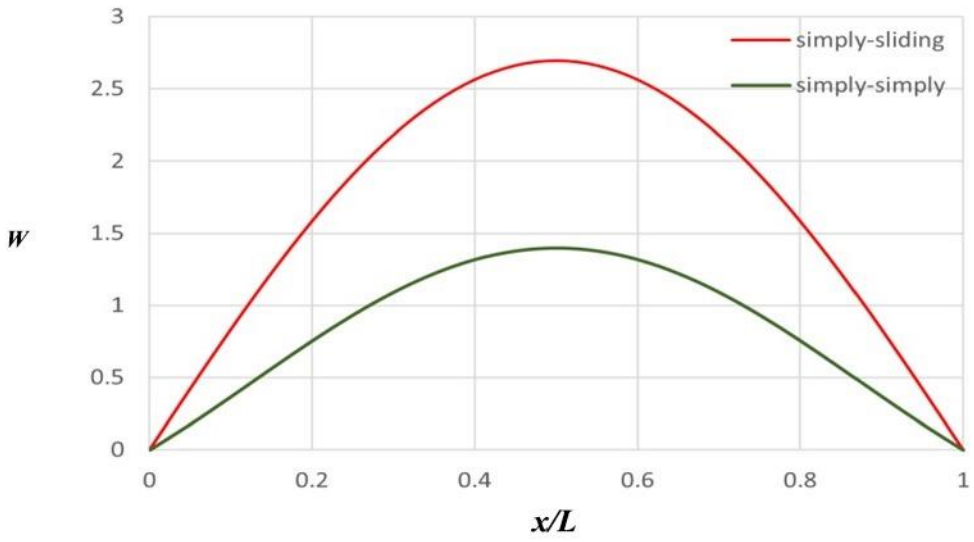

Figure 3.5 : Deflection (dimensionless) of antisymmetric [0/90] laminated composite beam with ρ = 20 under sinusoidal loading (Material 3)

3.1.2 Several Laminated Beams Under Uniform Load

This section introduces the analysis of uniformly ($p(x)= p_0$) loaded laminated beams with [0/90], [0/90/0], and [0/90/90/0] layouts. Both end fixed support conditions (CC) are applied to all lamination layouts, while the [0/90/0] layout is specifically examined under a clamped support condition. Table 3.2 displays the mid-span deflection values of a laminated beam, shown in Figure 3.6, which is produced with Material 1. These values are presented for various thickness ratios and numbers of elements. Table 3.2 also includes a comparison between the calculations made by the MHBT and the analytical solution provided by Khdeir and Reddy [78]. The suggested solution method consistently shows convergent behavior when exposed to CC boundary conditions, as shown in Table 3.2. It can be said that for all thickness ratios, the mixed finite element methods results are highly consistent with the analytical results. Another significant finding from Table 3.2 is that the deflection values faster convergence when the beam span-to-height ratio increases. During the analysis, same non-dimensionalization process for deflection given in equation (3.1) is followed.

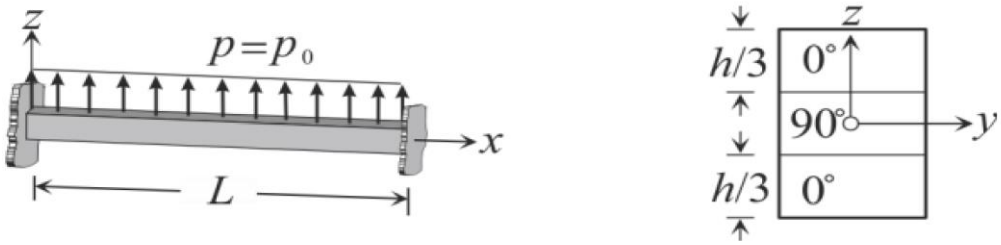

Figure 3.6 : Uniformly loaded and [0/90/0] oriented both ends fixed supported (clamped) beam

Table 3.2 : Symmetric laminated composite beam under uniform loading

		$\bar{w}$		
Layup	Theory	$\rho = 5$	$\rho = 10$	$\rho = 50$
[0/90/0]	MHBT $(n_e = 10)$	1.5265	0.5147	0.146
	MHBT $(n_e = 20)$	1.5487	0.5308	0.147
	MHBT $(n_e = 30)$	1.5533	0.5337	0.147
	MHBT $(n_e = 40)$	1.5532	0.5345	0.147
	Khdeir and Reddy	1.537	0.532	0.147

In Table 3.3, the deflection and stress results of a uniformly loaded composite beam with a simple support and symmetrical [0/90/90/0] layout, as depicted in Figure 3.7, is compared with those from the Third Order Theory solution and the elasticity solution. During this calculation the function of Nguyen-Xuan et al. function, which is given in Table 2.1, is used. The following equations are used to determine for calculating the nondimensional parameters in this table,

$$\bar{w} = \frac{10^2 E_2 h^3 b}{p_0 L^4} w(L/2, 0)\ ,\quad \bar{\sigma}_{xx} = \frac{h^2 b}{p_0 L^2}\sigma_{xx}(L/2, h/2)\ ,\quad \bar{\sigma}^{*}_{xx} = \frac{h^2 b}{p_0 L^2}\sigma_{xx}(L/2, -h/2) \tag{3.2}$$

calculated percentage (%) differences compared to the elasticity solution are presented in Table 3.3. The finite element formulation for the lamination and loading condition has a consistent convergence behavior, as shown in Table 3.3. It should be noted that the findings produced using the suggested method become more consistent with the elasticity solution as the beam span-to-thickness ratio grows. Additionally, it should be noted that the converged deflection and axial stress results of current theory, where $(\varepsilon_z \neq 0)$, are in a better agreement with the elasticity solution compared to the theory in which $\varepsilon_z = 0$ for all span length / thickness ratios. On the other hand, for the ratios $\rho = 10, 20,$ and 100 it is noticed that the results obtained from this study show a better agreement with the elasticity solution compared to the results obtained from the finite element solution based on Third Order Theory.

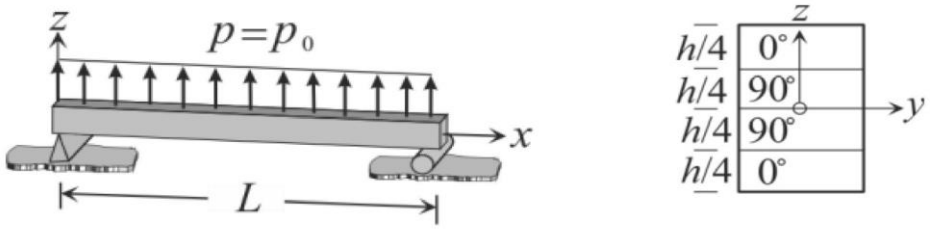

Figure 3.7 : Uniformly loaded and [0/90/90/0] oriented both ends simply supported beam

Table 3.3 : Mechanical parameters of the symmetrically laminated, simply supported, uniformly loaded composites obtained by the MHBT, analytical solution, and elasticity solution (% differences) (Material 2)

		$\rho=5$				$\rho=10$			
Theory	Mesh size	$\bar{w}$	$\bar{\sigma}_{xx}$	$\bar{\sigma}_{xx}^{*}$	$\bar{\sigma}_{xz}$	$\bar{w}$	$\bar{\sigma}_{xx}$	$\bar{\sigma}_{xx}^{*}$	$\bar{\sigma}_{xz}$
	$(n_e=10)$	2.92	1.96	0.95	6.27	1.92	0.64	0.33	6.36
MHBT	$(n_e=20)$	2.39	1.80	0.79	5.29	1.36	0.58	0.28	2.93
$(\varepsilon_z \neq 0)$	$(n_e=30)$	2.29	1.82	0.81	5.64	1.22	0.59	0.28	2.48
	$(n_e=40)$	2.26	1.81	0.80	5.95	1.21	0.59	0.28	2.47
$(\varepsilon_z=0)$	$(n_e=40)$	4.6	5.73	4.76	2.17	2.61	1.74	1.44	0.76
	Kapuria et al.	4.6	5.7	4.8	4.3	2.6	1.7	1.4	1.8
	Pagano	2.6748	1.0711	-	1.43	1.4343	0.9059	-	8.74
		$\rho=20$				$\rho=100$			
	$(n_e=10)$	1.17	0.16	0.09	7.51	0.82	0.01	0.01	9.4
MHBT	$(n_e=20)$	0.59	0.15	0.08	2.73	0.22	0.01	0.01	4.39
$(\varepsilon_z \neq 0)$	$(n_e=30)$	0.48	0.15	0.08	1.35	0.11	0.01	0.01	2.73
	$(n_e=40)$	0.44	0.15	0.08	0.80	0.07	0.02	0.02	1.92
$(\varepsilon_z=0)$	$(n_e=40)$	0.91	0.46	0.38	0.80	0.09	0.02	0.02	1.89
	Kapuria et al.	0.9	0.5	0.4	0.7	0.0	0.0	0.0	0.0
	Pagano	1.1152	0.8641	-	2.70	1.0123	0.8508	-	14.6

Table 3.4 presents the nondimensional representations of deflection and stress components within a uniformly loaded composite beam that is simply supported. The beam has two specific layouts which are symmetrical [0/90/0] and antisymmetric [0/90] as given in Figure 3.8. A comparison of Zenkour's [79] analytical solution with the results of the MHBT is made. Additionally, the analytical deflection results of Khdeir and Reddy [78] are used for comparison. This problem employes elasticity theory for the derivation of the transverse shear stress (σ_{xz}) components. The suggested mixed finite element solution demonstrates a steady convergence behavior, as shown in Table 3.4. The analytical results and mixed finite element solutions show a high level of compatibility for all of the provided span to thickness ratios. Noticeably, Table 3.4 shows that the axial normal stress (σ_{xx}) values converge faster than other parameters. The results coincide well enough with the analytical result even for very coarse mesh configuration, where ($n_e=10$),.

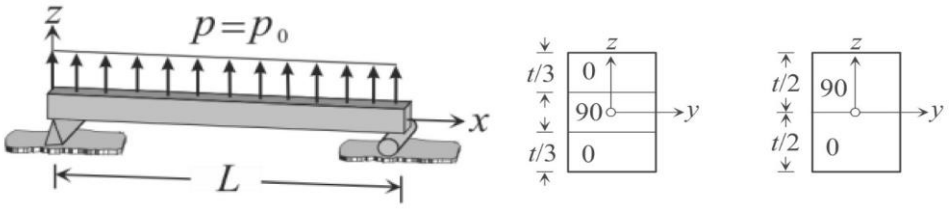

Figure 3.8 : Uniformly loaded [0/90/0] and [0/90] oriented both ends simply supported beam

Table 3.4 : Mechanical components of uniformly loaded composite beams with simply supported symmetrical and antisymmetric layer layouts (Material 1)

		$\rho=5$			$\rho=10$			$\rho=50$		
Layups	Theory	$\bar{w}$	$\bar{\sigma}_{xx}$	$\bar{\sigma}_{xz}$	$\bar{w}$	$\bar{\sigma}_{xx}$	$\bar{\sigma}_{xz}$	$\bar{w}$	$\bar{\sigma}_{xx}$	$\bar{\sigma}_{xz}$
	MHBT $(n_e=10)$	2.3919	-1.0654	0.4014	1.0888	-0.8494	0.4215	0.661	-0.7805	0.4297
[0/90/0]	MHBT $(n_e=20)$	2.4048	-1.0672	0.4013	1.0956	-0.8500	0.4283	0.665	-0.7805	0.4425
$(\varepsilon_z \neq 0)$	MHBT $(n_e=30)$	2.407	-1.0669	0.4012	1.0967	-0.8500	0.4289	0.666	-0.7805	0.4466
	MHBT $(n_e=40)$	2.408	-1.0672	0.4012	1.0971	-0.8500	0.4289	0.666	-0.7805	0.4484
$(\varepsilon_z = 0)$	MHBT $(n_e=40)$	2.413	-1.0069	0.515	1.0974	-0.8500	0.6111	0.666	-0.7805	0.6729
	Zenkour	2.4141	-1.0669	0.4057	1.0980	-0.8500	0.4311	0.661	-0.7805	0.4514
	Khdeir and Reddy	2.412			1.096			0.665		
	MHBT $(n_e=10)$	4.7431	0.2361	0.9022	3.6675	0.2342	0.9267	3.3179	0.2336	0.9347
[0/90]	MHBT $(n_e=20)$	4.7748	0.2361	0.9093	3.6893	0.2342	0.9473	3.3379	0.2336	0.9630
$(\varepsilon_z \neq 0)$	MHBT $(n_e=30)$	4.7798	0.2361	0.9091	3.6933	0.2342	0.9504	3.3417	0.2336	0.9723
	MHBT $(n_e=40)$	4.7815	0.2361	0.9090	3.6947	0.2342	0.9508	3.3430	0.2336	0.9767
$(\varepsilon_z = 0)$	MHBT $(n_e=40)$	4.7829	0.2361	0.2314	3.6948	0.2342	0.2743	3.3430	0.2336	0.2983
	Zenkour	4.7879	0.2362	0.9211	3.6973	0.2343	0.9572	3.3447	0.2336	0.9860
	Khdeir and Reddy	4.777			3.688			3.336		

In Figure 3.9 (laminated beam with the [0/90/0] layout), the profile of transverse shear stress distribution across the laminated beam's cross-section area is given. This distribution is computed through two methods: employing Hooke's law and using the equilibrium equations of elasticity. From the figure, it is noticed that the transverse shear stress distribution obtained by Hooke's law is unrealistic. The presence of different material constants at the material interfaces, where transverse shear strain components are continuous according to the assumptions of the HSDT, results in a discontinuous transverse shear stress distribution at these interfaces. Thus, the employment of the Hooke's law produces inaccurate transverse shear stress distributions. Figure 3.9 illustrates a significant difference between transverse shear stresses computed using Hooke's law and those calculated using the equilibrium equations, which produces a more accurate result.

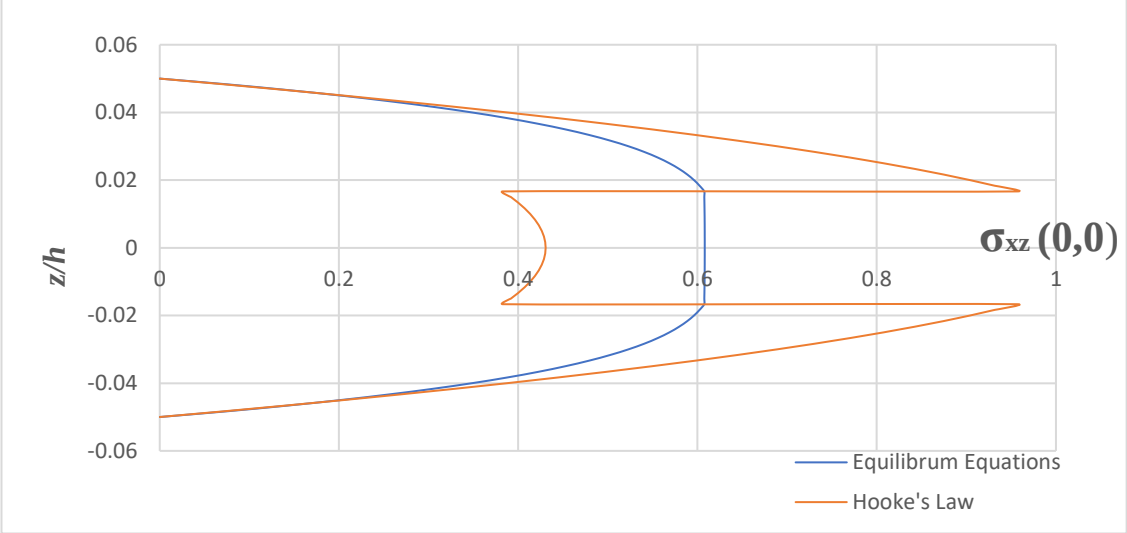

Figure 3.9 : Transverse shear stress distribution for symmetrical simply supported laminated composite beam with ρ = 20 ratio and 30 elements (Material 1)

By using the advantage of the mixed finite element formulation, stress resultants like shear force and moment are directly derived (shown in Figures 3.5, 3.6, and 3.7). Figure 3.10 illustrates the distribution of shear force within a uniformly loaded and simply supported laminated composite beam, using 30 elements for different ratios ($\rho = 5,10,50$). This distribution coincides across a significant part of the beam for various thickness ratios and displays minor differences near the supports. The reason for this difference is that the shear force reaches its extremum values near support locations.

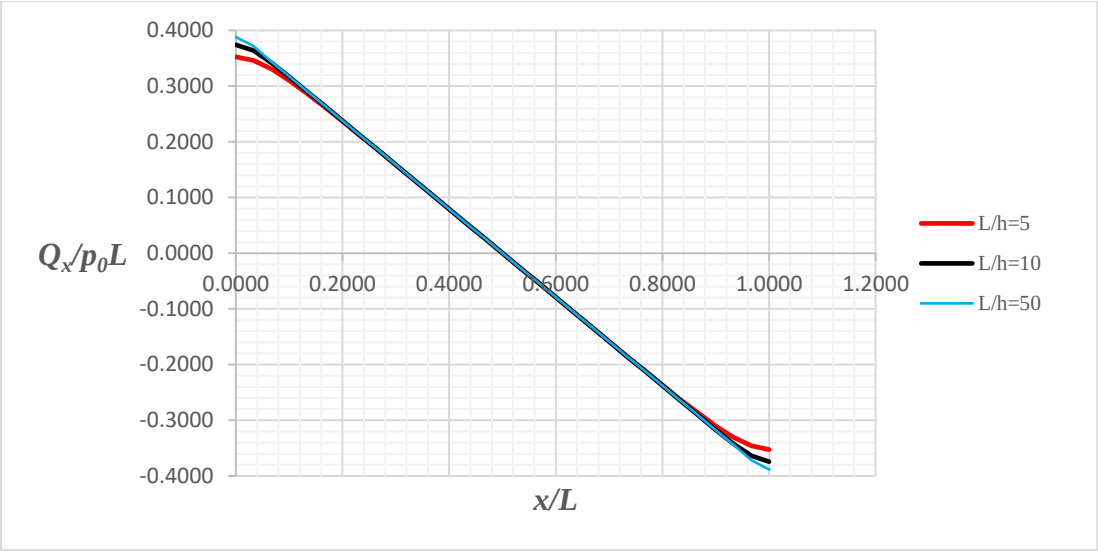

Figure 3.10 : Shear force distribution of symmetrical simply supported, uniformly loaded laminated composite beam with ρ = 20 ratio and 30 element (Material 1)

Figure 3.11 provides the moment distribution for different thickness ratios under the same beam configuration. In this distribution, both dimensionless moment values and analytical calculations for all thickness ratios overlap along the beam axis. Thus, it can be said that the moment values do not include the transverse shear effect considered by the higher order theory.

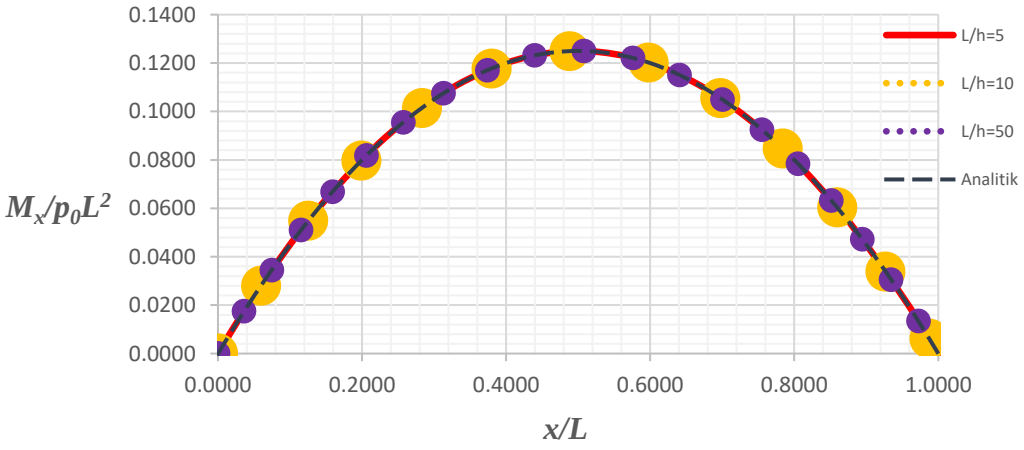

Figure 3.11 : Moment distribution of uniformly loaded, symmetrical simply supported laminated composite beam (Material 1)

Figure 3.12 displays higher order moment distributions for the same beam for various thickness ratios. The higher order moment values throughout the beam shows

slight variations for various thickness ratios because they are dependent on the transverse shear effect.

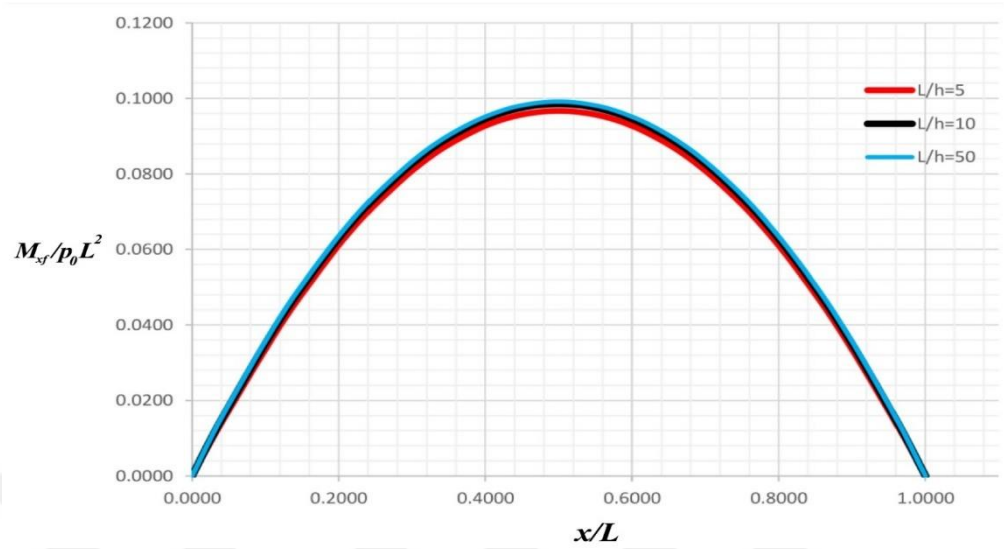

Figure 3.12 : Higher order Moment distribution of uniformly loaded, symmetrical simply supported laminated composite beam (Material 1)

Figure 3.13 shows the variation of the transverse normal stress for the beam which is symmetrical, uniformly loaded, fixed supported. As it can be noticed from the Figure 3.13 the solutions which are calculated by MHBT using the stress equilibrium equation (2.45) overlap each other; however the results of Hooke's Law show different variations among them. Also, the transverse normal stress distribution is added in Figure 3.13 which are calculated by the ANSYS program. Therefore, it appears that the distribution from Hooke's Law converge more to the ANSYS results than elasticity solutions.

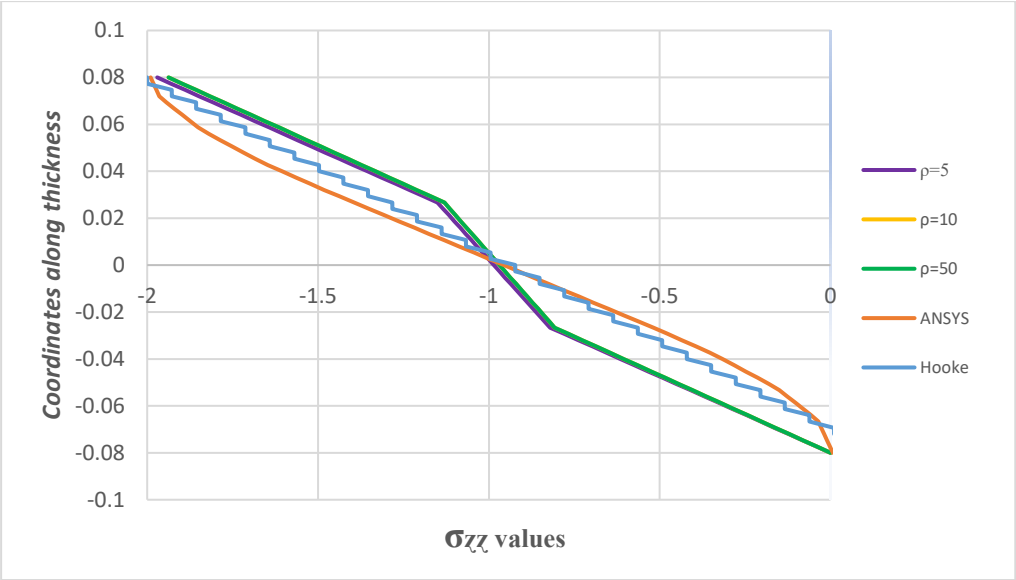

Figure 3.13 : Transverse normal stress distribution in a symmetrical, uniformly loaded, fixed supported beam comparison with the ANSYS results

3.2 Plate Examples

3.2.1 [0/90/90/0] Laminated Composite Plate under Sinusoidal Load

This example examines the bending of a laminated composite plate subjected to a sinusoidal loading $p(x) = p_0 \sin(\pi x/\mathrm{a})\sin(\pi y/\mathrm{b})$ with a [0/90/90/0] layout. The ratio of the plate's span to its thickness is taken as $\rho = a/h = 10, 20, 100$ and the soutions are performed for mesh configurations of 6x6, 12x12, 18x18, and 28x28. The shear function proposed by Touratier [71], Reissner [12], Reddy [11], and Nguyen-Xuan et al. [49] is utilized for this analysis. Pagano's study [80] is used for the purpose of verification, whereas Ferreira et al. [50] and Shi et al. [55] are used for comparison examples in this analysis. To follow the results presented in Tables 3.5-3.6 and 3.7 within a structural context, the following non-dimensionalization process has been carried out:

$$\bar{w} = \frac{10^2 E_2 h^3}{p_0 a^4} w\left(\frac{a}{2}, \frac{b}{2}, 0\right) \quad , \quad \bar{\sigma}_{xx} = \frac{h^2}{p_0 b^2} \sigma_{xx}\left(\frac{a}{2}, \frac{b}{2}, \frac{h}{2}\right)$$
$$\bar{\sigma}_{yy} = \frac{h^2}{p_0 b^2} \sigma_{yy}\left(\frac{a}{2}, \frac{b}{2}, \frac{h}{4}\right) \quad , \quad \bar{\sigma}_{xy} = \frac{h^2}{p_0 b^2} \sigma_{xy}\left(0, 0, \frac{h}{2}\right) \tag{3.3}$$

In Table 3.5-3.6 and 3.7, convergence analysis for all resultants of a plate which is symmetrical ([0/90/0] layout), sinusoidal loaded and simply supported is studied with

different ρ . From those tables it can be said that all shear functions given in Table 2.1 have consistent results when compared to the results of 3D elasticity solutions. The disparities between the findings of this study and the outcomes derived from 3D solutions are higher for thick plates compared to the results for thin plates. According to comparison, all the results of present theory have high differences with Ferreira's layer wise theory results. On the other hand, the current theory highly converges to Shi's higher-order theory in numerous examples results. Pagano's analytical results closely align with the present findings, primarily in terms of deflection and axial normal stress. When convergence results are compared, difference for in plane shear stress component $\bar{\sigma}_{xy}$ results higher than the other components. In addition, in present formulation, with including stretching effect, it can be said that for $\rho = 10$ (from Table 3.5) and $\rho = 20$ (from Table 3.6) each resultants (deflection and all of the stress components) of this study is better than the results where on the formulation with stretching effect is not considered. In other words, the difference between this study to analytical result is less for deflection and stress components.

3.2.2 [0/90/90/0] Laminated Composite Plate under Uniform Load

Resultants of a laminated composite plate, which is subjected to sinusoidal loading $p(x) = p_0 \sin(\pi x/\mathrm{a})\sin(\pi y/\mathrm{b})$ with a [0/90/90/0] layout is analyzed. During this analyze, the ratio of the plate's span to its thickness is taken as $\rho = 10, 20, 100$ and calculated for mesh sizes of 6x6, 12x12, 18x18, 20x20, 28x28 and 40x40. The shear function proposed by Reissner [24], Reddy [11], Touratier [71] and Nguyen-Xuan et al. [49] is utilized for this analysis. To validate the analysis, the 3D ABAQUS results by Kapuria and Kulkarni [75] are employed. Furthermore, for comparative purposes, the Third Order Zig-zag Theory by Kapuria and Kulkarni [75] as well as the Third Order Theory by Kulkarni and Kapuria [76] are used. To understand the results in Tables 3.5, 3.6, and 3.7 in a general structure, a simplification process named as nondimensionalization is used, which is expressed by equation (3.3).

Table 3.5 : Mechanical components of sinusoidal loaded composite plates with simply supported and [0/90/90/0] layout for $\rho=10$ (Material 1)

			Shear Function	$\bar{w}$	Diff. %	$\bar{\sigma}_{xx}$	Diff. %	$\bar{\sigma}_{xy}$	Diff. %	$\bar{\sigma}_{yy}$	Diff. %	$\bar{\sigma}_{yz}$	Diff. %	$\bar{\sigma}_{xz}$	Diff. %
$\rho=10$	MHPT (Present) ($\varepsilon_z \neq 0$)	6x6	Reissner	0.6824	8.16	0.535	4.37	-0.0253	8.28	0.381	5.53	0.1182	39.71	0.2869	4.69
			Reddy	0.6828	8.11	0.535	4.37	-0.0253	8.28	0.381	5.53	0.1182	39.71	0.2869	4.69
			Nguyen-Xuan	0.6945	6.53	0.548	1.98	-0.0259	6.17	0.385	4.41	0.1191	39.24	0.2835	5.8
		12x12	Reissner	0.7043	5.21	0.542	3.04	-0.0263	4.76	0.386	4.2	0.1718	12.36	0.3015	-0.18
			Reddy	0.7047	5.16	0.542	3.04	-0.0263	4.76	0.386	4.2	0.1718	12.36	0.3015	-0.18
			Nguyen-Xuan	0.7168	3.53	0.555	0.62	-0.0269	2.58	0.391	3.06	0.1732	11.65	0.298	1.00
		18x18	Reissner	0.7168	3.53	0.543	2.79	-0.0264	4.11	0.387	3.95	0.1832	6.54	0.297	1.16
			Reddy	0.7088	4.61	0.543	2.79	-0.0264	4.11	0.387	3.95	0.1832	6.54	0.297	1.16
			Nguyen-Xuan	0.721	2.97	0.557	0.37	-0.0271	1.91	0.392	2.81	0.1847	5.77	0.301	0.09
		28x28	Reissner	0.7103	4.39	0.544	2.68	-0.0265	3.81	0.388	3.83	0.1887	3.71	0.306	-1.54
			Reddy	0.7107	4.35	0.544	2.68	-0.0265	3.81	0.388	3.83	0.1887	3.71	0.306	-1.54
			Nguyen-Xuan	0.7229	2.7	0.558	0.25	-0.0271	1.6	0.392	2.69	0.1903	2.92	0.302	-0.34
	($\varepsilon_z = 0$)	28x28	Reddy	0.7134	3.9	0.5451	2.48	-0.0267	3.27	0.3885	3.61	0.1875	4.36	0.2388	0.83
	Shi et al.			0.7258	2.31	0.5479	1.99	0.0273	1.09	0.3888	3.52	0.1643	16.17	0.3035	0.83
	Ferreira et al.			0.7303	1.71	0.5487	1.84	0.0273	1.09	0.3966	1.59	-		0.2993	0.56
	Pagano			0.7430		0.559		0.0276		0.403		0.196		0.301	

Table 3.6 : Mechanical components of sinusoidal loaded composite plates with simply supported [0/90/90/0] layout for $\rho = 20$ (Material 1)

			Shear Function	$\bar{w}$	Diff. %	$\bar{\sigma}_{xx}$	Diff. %	$\bar{\sigma}_{xy}$	Diff. %	$\bar{\sigma}_{yy}$	Diff. %	$\bar{\sigma}_{yz}$	Diff. %	$\bar{\sigma}_{xz}$	Diff. %
$\rho = 20$	MHPT (Present) ($\varepsilon_z \neq 0$)	6x6	Reissner	0.4844	6.3	0.5287	2.63	-0.0218	5.4	0.2983	3.45	0.0950	39.1	0.3086	5.93
			Reddy	0.4845	6.28	0.5287	2.63	-0.0218	5.4	0.2983	3.45	0.0950	39.1	0.3086	5.93
			Nguyen-Xuan	0.4876	5.7	0.5335	1.74	-0.0219	4.83	0.2992	3.18	0.0953	38.93	0.3072	6.34
		12x12	Reissner	0.5	3.29	0.5364	1.22	-0.0225	2.12	0.3027	2.04	0.1376	11.8	0.3255	0.75
			Reddy	0.5001	3.26	0.5364	1.22	-0.0225	2.12	0.3027	2.04	0.1376	11.8	0.3255	0.75
			Nguyen-Xuan	0.5033	2.66	0.5413	0.31	-0.0226	1.53	0.3035	1.77	0.1380	11.53	0.2300	0.89
		18x18	Reissner	0.5030	2.7	0.5378	0.96	-0.0226	1.51	0.3035	1.78	0.1467	5.98	0.3274	0.18
			Reddy	0.5031	2.69	0.5378	0.96	-0.0226	1.51	0.3035	1.78	0.1467	5.98	0.3274	0.18
			Nguyen-Xuan	0.5062	2.08	0.5428	0.04	-0.0228	0.92	0.3044	1.5	0.1471	5.69	0.326	0.62
		28x28	Reissner	0.5044	2.45	0.5385	0.83	-0.0227	1.23	0.3039	1.65	0.1511	3.16	0.3288	-0.25
			Reddy	0.5045	2.42	0.5385	0.83	-0.0227	1.23	0.3039	1.65	0.1511	3.16	0.3288	-0.25
			Nguyen-Xuan	0.5076	1.81	0.5434	-0.08	-0.0229	0.63	0.3047	1.38	0.1515	2.86	0.3274	0.19
	($\varepsilon_z = 0$)	28x28	Reddy	0.5051	2.3	0.5388	0.8	-0.0228	1.1	0.3040	1.61	0.1511	3.11	0.2555	22.09
	Shi et al.			0.5093	2.31	0.5348	1.5	0.0229	0.4	0.3021	2.23	0.1317	15.58	0.3264	0.49
	Ferreira et al.			0.5113	1.71	0.5407	0.42	0.023	0.0	0.3073	0.55	-		0.3256	0.73
	Pagano			0.5170		0.543		0.023		0.309		0.3156		0.328	

Table 3.7 : Mechanical components of sinusoidal loaded composite plates with simply supported and [0/90/90/0] layouts for $\rho=100$ (Material 1)

			Shear Function	$\bar{w}$	Diff. %	$\bar{\sigma}_{xx}$	Diff. %	$\bar{\sigma}_{xy}$	Diff. %	$\bar{\sigma}_{yy}$	Diff. %	$\bar{\sigma}_{yz}$	Diff. %	$\bar{\sigma}_{xz}$	Diff. %
$\rho=100$	MHPT (Present) ($\varepsilon_z \neq 0$)	6x6	Reissner	0.4163	4.24	0.5283	1.99	-0.0204	4.49	0.2656	2.00	0.0858	39.17	0.317	6.5
			Reddy	0.4163	4.24	0.5283	1.99	-0.0204	4.49	0.2656	2.00	0.0858	39.17	0.317	6.5
			Nguyen-Xuan	0.4156	4.38	0.5302	1.63	-0.0204	4.64	0.2645	2.4	0.0856	39.28	0.3165	6.65
		12x12	Reissner	0.4297	1.15	0.5361	0.55	-0.0211	1.33	0.2695	0.55	0.1240	12.08	0.3333	1.69
			Reddy	0.4297	1.15	0.5361	0.55	-0.0211	1.33	0.2695	0.55	0.1240	12.08	0.3333	1.69
			Nguyen-Xuan	0.4290	1.3	0.5380	0.18	-0.0211	1.48	0.2684	0.96	0.1237	12.24	0.3327	1.85
		18x18	Reissner	0.4322	0.57	0.5375	0.28	-0.0212	0.74	0.2702	0.28	0.1321	6.31	0.3364	0.77
			Reddy	0.4322	0.57	0.5375	0.28	-0.0212	0.74	0.2702	0.28	0.1321	6.31	0.3364	0.77
			Nguyen-Xuan	0.4316	0.72	0.5395	-0.09	-0.0212	0.89	0.2691	0.69	0.1319	6.48	0.3358	0.93
		28x28	Reissner	0.4334	0.29	0.5382	0.15	-0.0213	0.46	0.2706	0.16	0.1360	3.51	0.3378	0.34
			Reddy	0.4334	0.29	0.5382	0.15	-0.0213	0.46	0.2706	0.16	0.1360	3.51	0.3378	0.34
			Nguyen-Xuan	0.4328	0.44	0.5401	-0.22	-0.0213	0.62	0.2695	0.56	0.1358	3.69	0.3373	0.5
	($\varepsilon_z = 0$)	28x28	Reddy	0.4335	0.3	0.5382	0.1	-0.0213	0.5	0.2706	0.15	0.1368	2.99	0.2621	22.69
	Shi et al.			0.4344	0.07	0.532	1.3	-0.0214	0.0	0.2675	1.29	0.1186	15.89	0.3355	1.03
	Ferreira et al.			0.4348	-0.02	0.5391	-0.02	-0.0214	0.00	0.2711	-0.04			0.3359	0.91
	Pagano			0.4347		0.539		-0.0214		0.271		0.141		0.339	

In the Table 3.8, it can be seen that deflection component of presented formulation, which is uniformly loaded composite plates with clamped boundary with 10x10 and 20x20 elements, converge Abaqus 3D better that TOT and TOT ZZ for all shear functions. For axial stress on x direction ($\bar{\sigma}_{xx}$), results using function of Nguyen-Xuan et al. shows the best convergence among all results. Moreover, $\bar{\sigma}_{yy}$ values for all shear functions with all elements have better convergence rate than TOT. Furthermore, when the shear function of Touratier is used, shear stress component for 20x20 elements has the best converge rate to Abaqus; in which the difference between presented study and analytical results is 3.16% . Also, when the results of the this study and the formulation in which stretching is ignored[81] is compared, especially for mesh number 10x10, it can be certainly said that presented study have less difference for all mechanical components given in Table 3.8.

Table 3.8 : Mechanical components of uniformly loaded composite plates with clamped boundary conditions and [0/90/90/0] layer layouts for $\rho = 5$ (Difference %) (Material 2)

			Diff. %			
		Shear Function	$\bar{w}$	$\bar{\sigma}_{xx}$	$\bar{\sigma}_{yy}$	$\bar{\sigma}_{xz}$
MHPT	10x10 ($\varepsilon_z \neq 0$)	Touratier	5.63	6.79	-0.88	-18.46
		Reissner	8.14	12.28	5.57	-23.68
		Reddy	8.12	12.28	5.57	-23.68
		Nguyen-Xuan	7.79	6.29	6.3	-7.50
	($\varepsilon_z = 0$)	Nguyen-Xuan	7.68	10.99	7.17	36.47
	20x20 ($\varepsilon_z \neq 0$)	Touratier	7.53	12.91	3.83	3.16
		Reissner	7.22	12.39	7.35	14.37
		Reddy	7.32	12.39	7.35	14.37
		Nguyen-Xuan	7.84	2.96	8.35	10.4
	($\varepsilon_z = 0$)	Nguyen-Xuan	6.98	-1.22	8.5	33.79
Kulkarni and Kapuria TOT			-6.92	-11.19	-9.43	14.37
Kapuria and Kulkarni TOT ZZ			-8.13	1.37	-4.60	7.84
Kapuria and Kulkarni ABAQUS 3D			1.1412	0.3222	0.3340	0.2356

In the Table 3.9, deflection values for all shear functions, without Reissner, with 28x28 converge to Abaqus 3D better than TOT results. $\bar{\sigma}_{xx}$ values with 20x20 and 28x28 elements are closer to the Abaqus 3D than TOT and TOT ZZ when the shear function of Nguyen-Xuan et al. is utilized. Also, this study for $\bar{\sigma}_{yy}$ with 12x12 mesh

numbers converges to 3D results better than TOT with every shear functions used in presented formulation. Transverse shear stress values of Reissner and Reddy's functions have the best convergence among all other shear functions and comparison studies (TOT and TOT ZZ). When Table 3.9 is checked for 28x28 mesh number, this study shows better convergence rate, for each mechanical component, than the study where $\varepsilon_z = 0$ [81].

Table 3.9 : Mechanical components of uniformly loaded composite plates with clamped boundary conditions and [0/90/90/0] layer layouts for $\rho = 10$ (Difference %) (Material 2)

			Diff. %			
		Shear Function	$\bar{w}$	$\bar{\sigma}_{xx}$	$\bar{\sigma}_{yy}$	$\bar{\sigma}_{xz}$
MHPT (Present) ($\varepsilon_z \neq 0$)	6x6	Touratier	7.51	2.79	-6.99	23.68
		Reissner	8.12	2.77	-2.76	22.88
		Reddy	8.00	2.77	-2.76	22.88
		Nguyen-Xuan	6.09	0.58	-3.95	-22.35
	10x10	Touratier	4.66	-0.92	-0.43	-13.51
		Reissner	7.21	1.36	3.00	-9.63
		Reddy	7.12	1.36	3.00	-9.63
		Nguyen-Xuan	5.44	-1.09	2.02	-3.89
	12x12	Touratier	4.63	-1.31	0.25	9.14
		Reissner	6.72	-1.53	2.29	7.42
		Reddy	6.67	-1.53	2.29	7.42
		Nguyen-Xuan	5.09	-5.5	1.12	8.41
	18x18	Touratier	3.60	0.16	1.28	3.12
		Reissner	5.63	2.31	4.34	3.37
		Reddy	5.52	2.31	4.34	3.37
		Nguyen-Xuan	4.41	-0.65	3.69	6.43
	20x20	Touratier	3.49	2.37	1.57	1.81
		Reissner	6.00	2.91	4.36	2.07
		Reddy	5.93	2.91	4.36	2.07
		Nguyen-Xuan	4.61	-0.43	3.71	7.77
	28x28	Touratier	3.09	2.26	1.93	11.85
		Reissner	5.63	3.33	4.73	2.07
		Reddy	5.52	3.33	4.73	2.07
		Nguyen-Xuan	4.41	0.11	4.19	4.14
($\varepsilon_z = 0$)	28x28	Nguyen-Xuan	3.95	0.16	4.52	32.11
Kulkarni and Kapuria TOT			-5.33	-3.42	-6.04	7.71
Kapuria and Kulkarni TOT ZZ			-3.46	-0.17	-1.19	2.04
Kapuria and Kulkarni ABAQUS 3D			0.4930	0.2691	0.2267	0.4109

According to Table 3.10, the results for the shear function of Touratier with 6x6 and 28x28 elements for deflection term, the shear functions of Reissner and Reddy with 20x20 elements for axial stress $\bar{\sigma}_{xx}$, and the shear function of Nguyen-Xuan et al. with 20x20 elements for transverse shear stress have the best convergence to 3D solution.

Table 3.10 : Mechanical components of uniformly loaded composite plates with clamped boundary conditions and [0/90/90/0] layer layouts for $\rho = 20$ (Difference %) (Material 2)

			Diff. %			
		Shear Function	$\bar{w}$	$\bar{\sigma}_{xx}$	$\bar{\sigma}_{yy}$	$\bar{\sigma}_{xz}$
MHPT (Present)	6x6	Touratier	0.20	-8.26	-2.47	26.27
		Reissner	2.56	-7.47	-2.76	27.41
		Reddy	2.52	-7.47	-2.76	27.41
		Nguyen-Xuan	1.43	-8.39	-3.95	27.11
	10x10	Touratier	0.93	-4.31	1.86	-5.01
		Reissner	3.47	-3.09	2.04	-4.90
		Reddy	3.43	-3.09	2.04	-4.90
		Nguyen-Xuan	2.35	-4.31	1.27	-3.74
	12x12	Touratier	0.93	-3.51	1.47	5.49
		Reissner	3.50	-2.30	2.29	3.37
		Reddy	3.46	-2.30	2.29	3.37
		Nguyen-Xuan	2.39	-3.76	1.12	6.43
	18x18	Touratier	0.76	-1.94	2.86	-2.63
		Reissner	3.47	-0.56	4.34	-3.52
		Reddy	3.43	-0.56	4.34	-3.52
		Nguyen-Xuan	2.39	-1.89	3.69	-1.12
	20x20	Touratier	0.68	-1.60	2.88	-1.80
		Reissner	3.41	-0.27	2.94	-3.28
		Reddy	3.38	-0.27	2.94	-3.28
		Nguyen-Xuan	2.35	-1.63	2.24	-0.19
	28x28	Touratier	0.43	-1.10	3.01	6.01
		Reissner	3.24	0.31	3.03	4.63
		Reddy	3.21	0.31	3.03	4.63
		Nguyen-Xuan	2.23	-1.04	2.39	8.94
Kulkarni and Kapuria TOT			-2.91	-0.67	-3.62	9.68
Kapuria and Kulkarni TOT ZZ			-0.95	0.08	-0.27	1.01
Kapuria and Kulkarni ABAQUS 3D			0.2824	0.2724	0.1448	0.5304

3.2.3 *[-θ / θ / -θ / θ]* Laminated Composite Plate under Sinusoidal Load

Laminated composite plate under sinusoidal loading $p(x) = p_0 \sin(\pi x/\mathrm{a})\sin(\pi y/\mathrm{b})$ is studied with $[-\theta/\theta/-\theta/\theta]$ layout of Material 3. Those θ angles are determined as $\theta = 15^o, 30^o, 45^o$. Span-thickness ratio is selected as ρ=10 for 28x28 elements and shear function of Reissner [12], Reddy [11] and Nguyen-Xuan et al. [49] is employed. Third Order Zig-zag Theory of Kapuria and Kulkarni [75] and Third Order Theory of Kulkarni and Kapuria [76] are used for comparing results, while 3D elasticity results of Piskunov et al. [87] are used for verification. To assess the results listed in Table 3.11 in a general structure, nondimensionalization processes have been carried out same as in the equation (3.3).

Table 3.11 : Mechanical components of sinusoidally loaded composite plates with simply supported conditions and $[-\theta/\theta/-\theta/\theta]$ layouts for $\rho = 10$ (Difference %) (Material 3)

Angle		Shear Function	$\bar{w}$	$\bar{\sigma}_{xx}$	$10^*\bar{\sigma}_{yy}$	$\bar{\sigma}_{xy}$
15	MHPT (Present) 28x28	Reissner	0.5688	0.4352	0.5951	0.6192
		Reddy	0.5691	0.4352	0.5951	0.6192
		Nguyen	0.5667	0.4438	0.6149	0.6139
	Kulkarni & Kapuria TOT		0.5886	0.4372	0.5858	0.7037
	Kapuria & Kulkarni ZZ		0.6103	0.4519	0.6000	0.5927
	Piskunov et al. Elasticity		0.6150	0.4453	0.6153	0.6739
30	MHPT (Present) 28x28	Reissner	0.4729	0.2782	0.1080	1.2739
		Reddy	0.4731	0.2781	0.1080	1.2739
		Nguyen	0.4719	0.2844	0.1108	1.2753
	Kulkarni & Kapuria TOT		0.4952	0.2701	0.1043	1.3129
	Kapuria & Kulkarni ZZ		0.5704	0.3081	0.1174	1.2039
	Piskunov et al. Elasticity		0.5619	0.2833	0.1115	1.3310
45	MHPT (Present) 28x28	Reissner	0.4399	0.1658	0.1658	1.6219
		Reddy	0.4401	0.1658	0.1658	1.6219
		Nguyen	0.4387	0.1698	0.1698	1.6427
	Kulkarni & Kapuria TOT		0.4619	0.1651	0.1651	1.5632
	Kapuria & Kulkarni ZZ		0.5597	0.1929	0.1929	1.5815
	Piskunov et al. Elasticity		0.5430	0.1749	0.1749	1.6420

According to Table 3.11, difference of present and comparison studies with 3D elasticity solution increases with the ply angle. Also, results, using the shear function

Nguyen-Xuan et al., $\bar{\sigma}_{xx}$ values have the best convergence to the three-dimensional solutions with all angles, and $\bar{\sigma}_{yy}$ values of all shear functions more converge to the 3D solutions than TOT and less converge than TOT ZZ for 15 degrees. $\bar{\sigma}_{xz}$ values have the less difference for all shear function than TOT and TOT ZZ.

3.2.4 [0/90/0] Laminated Composite Beams for Buckling Analysis

For this analysis, a composite laminated beam for ρ=5 and ρ=10 with both end simple support (SS) boundary condition is studied. During this analysis 4,8,12 and 16 mesh numbers are considered. Also, for this analysis Material 4 has been used. Moreover, for comparison of this study's result with the analytical results [83] for beams, non-dimensionalization formula of the critical load can be written as;

$$\overline{N_b} = \frac{N_{xx} L^2}{E_2 b h^3} \tag{3.4}$$

3.2.4.1 Buckling comparison of the beam with $\rho = 5$

When Figure 3.13 is checked, it can be definitely said that the study result converges at number of elemets 4 and 16 better than the other mesh frequencies. Besides, in this study, differences with analytical results in percentage for 4 and 16 elements 0.91% and 0.45% respectively. Also this convergence ratios are better than the convergence results of study [84] in which those results were 2.46% and 2.36% correspondingly.

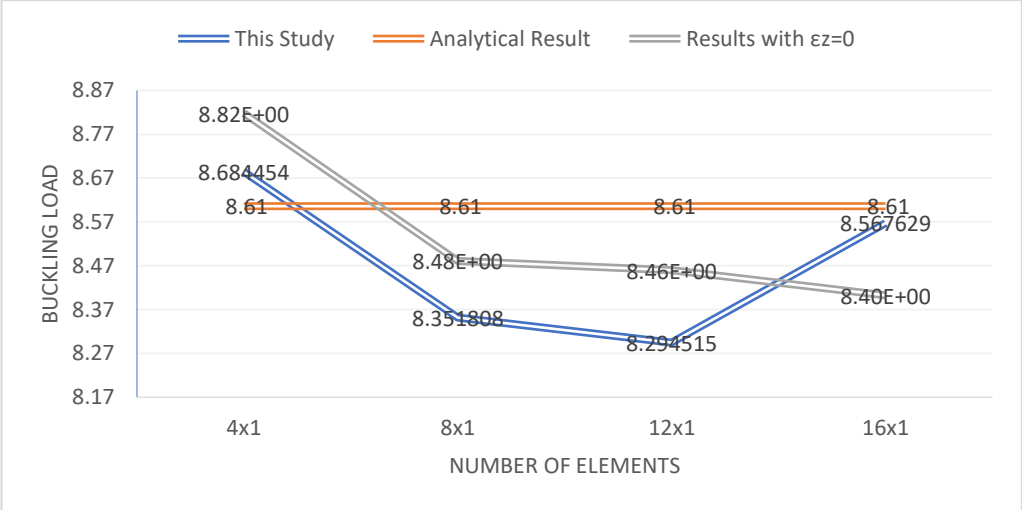

Figure 3.13 : Buckling load comparison of beam with [0/90/0] layup and ρ = 5 ratio and both end simply supported

3.2.4.2 Critical buckling load of the beam with $\rho = 10$ ratio

Also, for the same boundary conditions (SS), same layup ([0/90/0]) and with same material but for different ρ ratio, which is 10 in this example, buckling analysis is investigated and compared with the analytical results [83]. When Figure 3.14 is examined, it can be observed that in this time convergence is more regular than previous example. Also, it can be said that convergence rate is increasing proportionally with the mesh numbers. Moreover, for 12 and 16 elements the percentage errors are 0.06% and 0.19% respectively. For the results where the stretching effect is not added, the results for 12 element is 0.26%. To conclude, it can be said that this analysis almost overlaps with analytical results especially for the dense element numbers and shows better convergence when $\varepsilon_z \neq 0$ than $\varepsilon_z = 0$.

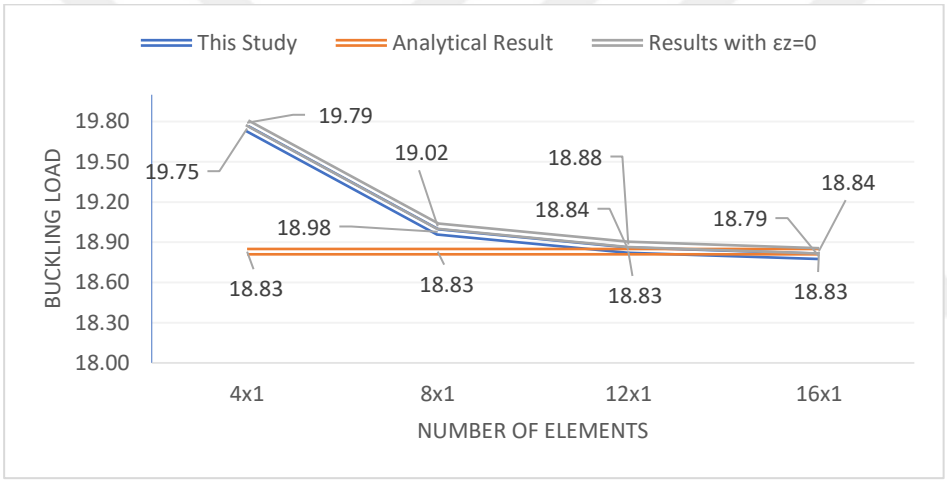

Figure 3.14 : Buckling load comparison of beam with [0/90/0] layup and ρ = 10 ratio and both end simply supported

Furthermore, the results for the buckling loads are taken for corresponded buckling modes which are generally observed in first mode as shown in Figure 3.15 as;

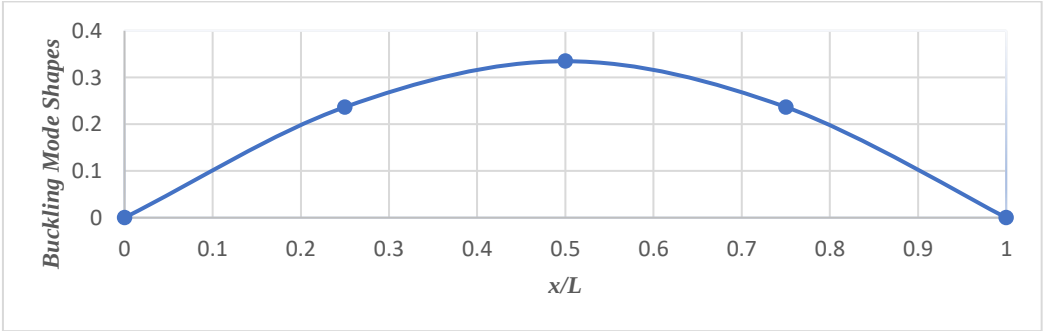

Figure 3.15 : Buckling mode shapes of beam with [0/90/0] layup and SS boundary conditions

3.2.5 Buckling analysis for isotropic plates

For the buckling effect on this analysis, the plate with the ρ=1000 with fixed support boundary condition is investigated. 4x4, 8x8, 12x12, 16x16 and 20x20 mesh frequencies are considered. Also, for this analysis isotropic material has been used which has its Young modulus as $E = 2*10^8\ Pa$ and Poisson's ratio $\upsilon = 0.3$. The non-dimensionalization formula which is used in this analysis can be given as follows [85];

$$\overline{N_b} = \frac{N_b b^2}{D} \tag{3.5}$$

Here, D denotes a constant ratio which depends on E, h and v as;

$$D = \frac{Eh^3}{12(1-v^2)} \tag{3.6}$$

When Figure 3.16 is checked, it can be definitely said that the study result converges directly proportional with the increasing number of elements without the 20x20 elements. As a proof for this judgement, the error observed as 0.13% for 16x16 mesh frequency.

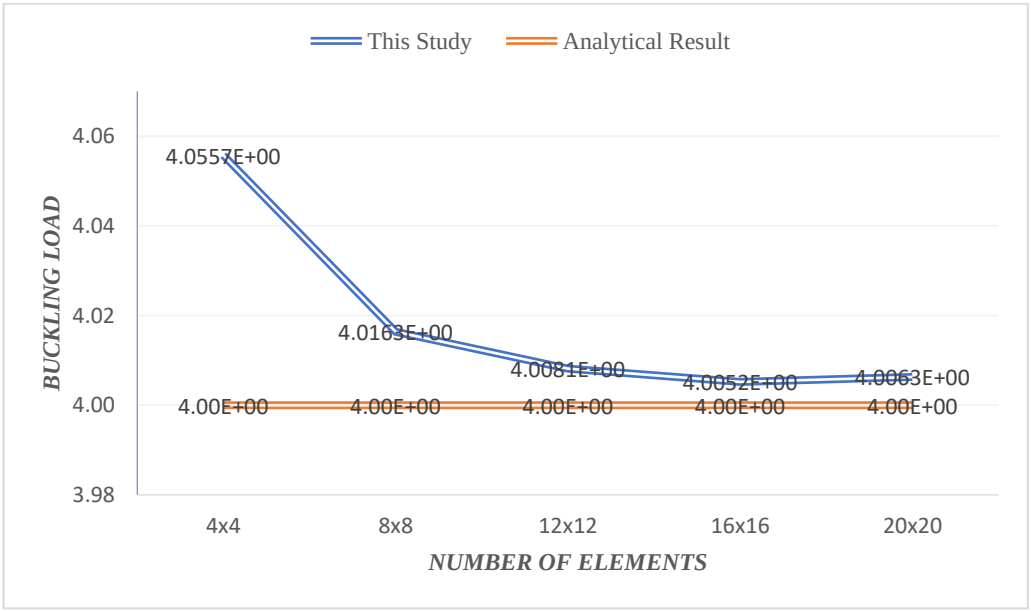

Figure 3.16 : Buckling load comparison between this study and analytical result [90]

Those results are barely corresponding for the buckling loads belongs the first mode. Moreover, the first mode shape versus the x and y dimensions of this plate is given in Figure 3.17 with the help of MATLAB program.

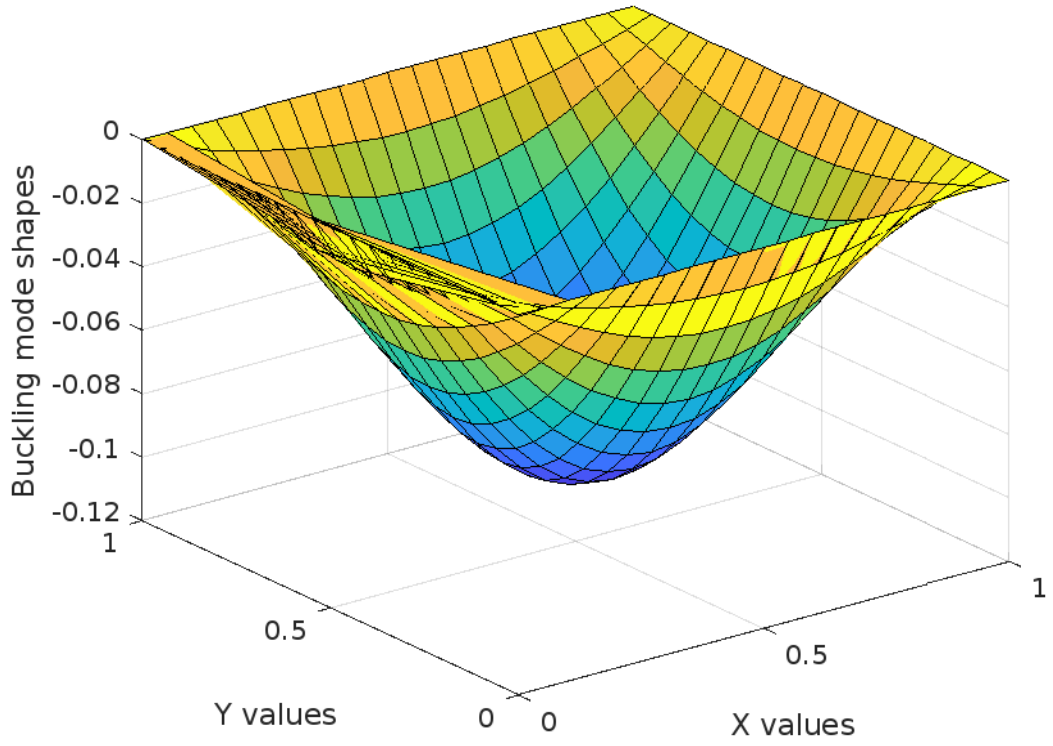

Figure 3.17 : Buckling mode shapes of the plate

It should be noted that the buckling mode shape given in Figure 3.17 for the used isotropic plate illustrates the form the plate assumes when subjected to the buckling load corresponding to the first mode.

4. CONCLUSION

A new formulation with higher order shear deformation theory is developed and applied to study of flexural and buckling analysis for laminated composite beams and plates by enforcing zero transverse shear stresses on the top and bottom surfaces, without the need for any shear correction factors. In this study, displacement and stress distributions are investigated under different boundary and loading conditions with including the stretching effect where $\varepsilon_z \neq 0$. For those analysis, four different shear functions are utilized. Moreover, in this thesis the mixed finite element method governing equations by applying Higher Order Beam and Plate Theory is presented. Finite element equations are derived using the Hellinger-Reissner variational principle are discretized using linear one-dimensional two-noded elements for the beam and quadrilateral four-noded elements with C^0 continuity. As an advantage of the mixed finite element formulation, force and moment components are calculated directly at the nodes alongside the displacement type field variables. In this way, strain components are obtained through matrix operations using cross-sectional compliance matrices. For laminated composite beam solutions, the axial normal stresses are calculated by Hooke's laws, and the transverse shear stress components are obtained by using the equilibrium equations of the theory of elasticity in such a way that continuity is ensured along the section Additionally, the transverse normal stress is determined using both elasticity solutions (for various length/thickness ratios) and Hooke's law. Moreover, for this resultant, ANSYS, which is an analysis program is also employed to check their relations. For plate solutions, the in-plane stress components are obtained from the Hooke's law while for transverse shear stress components are obtained by using the equilibrium equations of the elasticity. Additionally, buckling analysis for different length/thickness ratio is checked for the laminated composite beams and isotropic plate's by employing the presented formulation. Convergence and comparison analyses are performed in several numerical examples and it is observed that the results are in good agreement with the exact solutions obtained from the theory of elasticity, analytical solutions and finite element solutions. Also, with the given examples it has been proved that resultants of the present formulation generally shows better convergence than the resultants of the study in which stretching effect is disregarded $(\varepsilon_z = 0)$. Furthermore, in this study,

results more converges in beam analysis than plate results for both static and buckling analysis depending to the number of unknowns. It is observed that the obtained results are compatible with many advanced finite element solutions that stand out in the literature and produce better results, especially in stress calculations. It is thought that the proposed formulation offers the opportunity to be developed for many types of analysis in the future and to be adapted for various problems.

5. REFERENCES

[1] **Euler, L.** (1744). *Methodus inveniendi lineas curvas maximi minimive proprietate gaudentes*. apud Marcum-Michaelem Bousquet 331–1356

[2] **Bernoulli, J.** (1694). Curvatura laminae elasticae. *Acta Eruditorum Lipsiae*, 262– 276.

[3] **Boley, B. A.** (1963). On the Accuracy of the Bernoulli-Euler Theory for Beams of Variable Section. *Journal of Applied Mechanics*, 30(3), 373–378.

[4] **Modaress-Aval, A. H., Bakhtiari-Nejad, F., Dowell, E. H., Shahverdi, H., Rostami, H., & Peters, D. A.** (2020). Aeroelastic analysis of cantilever plates using Peters' aerodynamic model, and the influence of choosing beam or plate theories as the structural model. *Journal of Fluids and Structures*, 96, 103010.

[5] **Timoshenko, S. P.** (1921). LXVI. On the correction for shear of the differential equation for transverse vibrations of prismatic bars, *The London, Edinburgh, and Dublin Philosophical Magazine and Journal of Science*, *41*(245), 744-746

[6] **Wagner, W., & Gruttmann, F.** (2002). A displacement method for the analysis of flexural shear stresses in thin-walled isotropic composite beams. *Computers & Structures*, 80(24), 1843–1851.

[7] **Lee, U., & Jang, I.** (2010). Spectral element model for axially loaded bending–shear–torsion coupled composite Timoshenko beams. *Composite Structures*, 92(12), 2860–2870 10.

[8] **Lal, J. S.** (1966). *Damping of flexural vibrations in beams by viscoelastic materials* (Doctoral dissertation). Georgia Institute of Technology. 12. Reissner E. The effect of transverse shear deformation on the bending of elastic plates.pdf. Journal of Applied Mechanics. 1945;A69–77.

[9] **Reddy, J. N.** (2003). *Mechanics of Laminated Composite Plates and Shells*. CRC Press.

[10] **Dorduncu, M.** (2019). Stress analysis of laminated composite beams using refined zigzag theory and peridynamic differential operator. *Composite Structures*, 218, 193–203.

[11] **Reddy, J. N.** (1984). A Simple Higher-Order Theory for Laminated Composite Plates. *Journal of Applied Mechanics*, 51(4), 745–752. 16.

[12] **Reissner, E.** (1975). On transverse bending of plates, including the effect of transverse shear deformation. *International Journal of Solids and Structures*, 11, 569–573.

[13] **Soldatos, K. P.** (1992). A transverse shear deformation theory for homogeneous monoclinic plates. *Acta Mechanica*, 94(3–4), 195–220.

[14] **Chandrashekhara, K., & Bangera, K. M.** (1992). Free vibration of composite beams using a refined shear flexible beam element. *Computers & Structures*, 43(4), 719–727. 20.

[15] **Lekhnitskii, S. G.** (1935). Strength calculation of composite beams. *Vestnik inzhen i tekhnikov*, 9, 137–148

[16] **Kirchhoff, G.** (1869). Zur theorie freier flüssigkeitsstrahlen. *Journal für die Reine und Angewandte Mathematik*. 23.

[17] **Love, A. E. H.** (1888). XVI. The small free vibrations and deformation of a thin elastic shell. *Philosophical Transactions of the Royal Society of London.(A.)*, (179), 491-546 25.

[18] **Reissner, E., & Stavsky, Y.** (1961). Bending and stretching of certain types of heterogeneous aeolotropic elastic plates. *Journal of Applied Mechanics*, 28(3), 402–408.

[19] **Whitney, J. M., & Leissa, A. W.** (1970). Analysis of a simply supported laminated anisotropic rectangular plate. *AIAA Journal*, 8(1), 28–33 28.

[20] **Ewing, M. S., Hinger, R. J., & Leissa, A. W.** (1988). On the validity of the reduced bending stiffness method for laminated composite plate analysis. *Composite Structures*, 9(4), 301–317. 30.

[21] **Danielson, K. T., & Tielking, J. T.** (1988). Membrane boundary condition effects on unsymmetric laminates. *Journal of Engineering Mechanics*, 114(12), 2158–2172

[22] **Lin, C.-H., & Jen, M.-H. R.** (2005). Analysis of a laminated anisotropic plate by Chebyshev collocation method. *Composites Part B: Engineering*, 36(2), 155–169

[23] **Mindlin, R. D.** (1951). Influence of rotary inertia and shear flexural motions of isotropic, elastic plates. *Journal of Applied Mechanics*, 18(1), 31–38.

[24] **Reissner, E.** (1945). The effect of transverse shear deformation on the bending of elastic plates.pdf. *Journal of Applied Mechanics*, A69–A77. 36.

[25] **Noor, A. K., & Scott Burton, W.** (1989). Stress and free vibration analyses of multilayered composite plates. *Composite Structures*, 11(3), 183–204.

[26] **Voyiadjis, G. Z., & Pecquet, R. W.** (1988). Bending and stretching elements for analysis of thick composite plates. *Journal of Engineering Mechanics*, 114(11), 1973–1994

[27] **Auricchio, F., & Sacco, E.** (2003). Refined first-order shear deformation theory models for composite laminates. *Journal of Applied Mechanics*, 70(3), 381–390.

[28] **Dorduncu, M., Kaya, K., & Ergin, O. F.** (2020). Peridynamic analysis of laminated composite plates based on first order shear deformation theory. *International Journal of Applied Mechanics*, 12(3), 2050031-1–16

[29] **Ma, L. S., & Wang, T. J.** (2004). Relationships between axisymmetric bending and buckling solutions of FGM circular plates based on third-order plate theory and classical plate theory. *International Journal of Solids and Structures*, 41(1), 85–101.

[30] **Pai, P. F.** (1995). A new look at shear correction factors and warping functions of anisotropic laminates. *International Journal of Solids and Structures*, 32(16), 2295–2313.

[31] **Madabhusi-Raman, P., & Davalos, J. F.** (1996). Static shear correction factor for laminated rectangular beams. *Composites Part B: Engineering*, 27(3), 285–293

[32] **Di Sciuva Marco**. (2019). On the equivalence of displacement-based thirdorder shear deformation plate theories. *Journal of Engineering Mechanics*, 145(7), 04019044.

[33] **Mantari, J. L., Oktem, A. S., & Guedes Soares, C.** (2012). A new trigonometric shear deformation theory for isotropic, laminated composite and sandwich plates. *International Journal of Solids and Structures*, 49(1), 43–53.

[34] **Grover, N., Singh, B. N., & Maiti, D. K.** (2013). A general assessment of a new inverse trigonometric shear deformation theory for laminated composite and sandwich plates using finite element method: *Proceedings of the Institution of Mechanical Engineers, Part G: Journal of Aerospace Engineering*.

[35] **Thai, C. H., Ferreira, A. J. M., Bordas, S. P. A., Rabczuk, T., & NguyenXuan, H.** (2014). Isogeometric analysis of laminated composite and sandwich plates using a new inverse trigonometric shear deformation theory. *European Journal of Mechanics—A/Solids*, 43, 89–108

[36] **Akavci, S. S., & Tanrikulu, A. H.** (2008). Buckling and free vibration analyses of laminated composite plates by using two new hyperbolic sheardeformation theories. *Mechanics of Composite Materials*, 44(2), 145.

[37] **Grover, N., Singh, B. N., & Maiti, D. K.** (2013). Analytical and finite element modeling of laminated composite and sandwich plates: An assessment of a new shear deformation theory for free vibration response. *International Journal of Mechanical Sciences*, 67, 89–99. 57.

[38] **Thai, C. H., Kulasegaram, S., Tran, L. V., & Nguyen-Xuan, H.** (2014). Generalized shear deformation theory for functionally graded isotropic and sandwich plates based on isogeometric approach. *Computers & Structures*, 141, 94–112.

[39] **Aydogdu, M.** (2009). A new shear deformation theory for laminated composite plates. *Composite Structures*, 89(1), 94–101. 61.

[40] **Karama, M., Afaq, K. S., & Mistou, S.** (2009). A new theory for laminated composite plates. *Proceedings of the Institution of Mechanical Engineers, Part L: Journal of Materials: Design and Applications 223*(2), 53-62

[41] **Mantari, J. L., Oktem, A. S., & Guedes Soares, C.** (2011). Static and dynamic analysis of laminated composite and sandwich plates and shells by using a new higher-order shear deformation theory. *Composite Structures*, 94(1), 37–49 plates in the time domain.

International Journal for Numerical Methods in Engineering. 1994;37(23):4081–96.

[42] **Shankara, C. A., & Iyengar, N. G. R.** (1992). Analysis of composite plates with higher order shear deformation theory. *Mechanics Research Communications*, 19(4), 301–314.

[43] **Lim, J. K.** (1990). Mixed-type finite element formulation of higher order shear deformation theory for the linear and nonlinear analyses of a laminated composite plate. *KSME Journal*, 4(2), 109–114.

[44] **Ahmed, N. U., & Basu, P. K.** (1994). Higher-order finite element modelling of laminated composite plates. *International Journal for Numerical Methods in Engineering*, 37(1), 123–139.

[45] **Sadek, E. A.** (1998). Some serendipity finite elements for the analysis of laminated plates. *Computers & Structures*, 69(1), 37–51.

[46] **Cheung, Y. K., & Shenglin, D.** (1993). Analysis of laminated composite plates by hybrid stress isoparametric element. *International Journal of Solids and Structures*, 30(20),

[47] **Ferreira, A. J. M., Roque, C. M. C., & Martins, P. A. L. S. (2004).** Radial basis functions and higher-order shear deformation theories in the analysis of laminated composite beams and plates. *Composite Structures*, 66(1), 287–293.

[48] **Aydogdu, M.** (2009). A new shear deformation theory for laminated composite plates. *Composite Structures*, 89(1), 94–101

[49] **Nguyen, T. N., Thai, C. H., & Nguyen-Xuan, H.** (2016). On the general framework of high order shear deformation theories for laminated composite plate structures: A novel unified approach. International Journal of Mechanical Sciences, 110, 242–255.

[50] **Ferreira, A. J. M., Roque, C. M. C., & Jorge, R. M. N.** (2005). Analysis of composite plates by trigonometric shear deformation theory and multiquadrics. *Computers & Structures*, 83(27), 2225–2237

[51] **Mantari, J. L., Oktem, A. S., & Guedes Soares, C.** (2011). Static and dynamic analysis of laminated composite and sandwich plates and shells by using a new higher-order shear deformation theory. Composite Structures, 94(1), 37–49

[52] **Mantari, J. L., & Guedes Soares, C.** (2012). Analysis of isotropic and multilayered plates and shells by using a generalized higher-order shear deformation theory. Composite Structures, 94(8), 2640–2656

[53] **Nguyen-Xuan, H., Thai, C. H., & Nguyen-Thoi, T.** (2013). Isogeometric finite element analysis of composite sandwich plates using a higher order shear deformation theory. *Composites Part B: Engineering*, 55, 558–574.

[54] **Thai, C. H., Nguyen-Xuan, H., Bordas, S. P. A., Nguyen-Thanh, N., & Rabczuk, T.** (2015). Isogeometric analysis of laminated composite plates using the higher-order shear deformation theory. *Mechanics of Advanced Materials and Structures*, 22(6), 451–469.

[55] **Shi, P., Dong, C., Sun, F., Liu, W., & Hu, Q.** (2018). A new higher order shear deformation theory for static, vibration and buckling responses of laminated plates with the isogeometric analysis. *Composite Structures*, 204, 342–358.

[56] **Madenci, E., & Ozutok, A.** (2020). Variational approximate for high order bending analysis of laminated composite plates. *Structural Engineering and Mechanics*, 73(1), 97–108 82.

[57] **Kant, T., & Pandya, B. N.** (1988). A simple finite element formulation of a higher-order theory for unsymmetrically laminated composite plates. *Composite Structures*, 9(3), 215–246

[58] **Carrera, E.** (2003). Historical review of Zig-Zag theories for multilayered plates and shells. *Applied Mechanics Reviews*, 56(3), 287

[59] **Gherlone, M.** (2013). On the use of zigzag functions in equivalent single layer theories for laminated composite and sandwich beams: A comparative study and some observations on external weak layers. *Journal of Applied Mechanics*, 80(6), 061004–061004.

[60] **Tessler, A., Di Sciuva, M., & Gherlone, M.** (2010). A consistent refinement of first-order shear deformation theory for laminated composite and sandwich plates using improved zigzag kinematics. *Journal of Mechanics of Materials and Structures*, 5(2), 341–367.

[61] **Barut, A., Madenci, E., & Tessler, A.** (2013). C0-continuous triangular plate element for laminated composite and sandwich plates using the {2,2} – Refined Zigzag Theory. *Composite Structures*, 106, 835–853

[62] **Hasim, K. A., Kefal, A., & Madenci, E.** (2019). Isogeometric plate element for unstiffened and blade stiffened laminates based on refined zigzag theory. Composite Structures, 222, 110931

[63] **Dorduncu, M.** (2020). Stress analysis of sandwich plates with functionally graded cores using peridynamic differential operator and refined zigzag theory. Thin-Walled Structures, 146, 106468

[64] **Kutlu, A., Dorduncu, M., & Rabczuk, T.** (2021). A novel mixed finite element formulation based on the refined zigzag theory for the stress analysis of laminated composite plates. Composite Structures, 267, 113886.

[65] **Sahoo, R., & Singh, B. N.** (2014). A new trigonometric zigzag theory for buckling and free vibration analysis of laminated composite and sandwich plates. Composite Structures, 117, 316–332.

[66] **Cho, M., & Oh, J.** (2004). Higher order zig-zag theory for fully coupled thermo-electric–mechanical smart composite plates. International Journal of Solids and Structures, 41(5–6), 1.

[67] **Ermiş, M., Kutlu, A., Eratlı, N., & Omurtag, M. H.,** (2022) Free vibration of axially FG curved beam on orthotropic Pasternak foundation via mixed FEM.Journal of the Brazilian Society of Mechanical Sciences and Engineering

[68] **Pereira, E. M. B. R., & Freitas, J. A. T.** (1996). A hybrid-mixed finite element model based on Legendre polynomials for Reissner-Mindlin plates. Computer Methods in Applied Mechanics and Engineering, 136(1–2), 111–126.

[69] **Gendy, A. S., Saleeb, A. F., & Mikhail, S. N.** (1997). Free vibrations and stability analysis of laminated composite plates and shells with hybrid/mixed formulation. Computers & Structures, 63(6), 1149–1163

[70] **Kutlu, A., & Hakkı Omurtag, M.** (2012). Large deflection bending analysis of elliptic plates on orthotropic elastic foundation with mixed finite74 element method. International Journal of Mechanical Sciences, 65(1), 64–74.

[71] **Touratier, M.** (1991). An efficient standard plate theory. International Journal of Engineering Science, 29(8), 901–916.

[72] **Mantari, J., & Canales, F.** (2016). Finite element formulation of laminated beams with capability to model the thickness expansion. *Composites Part B: Engineering*, *101*, 107–115.

[73] **Keshava Kumar, S.** (2019). Review of Laminated Composite Plate Theories, with Emphasis on Variational Asymptotic Method. AIAA Journal, 57(10), 4182–4188.

[74] **Jones, R. M.** (1999). *Mechanics of composite materials*. CRC press

[75] **Kapuria, S., & Kulkarni, S. D.** (2007). An improved discrete Kirchhoff quadrilateral element based on third-order zigzag theory for static analysis of composite and sandwich plates. International Journal for Numerical Methods in Engineering, 69(9), 1948–1981.

[76] **Kulkarni, S. D., & Kapuria, S.** (2007). A new discrete Kirchhoff quadrilateral element based on the third-order theory for composite plates, Computational Mechanics, 39(3), 237-246.

[77] **Vidal, P., & Polit, O.** (2011). A sine finite element using a zig-zag function for the analysis of laminated composite beams. Composites Part B: Engineering, 42(6), 1671–1682.

[78] **Khdeir, A. A., & Reddy, J. N.** (1997). An exact solution for the bending of thin and thick cross-ply laminated beams. Composite Structures, 37(2), 195–203.

[79] **Zenkour, A. M.** (1999). Transverse Shear and Normal Deformation Theory for Bending Analysis of Laminated and Sandwich Elastic Beams. Mechanics of Advanced Materials and Structures, 6(3), 267–283.

[80] **Pagano, N. J.** (1994). Exact Solutions for Rectangular Bidirectional Composites and Sandwich Plates. Composites, 4(1), 15.

[81] **Bab, Y., & Kutlu, A.,** (2023) Stress Analysis of Laminated HSDT Beams Considering Bending Extension Coupling Turkish Journal of Civil Engineering 34, 5-10.

[82] **Piskunov, V. G., Verijenko, V. E., Adali, S., Tabakov, P. Y., Prisyazhnyouk, V. K., & Buryhin, S. G.** (2001). Rational transverse shear deformation higher-order theory of anisotropic laminated plates and shells. International Journal of Solids and Structures, 38(36–37), 6491–6523.

[83] **Khdeir, A., & Reddy, J. N.** (1994). Free vibration of cross-ply laminated beams with arbitrary boundary conditions. International Journal of Engineering Science 32(12), 1971–1980.

[84] **Kanığ D., Bab Y., Kutlu A., Omurtag M. H.,** 2023. Mixed finite element for the buckling analysis of laminated composite beams using HSDT, ICEARC 2023-3rd Internatıonal Civil Engineering and Architetectural Conference, October 12-14, Trabzon, Turkey.

[85] **Park, M., & Choi, D.** (2018). A simplified first-order shear deformation theory for bending, buckling and free vibration analyses of isotropic plates on elastic foundations. KSCE Journal of Civil Engineering, 22(4), 1235–1249.

6. APPENDICES

APPENDIX A : Stiffness matrix verification

APPENDIX B: Calculation of values of each component of stiffness matrix

APPENDIX C : Field variables

APPENDIX A

```
fz=sym('fz');
gz=sym('gz');
z=sym('z');
gprmz=sym('gprmz');
Zyeni=[1 0 0 z 0 0 fz 0 0 0 0 0 0 0;0 1 0 0 z 0 0 fz 0 0 0 0 0 0;0 0 1 0 0
z 0 0 fz 0 0 0 0 0; 0 0 0 0 0 0 0 0 gz 0 0 0 gz 0;0 0 0 0 0 0 0 0 0 gz 0
gz 0;0 0 0 0 0 0 0 0 0 0 gprmz 0 0]
ZT = transpose(Zyeni);
C11=sym('C11');
C12=sym('C12');
C16=sym('C16');
C13=sym('C13');
C22=sym('C22');
C26=sym('C26');
C23=sym('C23');
C66=sym('C66');
C33=sym('C33');
C55=sym('C55');
C44=sym('C44');
C45=sym('C45');
C54=sym('C54');
C36=sym('C36');
Q=[C11 C12 C16 0 0 C13;C12 C22 C26 0 0 C23;C16 C26 C66 0 0 C36;0 0 0 C44
C45 0 ;0 0 0 C54 C55 0;C13 C23 C36 0 0 C33]
sagcarpimyeni=Q*Z
sonucyeni=ZT*sagcarpim
```

APPENDIX B

```
aci=sym('aci')   %orientation degree
v31=sym('v31');  %poisson ratios
v32=sym('v32');
v21=sym('v21');
v23=sym('v23');
v12=sym('v12');
v13=sym('v13');

E1=sym('E1'); %Elastisities
E2=sym('E2');
E3=sym('E3');

I=1:60:1 %layer number
HL=linspace(-0.05,0.05,61) % z coordinates
he=0.1  %thickness
delta=1-v12.*v21-v23.*v32-v31.*v13-2.*v12.*v32.*v13 %delta factor

C13=E1.*(v31+v21.*v32)./delta
C23=E2.*(v32+v12.*v31)./delta
C33=E3.*(1-v12.*v21)./delta %C33=C33CİZGİ
C33cizgi=C33
C13cizgi=C13.*(cos(pi.*aci).^2) + C23.*(sin(pi.*aci).^2) %!!
C36cizgi=C13.*cos(pi.*aci).*sin(pi.*aci)-C23.*cos(pi.*aci).*sin(pi.*aci)
C23cizgi=C13.*(sin(pi.*aci).^2) + C23.*(cos(pi.*aci).^2)

Cler=[C13; C23]

%[C13cizgideneme;C36cizgideneme;C23cizgideneme]=saglama
M=[cos(pi.*aci).^2 sin(pi.*aci).^2; cos(pi.*aci).*sin(pi.*aci) -
cos(pi.*aci).*sin(pi.*aci); sin(pi.*aci).^2 cos(pi.*aci).^2 ];
%Transformation matrix given by Nguyen
saglama=M*Cler %for verification
FCRP5_81= cos(pi.*HL(I+1)/he)-cos(pi.*HL(I)/he)
FCRP6_81=(((HL(I+1)).*cos(pi.*HL(I+1)/he))-
((he)).*sin(pi.*HL(I+1)/he))/(pi)-(((HL(I)).*cos(pi.*HL(I)/he))-
((he)).*sin(pi.*HL(I)/he))/(pi)
FCRP7_81=((((he).*sin(2.*pi.*HL(I+1)/he))/(4.*pi)-(HL(I+1)/(2)))-
(((he).*sin(2*pi.*HL(I)/he))/(4.*pi)-(HL(I)/(2))))
FCRP8_81=(((((he).*sin(2.*pi.*HL(I+1)/he))-
(2.*pi.*HL(I+1))).*((pi)/(4.*he.^2)))-((((he).*sin(2.*pi.*HL(I)/he))-
(2.*pi.*HL(I))).*((pi)/(4.*he.^2))))
FCRP5_82=-((5*(HL(I+1)).^2)/(he.^2))-(-(5)*(HL(I+1)).^2)/(he.^2)
FCRP6_82=(-(10).*((HL(I+1)).^3)/(3.*he.^2))-(-
(10).*((HL(I)).^3)/(3.*he.^2))
FCRP7_82= (((10).*((HL(I+1)).^5)/(3.*he.^4))-
((25).*((HL(I+1)).^3)/(6.*he.^2)))-(((10).*((HL(I)).^5)/(3.*he.^4))-
((25).*((HL(I)).^3)/(6.*he.^2)))
FCRP8_82=((100).*((HL(I+1)).^3)/(3.*he.^4))-
((100).*((HL(I)).^3)/(3.*he.^4))
FCRP5_83=(-(4).*((HL(I+1)).^2)/(he.^2))-(-(4).*((HL(I)).^2)/(he.^2))
FCRP6_83=(-(8).*((HL(I+1)).^3)/(3.*he.^2))-(-(8).*((HL(I)).^3)/(3.*he.^2))
FCRP7_83=((32).*((HL(I+1)).^5)/(15.*he.^4))+(-
(8).*((HL(I+1)).^3)/(3.*he.^2))-((32).*((HL(I)).^5)/(15.*he.^4))+(-
(8).*((HL(I)).^3)/(3.*he.^2))
FCRP8_83=((64).*((HL(I+1)).^3)/(3.*he.^4))-((64).*((HL(I)).^3)/(3.*he.^4))
```

```
FCRP5_84=-6.*((HL(I+1)).^2)-
6.*((HL(I+1)).^2)/(he.^2)+10.*((HL(I+1)).^4)/(he.^4)-(-6.*((HL(I)).^2)-
6.*((HL(I)).^2)/(he.^2)+10.*((HL(I)).^4)/(he.^4))
FCRP6_84=((8).*((HL(I+1)).^5)/(he.^4))-((4).*((HL(I+1)).^3)/(he.^2))-
((8).*((HL(I)).^5)/(he.^4))-((4).*((HL(I)).^3)/(he.^2))
FCRP7_84= (5600.*((HL(I+1)).^9)-
9360.*((HL(I+1)).^7).*(he.^7)+7434.*((HL(I+1)).^5)*(he.^4)-
2205.*((HL(I+1)).^3)*(he.^6))/(630.*he.^8)-(5600.*((HL(I)).^9)-
9360.*((HL(I)).^7).*(he.^7)+7434.*((HL(I)).^5).*(he.^4)-
2205.*((HL(I)).^3).*(he.^6))/(630.*he.^8)
FCRP8_84=(((1600).*((HL(I+1)).^7))/(7.*he.^8))-
(((192).*((HL(I+1)).^5))/(he.^6))+(((48).*((HL(I+1)).^3))/(he.^4))-
(((1600).*((HL(I)).^7))/(7.*he.^8))-
(((192).*((HL(I)).^5))/(he.^6))+(((48).*((HL(I)).^3))/(he.^4))

%81=Touratier

J13_81=(FCRP5_81).*(C13cizgi);
J23_81=(FCRP5_81).*(C23cizgi);
J36_81=(FCRP5_81).*(C36cizgi);
L13_81=(FCRP6_81).*(C13cizgi);
L23_81=(FCRP6_81).*(C23cizgi);
L36_81=(FCRP6_81).*(C36cizgi);
O13_81=(FCRP7_81).*(C13cizgi);
O23_81=(FCRP7_81).*(C23cizgi);
O36_81=(FCRP7_81).*(C36cizgi);
P33_81=(FCRP8_81).*(C33cizgi);

J81=[J13_81;J23_81;J36_81]
L81=[L13_81;L23_81;L36_81]
O81=[O13_81;O23_81;O36_81]
P81=[P33_81]


%82=Reissner

J13_82=(FCRP5_82).*(C13cizgi);
J23_82=(FCRP5_82).*(C23cizgi);
J36_82=(FCRP5_82).*(C36cizgi);
L13_82=(FCRP6_82).*(C13cizgi);
L23_82=(FCRP6_82).*(C23cizgi);
L36_82=(FCRP6_82).*(C36cizgi);
O13_82=(FCRP7_82).*(C13cizgi);
O23_82=(FCRP7_82).*(C23cizgi);
O36_82=(FCRP7_82).*(C36cizgi);
P33_82=(FCRP8_82).*(C33cizgi);

J82=[J13_82;J23_82;J36_82]
L82=[L13_82;L23_82;L36_82]
O82=[O13_82;O23_82;O36_82]
P82=[P33_82]


%83=Reddy

J13_83=(FCRP5_83).*(C13cizgi);
J23_83=(FCRP5_83).*(C23cizgi);
J36_83=(FCRP5_83).*(C36cizgi);
L13_83=(FCRP6_83).*(C13cizgi);
```

```
L23_83=(FCRP6_83).*(C23cizgi);
L36_83=(FCRP6_83).*(C36cizgi);
O13_83=(FCRP7_83).*(C13cizgi);
O23_83=(FCRP7_83).*(C23cizgi);
O36_83=(FCRP7_83).*(C36cizgi);
P33_83=(FCRP8_83).*(C33cizgi);

J83=[J13_83;J23_83;J36_83]
L82=[L13_83;L23_83;L36_83]
O82=[O13_83;O23_83;O36_83]
P82=[P33_83]


%84=Nguyen-Xuan et al.


J13_84=(FCRP5_84).*(C13cizgi);
J23_84=(FCRP5_84).*(C23cizgi);
J36_84=(FCRP5_84).*(C36cizgi);
L13_84=(FCRP6_84).*(C13cizgi);
L23_84=(FCRP6_84).*(C23cizgi);
L36_84=(FCRP6_84).*(C36cizgi);
O13_84=(FCRP7_84).*(C13cizgi);
O23_84=(FCRP7_84).*(C23cizgi);
O36_84=(FCRP7_84).*(C36cizgi);
P33_84=(FCRP8_84).*(C33cizgi);

J84=[J13_84;J23_84;J36_84]
L84=[L13_84;L23_84;L36_84]
O84=[O13_84;O23_84;O36_84]
P84=[P33_84]
```

APPENDIX C

$$N_{xx} = \sum_{i=1}^{4} N_{xx}{}^{i}\varphi_i \quad N_{yy} = \sum_{i=1}^{4} N_{yy}{}^{i}\varphi_i \quad N_{xy} = \sum_{i=1}^{4} N_{xy}{}^{i}\varphi_i$$

$$M_x = \sum_{i=1}^{4} M_x{}^{i}\varphi_i \quad M_y = \sum_{i=1}^{4} M_y{}^{i}\varphi_i \quad M_{xy} = \sum_{i=1}^{4} M_{xy}{}^{i}\varphi_i$$

$$M_{xx}^{f} = \sum_{i=1}^{4} M_{xx}^{f\,i}\varphi_i \quad M_{yy}^{f} = \sum_{i=1}^{4} M_{yy}^{f\,i}\varphi_i \quad M_{xy}^{f} = \sum_{i=1}^{4} M_{xy}^{f\,i}\varphi_i \quad M_{zz}^{f} = \sum_{i=1}^{4} M_{zz}^{f\,i}\varphi_i \quad M_{xz}^{f} = \sum_{i=1}^{4} M_{xz}^{f\,i}\varphi_i \quad M_{yz}^{f} = \sum_{i=1}^{4} M_{yz}^{f\,i}\varphi_i$$

$$V_{yz} = \sum_{i=1}^{4} V_{yz}{}^{i}\varphi_i \quad V_{xz} = \sum_{i=1}^{4} V_{xz}{}^{i}\varphi_i$$

$$u = \sum_{i=1}^{4} u^{i}\varphi_i \quad v = \sum_{i=1}^{4} v^{i}\varphi_i \quad w = \sum_{i=1}^{4} w^{i}\varphi_i$$

$$\theta_x = \sum_{i=1}^{4} \theta_x{}^{i}\varphi_i \quad \theta_y = \sum_{i=1}^{4} \theta_y{}^{i}\varphi_i \quad \beta = \sum_{i=1}^{4} \beta^{i}\varphi_i$$

$$k_1 = \int_{L^e} \varphi_i \varphi_j dx \quad k_2 = \int_{L^e} \varphi_{i,x} \varphi_j dx \quad k_2^T = \int_{L^e} \varphi_i \varphi_{j,x} dx \quad k_3 = \int_{L^e} \varphi_{i,y} \varphi_j dx \quad k_3^T = \int_{L^e} \varphi_i \varphi_{j,y} dx$$

$$k_4 = \int_{L^e} \varphi_{i,x} \varphi_{j,x} dx \quad k_5 = \int_{L^e} \varphi_{i,y} \varphi_{j,y} dx \quad k_6 = \int_{L^e} \varphi_{i,x} \varphi_{j,y} dx \quad k_6^T = \int_{L^e} \varphi_{i,y} \varphi_{j,x} dx$$

(i=1, 2, 3, 6 ; j = 1, 2, 3, 6)

$$N = \left\{ N_x \quad N_y \quad N_{xy} \right\}$$

$$M = \left\{ M_x \quad M_Y \quad M_{xy} \right\}$$

$$M^{f} = \left\{ M_{xx}^{f} \quad M_{yy}^{f} \quad M_{xy}^{f} \quad M_{zz}^{f} \right\}$$

$$V = \left\{ V_{yz} \quad V_{xz} \right\}$$

$$U = \left\{ u \quad v \quad w \right\}$$

$$R = \left\{ \theta_x \quad \theta_y \quad \beta \right\}$$

$$k^e_{NN} = \begin{bmatrix} -A'_{11}k_1 & -A'_{12}k_1 & -A'_{16}k_1 \\ -A'_{21}k_1 & -A'_{22}k_1 & -A'_{26}k_1 \\ -A'_{61}k_1 & -A'_{62}k_1 & -A'_{66}k_1 \end{bmatrix} \quad k^e_{NM} = \begin{bmatrix} -B'_{11}k_1 & -B'_{12}k_1 & -B'_{16}k_1 \\ -B'_{21}k_1 & -B'_{22}k_1 & -B'_{26}k_1 \\ -B'_{61}k_1 & -B'_{62}k_1 & -B'_{66}k_1 \end{bmatrix}$$

$$k^e_{NM^f} = \begin{bmatrix} -E'_{11}k_1 & -E'_{12}k_1 & -E'_{16}k_1 \\ -E'_{21}k_1 & -E'_{22}k_1 & -E'_{26}k_1 \\ -E'_{61}k_1 & -E'_{62}k_1 & -E'_{66}k_1 \\ -J'_{13}k_1 & -J'_{23}k_1 & -J'_{36}k_1 \end{bmatrix}$$

$$k^e_{NU} = \begin{bmatrix} k_2^T & 0 & 0 \\ 0 & k_3^T & 0 \\ k_3^T & k_2^T & 0 \end{bmatrix} \qquad k^e_{M^f R} = \begin{bmatrix} k_2^T & 0 & k_3^T & 0 \\ 0 & k_3^T & k_2^T & 0 \\ 0 & 0 & 0 & k_1 \end{bmatrix}$$

$$k^e_{MM^f} = \begin{bmatrix} -F'_{11}k_1 & -F'_{12}k_1 & -F'_{16}k_1 \\ -F'_{21}k_1 & -F'_{22}k_1 & -F'_{26}k_1 \\ -F'_{61}k_1 & -F'_{62}k_1 & -F'_{66}k_1 \\ -L'_{13}k_1 & -L'_{23}k_1 & -L'_{36}k_1 \end{bmatrix} \qquad k^e_{MM} = \begin{bmatrix} -D'_{11}k_1 & -D'_{12}k_1 & -D'_{16}k_1 \\ -D'_{21}k_1 & -D'_{22}k_1 & -D'_{26}k_1 \\ -D'_{61}k_1 & -D'_{62}k_1 & -D'_{66}k_1 \end{bmatrix}$$

$$k^e_{VV} = \begin{bmatrix} A^s_{11} & A^s_{12} \\ A^s_{21} & A^s_{22} \end{bmatrix} \qquad k^e_{M^f M^f} = \begin{bmatrix} -H'_{11}k_1 & -H'_{12}k_1 & -H'_{16}k_1 & -O'_{13}k_1 \\ -H'_{21}k_1 & -H'_{22}k_1 & -H'_{26}k_1 & -O'_{23}k_1 \\ -H'_{61}k_1 & -H'_{62}k_1 & -H'_{66}k_1 & -O'_{36}k_1 \\ -O'_{13}k_1 & -O'_{23}k_1 & -O'_{36}k_1 & -P_{33}k_1 \end{bmatrix}$$

$$k^e_{VR} = \begin{bmatrix} 0 & k_1 & 0 \\ k_1 & 0 & 0 \end{bmatrix}$$

$$k^e_{MU} = \begin{bmatrix} 0 & 0 & k_4 \\ 0 & 0 & k_5 \\ 0 & 0 & k_6 + k_6^T \end{bmatrix}$$

$$k^e = \begin{bmatrix} k^e_{NN} & k^e_{NM} & k^e_{NM^f} & 0 & k^e_{NU} & 0 \\ & k^e_{MM} & k^e_{MM^f} & 0 & k^e_{MU} & k^e_{MR} \\ & & k^e_{M^f M^f} & 0 & 0 & k^e_{M^f R} \\ \vdots & & & k^e_{VV} & k^e_{VU} & k^e_{VR} \\ & sym & & & 0 & 0 \\ & & \cdots & & & k^e_{M^f R} \end{bmatrix}$$

For simplicity, form of load vector in transverse direction can be stated as:

$$f^e = \begin{Bmatrix} f_N^e \\ f_M^e \\ f_{Mf}^e \\ f_V^e \\ f_U^e \\ f_R^e \end{Bmatrix} = \begin{Bmatrix} 0 \\ 0 \\ 0 \\ 0 \\ f_U^e \\ f_R^e \end{Bmatrix} =, \; f_U^e = \begin{Bmatrix} 0 \\ 0 \\ \int_\varphi q(\delta w)\varphi_i dx \end{Bmatrix}, \; f_R^e = \begin{Bmatrix} 0 \\ 0 \\ \int_\varphi q(g(\frac{h}{2})\delta\beta)\varphi_i dx \end{Bmatrix}$$

7. CURRICULUM VITAE

Name Surname : Doğan KANIĞ

EDUCATION

- **B.Sc.** **:** 2020, Istanbul Technical University, Civil Engineering Faculty, Civil Engineering Department
- **B.Sc.** **:** 2022, Istanbul Technical University, Faculty of Architecture, Urban and Regional Planning (Minor Degree)
- **M.Sc.** **:** 2023, Istanbul Technical University, Graduate School, Structural Engineering Department

PUBLICATIONS, PRESENTATIONS AND PATENTS ON THE THESIS:

• **Kanığ D.,** Kutlu A., 2021. Stress and Bending Analysis in Laminated Composite Beams Based on HSDT Considering Stretching Effect (in Turkish). *Proceedings 23. National Mechanics Congress*, September 04-07, Konya, Türkiye.

• **Kanığ D.,** Bab Y., Kutlu A., Omurtag M. H., 2023. Mixed finite element formulation for the buckling analysis of laminated composite beams using HSDT, *ICEARC 2023- 3rd Internatıonal Civil Engineering and Architecture Conference*, October 12-14, Trabzon, Turkey.